Dissertation
submitted to the
Combined Faculties for the Natural Sciences and for Mathematics
of the Ruperto-Carola University of Heidelberg, Germany
for the degree of
Doctor of Natural Sciences

Put forward by

Master of Science: Sarah A. Biela

Born in: Bonn, Germany

Oral examination: July 8th, 2009

Stimulation of vascular cells by extracellullar signals

- A biophysical analysis

Referees: Prof. Dr. Joachim P. Spatz

Prof. Dr. Rainer H. A. Fink

Stimulierung von Gefäßzellen durch extrazelluläre Signale

Die Behandlung von Herz-Kreislauf-Erkrankungen erfordert häufig die selektive Stimulierung von Endothel- (ECs) und glatten Muskelzellen (SMCs). Die zwei Gefäßzelltypen sind wichtig für die Einheilung von sog. Stents. Die moderne Forschung befasst sich mit der Entwicklung neuer Materialien und Beschichtung für Stents, um den komplexen Einheilungsprozess zu verbessern. Das Ziel meiner Arbeit war es, durch Oberflächen-Chemie, -Topographie und andere stimulierende Faktoren wie elektrische Felder oder mechanische elastische Dehnung verschiedene Reaktionen der zwei vaskulären Zelltypen (ECs und SMCs) zu finden und zu untersuchen. Auf verschiedenen Iridium-Oxid Stent-Beschichtungen erscheinen ECs empfindlicher als SMCs. Auf micro-nano-Strukturen aus PDMS richten sich ECs und SMCs nicht signifikant unterschiedlich aus. Experimente mit biofunktionalisierten Nanostrukturen machen deutlich, dass es eine universelle Liganden-Abstand-Abhängigkeit für beide Zelltypen geben muss. Unter uniaxialer mechanisch elastischer Dehnung oder einem gerichteten elektrischen Feld, zeigen ECs und SMCs signifikant verschiedene Reaktionen. Die allgemeinen Eigenschaften der zwei Zelltypen können mit einem automatischen Controller-Modell quantitativ beschrieben werden. Die Ergebnisse machen zuversichtlich, in kommenden Untersuchungen die Implantat-Einheilung zu verbessern und sogar künstliche Formation neuer Blutadern (Angiogenese) zu ermöglichen.

Stimulation of vascular cells by extracellullar signals

Treatment of vascular diseases often requires the selective addressing of endothelial (ECs) and smooth muscle cells (SMCs). The two vascular cell types are important for the wound healing after stent implantation. Recent research designs new materials and coatings for stents to improve the complex healing process. The aim of my work was to find and investigate different reactions in the two vascular cell types (ECs and SMCs) through surface chemistry, topography and other stimulating factors like electrical fields or applied external stretching forces. On various iridium-oxide stent coatings ECs seem to be more sensitive to chemical differences than SMCs. On PDMS micro-nano-grooves ECs and SMCs align not significant differently to the structure. Cell assays on nano-structured and bio-functionalized surfaces reveal a universal ligand distance dependency for both cell types. Upon application of uniaxial mechanical stretch or an directed electrical field, ECs and SMCs show significant different responses. General characteristics of the two cell types can be quantitatively described by an automatic controller model. These findings are promising for further studies to improve wound healing after implantation and even more to allow the artificial generation of new blood vessels (angiogenesis).

Contents

Introduction and objective

One of the key organ systems of the human body is the vascular system. Through development and response to injury it sustains normal human physiology [114]. Blood vessels are built up from and regulated by an inner monolayer of endothelial cells (ECs) surrounded by an outer thicker shell of smooth muscle cells (SMCs) [32, 211] The two vascular cell types are key players in vascular disease, still one of the major medical concerns in modern society. The common treatment by coronary angioplasty (stent insertion) still suffers from problems like inflammations, thrombosis and re-occlusion by SMC growth (restenosis) [204, 153]. Another interesting phenomenon, where signaling pathways modulate EC and SMC growth, is the formation of new blood vessels (angiogenesis) in development and tumor growth, whose understanding and artificial modulation offers great hope for treatment of cancer and a vast spectrum of other diseases [61, 62]. A complete understanding of both cell types requires a systematic, structural, and separate analysis of the multiple-interdependent signaling pathways in the cells, the surrounding tissue and the blood [87]. Thereby, a multitude of stimulating signals, such as messenger molecules, extracellular matrix, pulsatile blood flow and endogenous electrical fields exist in and around the vasculature, see Figure 0.1 [190, 181, 172].

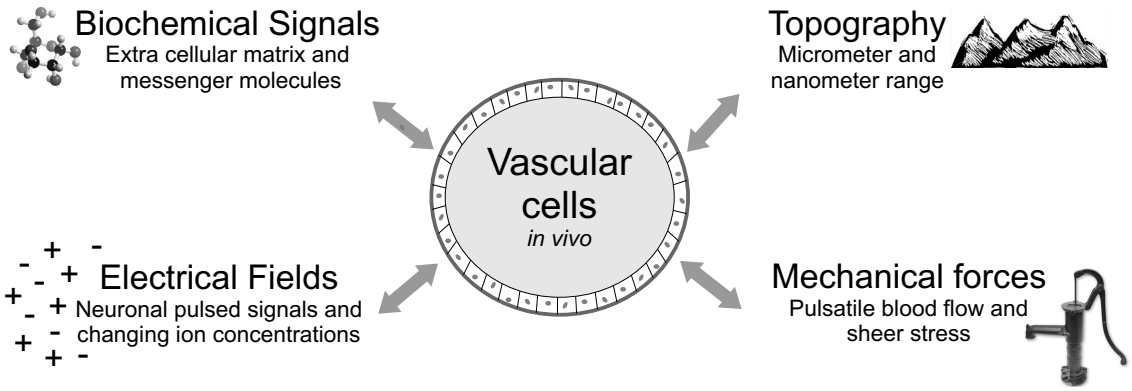

Figure 0.1: Overview of extra cellular signals interacting with vascular cells.

In order to increase the knowledge and improve developments in medical treatment, current research seeks to gain a deeper understanding of the response and function of ECs and SMCs and their cell type specific interaction with extracellular signals in their surrounding [63, 85, 120].

Research on cell environments has attained much interest in recent *in vitro* investigations. A promising approach to improve implantation is the stimulation of cells by surface topography, which is systematically studied, see [29, 126, 44, 94, 232]. The topography and chemistry of a material surface can regulate diverse cellular responses, including survival, adhesion, spreading, migration, proliferation, and expression of differentiated phenotypes [138, 25, 31, 51], which altogether regulates tissue development in a complex manner. Several studies on vascular and other cell types show responses to stimulating factors such as mechanical stretch and electric charges [97, 93, 7, 108]. Recent investigations combine mechanical stress and electrical charge effects [139], which indicate that piezoelectric charges produced under stress in extra cellular materials may stimulate cellular response and thus the growth and healing of these tissues [133, 12, 178, 113]. Considering this diversity of signals and cell responses, the focus of this thesis is on the quantitative model-inspired analysis of cell-type specific responses of ECs and SMCs to several physical signals. Thus the following questions are addressed: Can cell type specific responses of ECs and SMCs be stimulated by (i) chemically inert and topographically modified surfaces, (ii) nanostructured and cell specifically biofuncionalized surfaces, (iii) applied mechanical cyclic stretch or (iv) variations in directed electrical fields? Moreover, to increase the insight into the cell response characteristics a quantitative model of the cell as an automated controller is applied to the various experimental data. In order to address the above mentioned questions, a variety of experimental techniques and setups have been developed and used. Cells on modified surfaces, under applied cyclic stretch or electrical fields were observed *in vitro* with phase contrast, fluorescence and time-lapse microscopy. This thesis is divided in four parts. In the first part, an introduction to the physiological, biological and physical background of vascular cells and their surrounding is given. In the second part, the most important methods, such as surface preparation and application of stimulating signals are presented. Furthermore, observation and analysis techniques are introduced. The third part presents results of an industrial cooperation project with authentic stents. The last and main part of this thesis shows the results of studies about the behavior of ECs and SMCs under application of various signals such as surface topography, biochemistry, mechanical cyclic stretch and electrical fields.

Part I

Review on blood vessel physiology

1 Cell system and biology

The tissue of human blood vessels is built up from an inner monolayer of endothelial cells (ECs) surrounded by an outer thicker shell of smooth muscle cells (SMCs). The properties and interactions of these different cell types are important for the physiological functions of the vascular system and will be briefly explained in this chapter. ECs and SMCs are also key players in vascular disease, one of the major medical concerns in modern society. The common treatment by coronary angioplasty (stent insertion) leads to disruption of the endothelial layer leaving a highly prothrombotic surface exposed to the blood stream. In order to increase the chance of appropriate healing, current research on coronary implants seeks to gain a deeper understanding of the response and function of these two cell types (ECs and SMCs) and their interaction with the stent surface, see sections 1.2 and 1.2.1. Within the focus of this thesis the function and intercation of ECs and SMCs are studied in several cell sourroundings and under various extracellular stimuli.

1.1 Blood vessel physiology

The inner monolyer of a vessel wall, called intima, is build up by endothelial cells, which form the endothelium [177]. They are mostly aligned along the longitudinal axis of the blood vessel or lymph. Independent of the kind of vessel, ECs are flat, around $1 - 2\,\mu$m thick with a dimater of $10 - 20\,\mu$m. ECs play important roles in several physiological processes. They not only regulate the nutrient exchange between tissue and blood, but also produce important biochemical factors for the regulation of the blood pressure like nitrigenmonoxide (NO), which interacts with the smooth muscle cells that sourround the endothelium and modulate the vascular tone. Furthermore, ECs influence the flow of the blood and thereby, activating or inhibiting coagulation processes. Upon inflammation, ECs locally activate several microbial substances to attract leukocytes from the blood to adhere to the ECs and be activated. The activated leukocytes migrate then into the tissue beneath the endothelium and alleviate the infection.
Another crucial biological process, where ECs are involved is angiogenesis. The formation of new blood capillaries is of high importance in embrionic development, but is also an important matter in the field of cancer and tumor research [61, 62, 85].
Smooth muscle tissue is the contractile tissue of many hollow organs, blood and lymph vessels and other structures in the human body. In opposite to the skeletal muscles, smooth muscles are controlled by the autonomic nervous system. Smooth muscle cells are able to synthesize collagen and other proteins that build up the extra cellular matrix. They interact with ECs via messenger molecules and regulate the blood pressure [177, 6, 114, 85]. In figure 1.1 the typical anatomy of a blood vessel is shown schematically.

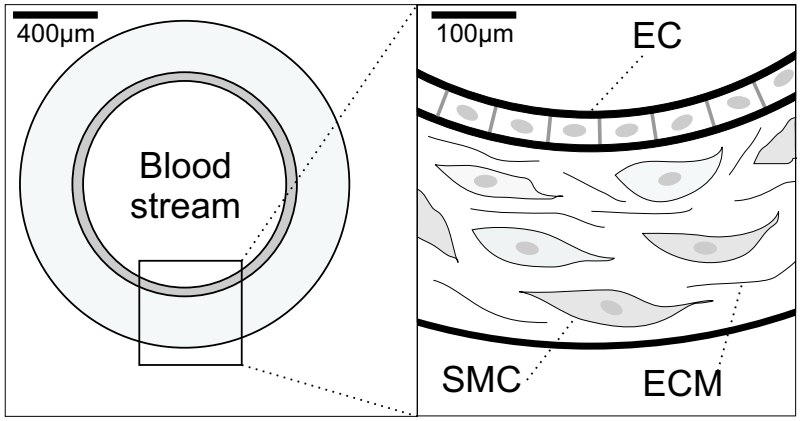

Figure 1.1: Schematic view of the inner blood vessel consisting of endothelial cells (ECs), smooth muscle cells (SMCs) and extracellular matrix (ECM).

1.1.1 Cell culture of vascular cells

In order to analyse the diverse physiological functions independently of the surrounding tissue, ambitious efforts have been made to isolate and culture ECs and SMCs, see [50]. During the past three decades, the development of isolation and culture techniques of ECs and SMCs from numerous vascular regions and species has revolutionized our understanding of vascular cells' function. Apart from the use of freshly isolated, primary EC and SMC cultures, there is also a variety of cell preparations commercially available. The cells used for the studies of this thesis were commercially aquired at PromoCell, Germany (see appendix 3 for details). In addition, a number of endothelial and smooth muscle cell lines have been generated from ECs and SMCs of micro- and macrovascular origin. However, the great disadvantage of cell lines is that cell morphology and function may change during long-term culture. To overcome this problem, the cells used in this thesis were isolated human primary ECs and SMCs. Typical morphologies of both cell types in a cell culture flask are shown in figure 1.2.

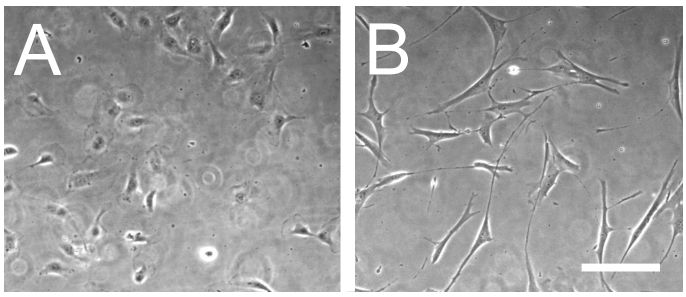

Figure 1.2: Phase contrast images of endothelial cells (A) and smooth muscle cells (B) in cell culture flasks obtained with a CCD camera attached to an optical microscope; scalebar represents 200 μm.

1.2 Cardiovascular disease

Endothelial cells may modulate the vascular diameter, and hence the tone by releasing vasoactive substances in response to various stimuli and these regalutory mechnanisms may play a role in the pathophysiology of cardiovascular disease. The endothelium plays a crucial role in the local control of vascular smooth muscle tone, in hemostasis and as a primary target organ in cardiovascular diseases such as atherosclerosis, hypertension and diabetes, [127]. The functional role of the vascular endothelium in the circulation includes: (a) prevention of adhesion of platelets, leukocytes and monocytes; (b) production of factors that are involved in blood clotting; (c) capillary transport and exchanges between blood and tissue; (d) activation and inactivation of circulating hormones and other plasma constitutes, and (e) synthesis and secretion of vasodilator and vasoconstricttor substances. In addition, ECs produce a heparin-like cell growth inhibitor as well as distinct growth factors, which may regulate the growth of underlying vascular smooth muscle [127]. Arteriosclerosis is one of the most frequent cardiovascular deseases and mainly responsible for heart infactation and strokes. The local phenomenon in in the artery is the concretion of lipids, blood products and calcium carbonate. These concretions occluse and harden the blood vessel and disturb the blood flow. This desease is treated by rotational angioplasty, Laser angioplasty, bypass-operation, and the insertion of stents [200, 147, 116]. Restoration of an intact endothelium, therefore, represents a crucial process in reestablishing an intact vessel surface. However, enhanced SMCs proliferation often leads to restenosis, which describes the re-occlusion of the blood vessel by SMC proliferation. Current studies have shown that restenosis is not dependent on the material or the design of the stent, and takes place in about 30% of the cases of stent insertion [49, 116, 115].

1.2.1 Stent treatment and current stent materials

The implantation of a stent is performed using an inflatable baloon at the end of a long catheter, which is introduced into the blood vessel. The stent sticks around the compressed baloon, and is expanded when the catheter reaches the inflamed and narrowed part of the vessel. The insertion of the stent is shown schematically in figure 1.3. For the current treatment several stent designs and materials are available on the market. There is a great variety of stent materials ranging from pure metallic stents over polymer coated and drug eluting stents to biodigradable stents fully made out of polymers [152, 116, 115, 155, 101, 76, 131, 57, 27, 171]. The mentioned studies and reviews summarize the different components of stent design that are important in term of biological response of the arterial wall and clinical outcome. The original approach used pure metallic stents [101, 159], but due to the problem of restenosis, drug eluting stents were developed to delay the healing process [57]. Since then researchers try to elucidate the healing process and investigate the role of stent design and coatings on restenosis and thrombosis [76]. Especially drug eluting stents are investigated since sudden occurence of thrombosis after long term insertion of stents diminish the superiority of this treatment approach of vascular desease [164, 192]. It is believed that a better understanding of the basic biologic interactions is the correct path to significant improvement. Newest findings suggest alternatives for the conventional drug eluting stents e.g. polymer coatings releasing epigallocatechin gallate [28], pure polymer coatings [75], nitiniol carbolfilm coatings [163], or DNA-releasing coatings with ultrathin polyelectrolyte films [90]. Further studies show that gene eluting stents are indeed a

promising new field [58, 179], since they may reduce vascular injury and accelerate vessel healing. Another alternative to the current drug eluting stents, which is further pursued, is the treatment with bioresorbable (also called biodegradable) polymeric stents [180], that hopefully may provide more precise answers to stent implantation and improve the clinical outcome [171]. In addition, some of these biodegradable stent materials are even able to elute drugs, see e.g. [27].

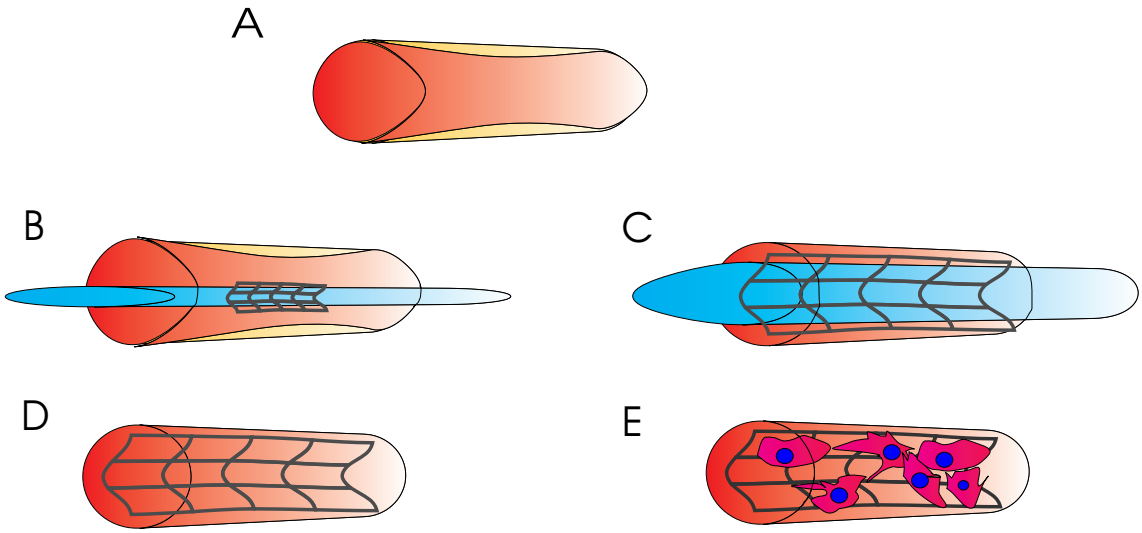

Figure 1.3: Scheme of stent implantation. A: Blood vessel narrowing by plaque and inflammation. B: Stent is introduced by an inflatable baloon catheter. C: Catheter and stent are expanded. D: Expanded stent in opened blood vessel after removal of the catheter. E: SMC proliferation on the stent starts to re-occlude the blood vessel (restenosis).

2 Recent research

The idea of this thesis was to find new solutions to wound healing after stent implantation and to increase endothelialization instead of increased smooth muscle cell (SMC) proliferation. As there are several factors in the body stimulating and exciting cell growth, they were tested seperately on the cells in the presented experiments. In the following sections an overview of ongoing research on this topic and motivations for the different studies and experimental setups are given, which will be described in detail in part II. The results of the studies are presented in part III and IV.

2.1 Samples and surfaces

Seeding cells on surfaces and observing their spreading and proliferation behavior with microscopy (see chapter 4) opens many possibilities for *in vitro* studies of the interaction of cells and materials. In this theses two approaches were pursued: topographic and biochemical stimulations of vascular cells with the help of surface modifications.

2.1.1 Topography

In order to increase the chance of appropriate healing, current research on coronary implants seeks to gain a deeper understanding of the response and function of vascular cells and their interaction with the implant surfaces (e.g. stents). Consequently new materials and surface modification including micro or nano-structured surfaces, polymers, and drug-releasing coatings [131] have been studied resulting in different improvements and drawbacks [104, 192]. As a result, increasing interest has been focused on the analysis of cell-type-specific functions and responses [204, 153] to stent surface features and recent research has tried to elucidate mechanisms by which the independent stimulation of endothelial (ECs) and smooth muscle cells (SMCs) may be achieved via surface modification [29]. Among others, a common approach for controlling cell adhesion to implant surfaces is the introduction of surface topographies either in the micrometer or in the nanometer range [29, 138, 126, 44]. It is well documented that many cells respond to these topographical surface features by changing their proliferation, adhesion, or by directed migration and cell orientation often called contact guidance [40, 20, 2, 197]. Such cell alignment along surface structures and directed migration are powerful indicators of the cells' ability to sense their environmental topography. Loesberg *et al.* showed, for example, that the orientation response of fibroblasts to hypergravity can be significantly increased by a combination with micrometer-sized grooves [126]. In a different study, the influence of channel width on the alignment of smooth muscle cells by high-aspect-ratio microstructures was

demonstrated [70]. However, comparable studies of several cell types and their responses to topography are rare but necessary to address the question of cell-type specificity.

Therefore, in this thesis the alignment and migration of vascular cells exposed to defined grooved surface topographies with sub-cellular nano-micro dimensions was systematically examined, see chapter 6. The cells responded to the input signal by alignment parallel to the grooves. This cell response and the directed migration are quantified in order to elucidate possible differences between the cell types. Response differences may provide an opportunity to selectively trigger behaviors of cells towards implant materials in the body.

2.1.2 Surface bio-chemistry

In fundamental cellular functions including motility, proliferation, differentiation, and apoptosis cell-cell and cell-extracellular matrix (ECM) adhesion are involved. They are complex, highly regulated processes, investigated in various studies [15, 227, 66]. Responsible for cell-ECM attachment and adhesion-mediated signaling are focal adhesions. These complex multi-molecular assemblies consist of transmembrane integrin receptors linked to the actin cytoskeleton [227, 36, 140, 8]. Integrins are heterodimers formed by noncovalent association of α and β subunits that bind to a lipid sequence present in ECM proteins. For fibroblast cells the main motif is the RGD (Arg-Gly-Asp) motif, a sequence of fibronectin. Other cell types, expressing different integrins are attracted by other motifs, such as REDV (Arg-Glu-Asp-Val) or VAPG (Val-Ala-Pro-Gly), studied by Massia *et al.* and Plouffe *et al.* [134, 161]. They show that REDV preferentially binds via $\alpha_4\beta_1$ to endohelial cells (ECs), and VAPG binds to SMCs [134, 161, 71] while RGD can bind mediated by the $\alpha_5\beta_3$ integrin to fibroblasts as well as both ECs and smooth muscle cells (SMCs) [78, 96]. In the *in vivo* surrounding of vascular cells, not only cell-ECM-contacts, but also cell-cell contacts are important. One of the major families of cell surface receptors is the cadherins that forms intercellular junctions [67]. Especially ECs, usually connected to each other via vascular endothelial cadherins (VE-Cad) are of researchers interest, since finding mechanisms to trigger cells migration (angiogenesis) and monolayer formation on implants (stents) via cell-cell or cell-ECM contacts is promising [91, 225, 84, 81, 203, 110]. Furthermore it is of interest to decrease SMC proliferation on implant surfaces as it causes inflammation and re-occlusions of blood vessels [217, 83]. In addition not only the surface biochemistry plays an important role triggering cellular reactions, also the nanostructure at the interface, see e.g. [138].

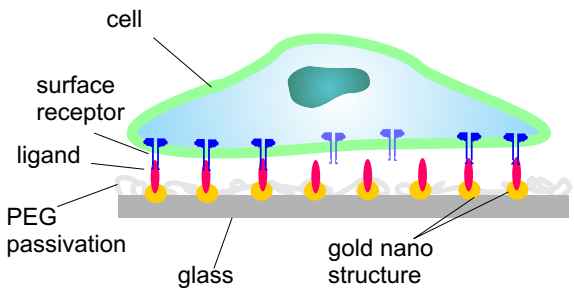

Figure 2.1: Schematic representation a cell on a surface decorated with gold nano structures and biofunctionalization. The cells' surface receptors bind to the ligands immobilized in the nanostructure. The surface between the gold structure is passivated with polyethylene glycol (PEG), [69, 4].

Whether cells adhere via integrins or cadherins to interfaces modified with appropriate ligands depends on many factors [66, 78, 24]. Affinity and specifity of the ligands to the particular integrin, mechanical strength of the ligand support, spacer length, overall ligand concentration, surface topography and ligand density are important surface characteristics, which have to be considered in the experimental setup. To address the precise molecular topology of focal adhesions and cadherins functional nanostructured surfaces were created before [69, 4, 188], where adhesive spots with molecular dimensions are separated by non-adhesive regions so that individual integrins or cadherins can interact specifically with such surfaces. In the mentioned studies, gold-nano structures build up a regular pattern on glass surfaces, which can be passivated by polyethylene glycol (PEG) [52, 129, 214, 112, 16]. This is a powerful approach since it allows the tuning of the properties of cellular material i.e. peptide composition, nanotopography and spatial nanopatterning of signaling molecules. It provides a promising possibility to test specific cellular responses, i.e. cell spreading and adhesion, integrin and cadherin clustering, depending on the presented ligand and its lateral distribution on the surface, see figure 2.1 [24, 4, 22].

In this thesis the approach by Arnold *et al.* [4] is used to stimulate vascular cells (ECs and SMCs) with three linker systems, see chapter 7. Peptide sequences of the extracellular matrix and VE-cadherins typical for endothelial cell-cell contacts are used to observe specific ligands and/or distance dependence of the spreading and adhesion characteristics of the two cell types. The here presented data in comparison with recent studies [4, 5], indicate a universal distance dependence for integrin clustering and focal adhesion formation. This finding together with further insight into cell-cell and cell-ECM interactions will be helpful in the future to stimulate vascular cells for vessel formation (angiogenesis) and wound healing.

2.2 External signals

Topographical and bio-chemical stimulations can be tested in a simple way *in vitro* seeding cells on various modified surfaces and observe their behavior. Application of external guiding signals is a different approach. To observe their effects with the standard methods, new aperatures had to be built in our labs, which are described in chapter 3.

2.2.1 Mechanical forces

The function of many tissue and cell types is regulated by mechanical forces. These forces can be externally applied or internally generated. In this manner, gravitational compressive forces control the deposition of bone composites, just as isotonic tension causes muscles to grow [111, 26]. In the vascular system hemodynamic forces such as stretch and shear stress are required to maintain the structural organization and functional activity of ECs and SMCs that form the vessel wall [47]. Shear stress is generated by the pulsatile blood flow, and circumferential stress is caused by the pulsatile blood pressure [190, 181]. At the interface between the bloodstream and the vessel wall endothelial cells are continuously subjected to mechanical stimulation *in vivo*. When exposed to mechanical loading, endothelial cells act like mechanical sensors. Endothelial cells, exposed to cyclic stretching, hydrostatic pressure and fluid shear stress, orient along the vascular axis *in vivo* [60, 226]. Not only their morphology and structure, but also their functions change with the application of tensile or shear loadings [167, 13, 187]. This response is thought to be the result

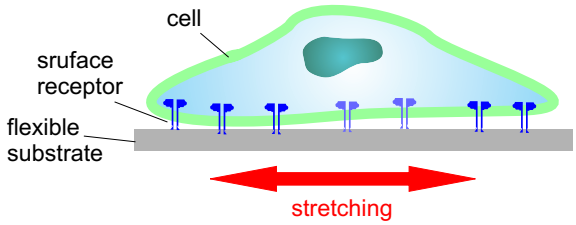

Figure 2.2: Schematic representation of a cell on a stretchable membrane.

of adaptation to or survival from such mechanical environments [196]. However, the elevation of circumferential tensile stress in an arterial wall may result in endothelial damage, plaque formation and atherosclerosis [167, 118]. The orientation and structural network of the smooth muscle cell (SMC) layers, that build up the arterial wall are very important for maintaining its mechanical strength and function and also for providing the flexibility required for pulsatile blood flow [199, 56, 191]. SMCs are primarily aligned in the circumferential direction in the arterial wall, which is a result of the complicated mechanical environment *in vivo*. It is mainly the cyclic nature of vessel stretch resulting from arterial pressure waveforms generated by the left ventricle, that is responsible for that [97, 218]. The mechanical stimuli from pulsatile blood flow were considered to be one of the key factors to regulate vascular remodeling during development and pathogenesis [222, 123, 141]. Cultured SMCs *in vitro* can be induced to reorient to a uniform perpendicular alignment into the direction of principal uniaxial mechanical stretch [191, 231, 98]. The cell orientation response strongly depends on the stretching magnitude [210, 46] and is consistent with the response found in other cell types [210, 212, 213]. These investigations provide useful information for understanding the role of cyclic strain in regulating the alignment of vascular ECs and SMCs. In the context of tissue engineering, applied forces are important for creating functional vessels that can withstand the mechanical stresses present *in vivo* [193]. Cellular responses to mechanical stimuli have been studied extensively through exposure of cultured cells or arterial segments to cyclic loading. The parameters investigated are manifold. Among them are changes in cell morphology, structure, mechanical properties, protein synthesis and modification, gene expression, angiogenesis, cell migration, ion flux, cell proliferation and vessel tone [190, 182, 132, 142, 183, 206]. The responses depend on external stresses or on intracellular processes like the contractile cytoskeleton-motor protein complex [51, 82, 88]. The details of biochemical mechano transduction and pathways are not fully understood, yet for basic biological science a profound knowledge of cell responses to mechanical signals is important [205, 89]. Recent research uses many different methods to investigate the influence of mechanical signals on cells [11]. One common method of examining cell responses to mechanical stress is the use of flexible membranes as culture substrates [117, 10]. Cells adherent on an expandable elastomeric substrate coated with extracellular matrix molecules like fibronectin or collagen can be exposed to a mechanical strain, see figure 2.2 [149]. Several studies have shown that cells on uniaxial cyclically stretched substrates mostly reorient themselves nearly perpendicular to the direction of stretch [97, 210, 46, 212, 149, 108, 143, 148]. Furthermore, it was observed that the actin cytoskeleton is reorganized perpendicular to the stretch direction [86, 45]. In the studies mentioned similar orientation responses have been found in many different cell types such as endothelial cells, smooth muscle cells, osteoblasts or fibroblasts.

The results support the common hypothesis that cell alignment is an avoidance reaction of the cells to stress by stretching. It is believed that the sensing of cells is mediated by focal adhesions that mechanically link the extra cellular matrix with the cytoskeleton [14]. Despite many experimental studies, only limited information about the dynamics of cell reorientation is available to this date. Neidlinger-Wilke *et al.* showed, for example, that fibroblasts tend to reorient within the first three hours during cyclic stretch [148]. Liu *et al.* demonstrated a frequency dependence for the alignment of arterial smooth muscle cells observed in time steps of 3 hours [123]. Jungbauer *et al.* systematically investigated the influence of dynamical frequency and amplitude changes on fibroblasts [93]. Detailed quantitative examination of the temporal behavior of cells under cyclic stretch could be helpful for understanding the molecular mechanisms involved and is crucial for theoretical modeling [48]. One mechanism observed is the remodeling of the actin cytoskeleton during cell reorientation of ECs and SMCs to minimize the mechanical strains acting on actin filaments and cells, respectively [196, 196, 124, 215]. The detailed response of actin stress fibers to such mechanical stimuli, specifically the orientation angle and location of stress fibers with respect to the stretch axis, is not fully understood.

In this thesis the effects of stretch frequency on the temporal dynamics of EC and SMC reorientation are compared, see chapter 8. Experimental measurements with a high temporal resolution were conducted. For the two cell types a characteristic difference in the behavior of cell reorganization in the frequency range from 0.01 to 1 Hz is demonstrated. Furthermore, not only reorientation of the whole cell body is shown, but also differences in the intracellular actin network and the focal adhesion orientation are presented.

2.2.2 Electrical fields

Endogenous direct current electrical fields (dcEFs) are present in all developing and regenerating animal tissues, and are important for wound healing [168, 136]. *In vitro* studies with neurits, corneal epithelial and endothelial cells have shown that even small EFs ($5 - 1600\,\mathrm{mV/mm}$) have an effect on cell proliferation rates, the orientation of the axis of cell division, and migration direction [136, 185, 209]. Furthermore, the application of small dcEFs may upregulate some growth factor receptors and increase growth factor release [99, 230, 59]. These changes are important for migration of many cell types, including human umbilical vein endothelial cells (HUVECs) and bovine aortic endothelial cells [229, 119]. *In vivo*, injured and ischemic tissues are polarized electrically which can produce a dcEF of 5.8 mV/mm across an 8-mm zone at the boundary with undamaged tissue [35]. Endogenous EFs also exist in and around the vasculature. For example, ζ-potentials arise from the flow of blood in large blood vessels and are 100 to 400 mV at the blood-endothelial cell (EC) interface [172]. This generated EF may be one of the mechanisms involved in maintaining a healthy state at the EC interface, which is a common interest in recent research. In addition to having an effect in the health of established blood vessels, electrical stimulation has emerged as an approach to induce angiogenesis *in vivo* [99, 158, 37]. The modulation of new blood vessel formation, either to increase the blood supply to ischemic tissue or to inhibit blood supply to an undesired neoplasm such as cancer, offers great hope for treatment of a vast spectrum of diseases [61]. New blood vessel formation is based on the capacity of ECs to migrate, proliferate, elongate, and organize in 3 dimensions into tubules. Bai, *et al.* and others have shown that electrical stimulation can induce reorientation, direct migration, and stimulate elongation [229, 119, 7] of ECs

and SMCs, two cell-types important in angiogenesis.

In addition to the existence of and physiological roles for steady dcEFs in development and in wound healing, there are many situations where external EFs arise from repetitive, pulsatile firing of action potentials or synaptic activity, particularly within the tight constraints of the extracellular spaces of the central nervous system [135, 55]. This indicates that, in addition to dcEFs, pulsed EFs may also be important for the induction of alternate cellular behaviors. Under uniform pulsed EFs, neurites showed a preferential orientation toward the cathode pole of the field in a manner similar to that previously found for dcEFs [55]. Application of extremely low frequency pulsed dc electric fields (ELFP- EFs), can lead to exaggerated neutrophil extension and metabolic resonance [109]. The study of Baldi, *et al.* suggests that a full investigation into the effect of extremely low frequency pulsed electromagnetic fields on the cardiovascular system is justified [9].
Directional shapes and movements during cell migration are controlled by several factors such as contact inhibition, chemotaxis, haptotaxis, and contact guidance [195]. These are functions of cells having a goal-seeking system or, in other words, an automatic controller that has a closed-loop feedback system [108]. The ability of some cells to direct their movement and their orientation along extra-cellular signals seems to be a general phenomenon. Directed migration and orientation is obtained if the cells have the ability to measure the direction of the extracellular guiding signal, in this study the electrical field. The result is a directed response where the cells migrate in the direction parallel or align in the direction perpedicular to the guiding signal. The mechanism responsible for directed migration and orientation is an automatic controller found in different cell types like granulocytes, monocytes, neural crest cells, and sperm that responds to different guiding signals like concentration gradients of chemotactic molecules and electrical fields [108, 74, 73].

In this thesis, ECs and SMCs were observed under dcEFs and ELPF-EFs, see chapter 9. Differences in their orientation and migration characteristics could be measured and analyzed in detail with the controller model of Kemkemer, *et al.* [108, 74], which extracts important information from the raw data (see also section 4.4). It can be shown, how the intracellular signal transformer measures the extracellular signal and how the statistical signal in the automatic controller can be quantified by a characteristic time. ECs and SMCs apparently have a controller mechanism in their orientation and directed migration response towards dcEFs and ELFP- EFs. Furthermore ECs and SMCs migrate in different directions under applied EFs. This intriguing directional selectivity indicates that a dc or pulsed electric signal as a directional cue may be able to play a role in the spatial organization of vascular structure and may be used in the future for selective tissue engineering.

Part II

Experimental design and measurement techniques

3 External signal stimulations

3.1 Nano-micro grooves

The nano-micro-structured substrates were fabricated as described previously in Jungbauer *et al.* [94]. Briefly, master substrates (silicon-100 wafers) were structured by a photolithographic process resulting in rectangular parallel grooves of different depths (50, 100 and 200 nm), and groove widths (2, 3, 5 and 10 μm) (see figure 3.1). These master substrates were used as a mold for the pattern transfer to poly(dimethylsiloxane) (PDMS) substrates [216]. PDMS (Sylgard 184, Dow Corning) was polymerized by mixing the prepolymer with the curing agent at a ratio of 10:1. The mixture was cured on the master substrates at 65 °C for 24 hours. Once peeled of the master, the substrates were treated with oxygen plasma (200 W, 1 mbar, Tepla RIE, Germany) for 5 sec to increase surface wettability and cell adhesion. They were sterilized with 70% ethanol, washed with PBS and finally used in the experiments. The surface topography of the PDMS substrates was verified by atomic force microscopy and scanning electron microscopy (SEM) as described in [106].

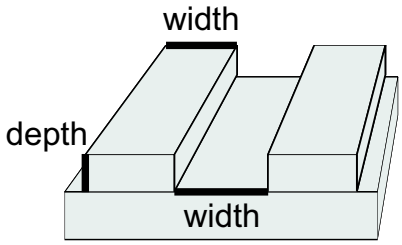

Figure 3.1: Schematic representation of PDMS grooves.

3.2 Gold nano structures

As described in previous studies [69, 68, 188, 189], the herein performed substrate patterning strategy is based on self-assembly of diblock copolymer micelles. Highly regular monomicellar films are prepared by dipping a glass slide into a 5 mg/ml toluene solution of PS(x)-b-P2VP(y) diblock copolymers and then retracting the glass slide after a few seconds with a speed of 12 mm/min as shown schematically in figure 3.2. The molecular weights of the diblock copolymers varied according to table 3.1.
In all cases, a part of the 2VP units were neutralized by addition of $HAuCl_4$ to the toluene solution and were then stirred for at least 48 h, i.e. PS-b-P[2VP($HAuCl_4$)x]. After air-evaporating the toluene solvent from the substrate, the monomicellar polymer films were

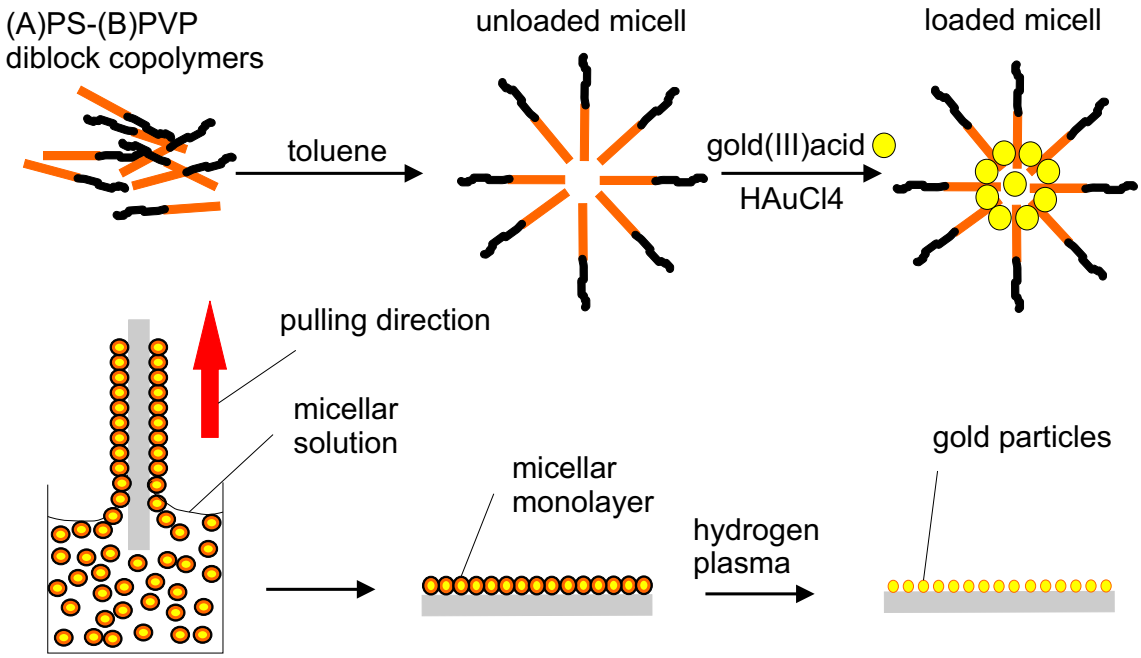

Figure 3.2: Schematic representation micellular nanolithography on glass slides; image adapted from [4, 69].

removed completely with a H_2-plasma treatment (0.4 mbar pressure, 150 Watt output, 0.4 ml/sec gas flow, for 45 min). This results in extended and highly regular Au nanodots, deposited into a nearly perfect hexagonal close-packed Au dot pattern on glass. In figure 4.1 the pattern is shown as bright spots in scanning electron microscopy (SEM) image, see section 4.1. Separation between Au dots can be varied by the molecular weight of the diblock copolymers used in each case (diblock copolymers varied according to table 3.1). To suppress cell binding to the areas between the Au dots, these regions were passivated by polyethylene glycol (PEG).

Particle distance [nm]	**Polymer*** PS(x)-b-P2VP(y)
30 - 45	240 - b - 143
90 - 120	1056 - b - 495

Table 3.1: Table of used diplock copolymers to gain different gold particle distances on the surface.(*): x and y give the numbers of theoretical repeat units as calculated by the initial monomer/initiator feed ratio.

3.2.1 Passivation of the surfaces with polyethylene glycol (PEG2000)

Polyethylene glycol (PEG) based substrates are widely used as biologically inert interfaces due to the fact that they repeal protein absorption [52, 214]. Glass samples with gold nanostructure were pre-activated in an O_2-plasma machine for 2 min at a pressure of 0.4 mbar at 150 Watt. All flasks were cleaned with permonosulfuric acid called Piranha

(4 : 1 of $H_2SO_4 : H_2O_2$), rinsed with Millipore water, and treated with ultrasound. In order to avoid the presence of undesired H_2O in the process, the toluene p.a. was dried over a molecular sieve and stored under nitrogen. The plasma treated substrates were then transferred into a nitrogen filled flask and filled with 10 ml dried toluene. A small amount of PEG was added to the toluene under nitrogen, as well as a drop of triethylamine. The flask was then heated to 80 °C. After 24 hours the substrates are intensively rinsed with ethyl acetate and methanol and blow-dried with nitrogen.

3.3 Surface biofunctionalization

The gold dots produced under the conditions chosen for this study have approximately a diameter of 8 nm, providing anchor points to which only single integrin molecules can bind, because the diameter of integrins in the cell membrane is between 8 and 12 nm [220, 221, 53]. Given that each nanodot can anchor only a single linker molecule, a uniform patterning of extensive substrate areas produced by the tuneable self-organization of diblock copolymers [156, 144, 17] can provide an accurate control of inter-ligand lateral spacing, which is essential for cell adhesion. To serve as specific ECM-mimetic structures, Au dots are biofunctionalized with ^{TM}c(RGDfK)-thiols (the cyclic peptide linked via the spacer aminohexanoic acid to mercaptopropione acid) or REDV-peptides or with VE-cadherins [160, 77].

3.3.1 Biofunctionalization with cyclic RGD-Thiol

For binding the RGD motif to the gold nanostructure, a peptide with RGD-motif and thiol-groups was used as described in [160, 77]. Thiols can form a stable binding to gold (Lewis base and acid). After the PEG passivation, substrates were incubated for 2 hours at room temperature with 20 μl of 25 μM RGD-thiol-solution. After that, the substrates were incubated with Millipore water over night. Finally, the samples were washed several times in PBS-buffer and prepared in cell dishes for the cell experiments.

3.3.2 Biofunctionalization with REDV

The herein used REDV peptide (American Peptide Company Inc., USA) exhibits no thiol groups, which made the binding to gold more elaborate. It is performed by a carbonic acid, which has S-S-groups. Since carbonic acid is extremely sensitive to hydrolysis, it is previouslydissolved in acetonitrile and then the sample is incubated in this solution for 30 min. After that the substrate is washed with acetonitrile and blow-dried in a steam of nitrogen. Then it is incubated for 1 hour with 20 μl of a 5 mM REDV-solution, and left over night in Millipore water. For cell experiment preparation it is washed with PBS.

3.3.3 Biofunctionalization with VE-Cadherins

Each sample was incubated at 48 °C over night with 20 μl of 100 μM nitrilotriacetic acid (NTA)-ethanol solution. Subsequently it was washed 20 min in Millipore water and 20 min in HBS-buffer. Then the substrate was incubated for 15 min at room temperature with 10 mM nickel(II)-chloride-solution. After repeated washing with HBS, the protein can be bound to gold without disturbing the proteins activity. The sample is incubated

over night with 30 μl of an aqueous 20 μM VE-cadherin-solution (Recombinant Human VE-Cadherin/Fc Chimera, R&D Systemy, Inc.), and 2 mM Ca^{2+} concentration. After 3 washing repetitions with HBS, the sample can be prepared for the cell experiments.

3.4 Mechanical stretch

The here applied mechanical force is cyclic strain, executed by a stretching device built in our labs by Simon Jungbauer [92].

Cell stretching device and experiment The customized stretching device applied a periodical mechanical strain to an elastomeric membrane which served as cell culture substrate [93]. The stretching device was mounted on a motorized inverted light microscope (Axiovert 200M, 10x/0.25 Ph1 objective, Zeiss, Germany) equipped with a CCD-camera (PCO Sensicam, Germany) and an environmental chamber to control the temperature and the CO_2 concentration of the atmosphere. In each experiment a stretching frequency of 0.01, 0.1 or 1 Hz, was selected. The stretching amplitude was 8% for all experiments. Phase contrast images were acquired in the non-strained position at intervals of 100 sec. Each image was focused before acquisition by a software-based auto focusing routine. The cells were plated on a 20×20 mm poly(dimethylsiloxane) (PDMS, Corning Sylgard 184, USA) membrane with an elastic modulus of approximately 1 MPa. The suitability of PDMS dishes for cell culture was previously shown for example by Neidlinger-Wilke [149], Lee [117], and Jungbauer [93]. Before cell seeding, the stretching chambers were sterilized with ethanol and rinsed several times with phosphate buffered saline (PBS), and coated by incubation ($12-14$ hours) with a 20 μg/ml fibronectin solution overnight (Sigma, Germany), then again washed with PBS.

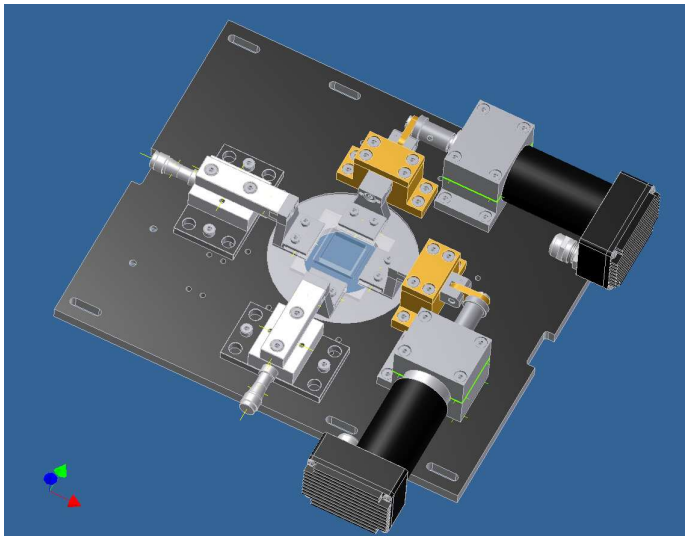

Figure 3.3: AutoCad drawing of the stretch device, which is put on top of a microscope to observe cells during application of frequent stretch; kindly provided by Martin Deibler.

Cells were cultured and prepared like in appendix 3.1. To avoid bacteria contamination, 100 units/ml of penicillin-streptomycin (Gibco, Germany) was added to the medium. After

cell seeding, the culture dishes were placed in a cell culture incubator (37 °C, 5% CO_2, high humidity) for 24 h before they were mounted on the stretching setup. After the experiments, cells were fixed and stained as described in appendix 3.3. Fluorescence images were acquired by an AxioImager microscope (Zeiss, Germany) with a 63x water-immersion objective. Images of each z-stack were merged to a single image (extended depth focus, Zeiss). The analysis of the actin stress fibers and the focal adhesions is explained in appendix 3.4.

3.5 Electrical field

Direct current and extremely low frequency pulsed electrical fields (dcEFs and ELFP-EFs) were applied within 24 hours after the cells were seeded correspondingly to appendix 3.1. Agar-salt bridges not less than 15 cm long were used to connect silver/silver chloride electrodes in beakers of phosphate buffered solution (PBS, Gibco, USA) to pools of excess culture medium at either side of the chamber. This prevents diffusion of electrode products into the cultures (see figure 3.4). Field strengths were measured during the whole observation period with two platin electrodes at two sides of the chamber. Only few fluctuations in field strength were observed (see figure 9.2 in chapter 9). ELFP-EFs were generated by using a controlled switch-device attached to the feed cables between the direct current generator and the electrodes. The pulse duration of the applied field was 1sec, the time between pulses varied from 2 to 16 sec, consequently the pulse dose (pulses per minute, PpM) differed as well.

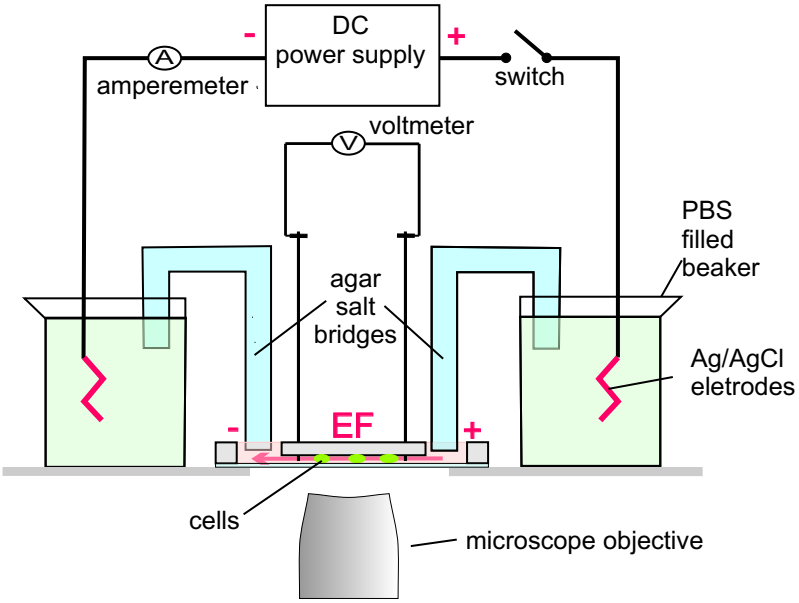

Figure 3.4: Schematic representation of the electrical field setup with cell chamber on top of a microscope (here only a microscope objective is shown).

The protocols used are based on those pioneered and used by a handful of laboratories to apply electrical fields to cells *in vitro* [157, 228, 145, 54, 150, 34] and to calculate the relevant bioelectrical properties of the system. We have modified and used electrotactic chambers cast of PDMS on top of a thin glass plate to accommodate cells growing in planar

culture (figure 3.5). The glass subtrate was immersed with 10 μg/ml fibronectin solution (Sigma, Germany) 24 h before seeding the cells. For observation of the cells, the setup was put on a microscope (CK40, Olympus, Germany) with phase contrast objectives (4× or 10× magnification) and an attached CCD-camera (CS8420Ci, Imaging Development Systems, Germany), which images the cells every 5 to 10 minutes, controlled by NIH image software for Macintosh. The cells viability could be maintained placing an incubator around the microscope with an additional humidity and 5% CO_2 supply, at a temperature of 37°C. For those experiments cell medium containing 5% FBS and 100 units/ml of penicillin-streptomycin (Gibco, Germany) was used to diminish the risk of bacterial contamination during the experiments.

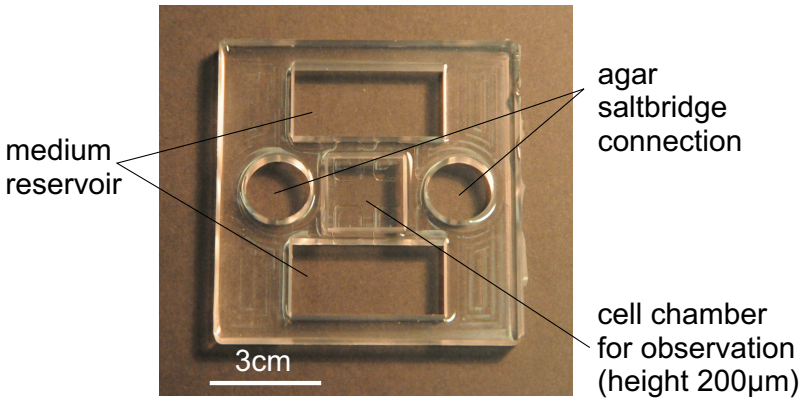

Figure 3.5: Example of a PDMS-chamber designed for the observation of cells in an electrical field (EF). The EF is apllied via agar salt bridges; connections are indicated in the image. The cell observation chamber is connected via channels to medium reservoirs.

4 Methods of characterization

4.1 Scanning electron microscopy

Substrates decorated with gold nano structures (see 3.2) were characterized with scanning electron microscopy (SEM) in order to verify the correct distance of the gold dots. Electron microscopes work comparable to light microscopes, but using fast electrons instead of light. They allow examination of samples below the resolution of light microscope down to $\approx 1.3{\cdot}10^{-10}$m due to the shorter wavelength of the e-beam. The electrons are focused in a thin beam with the help of electric and magnetic fields (so called projection lenses). With the electron beam the sample is scanned point by point and the signal is captured by a detector. Various signals arising from the interaction of the electrons with the sample are used to obtain information about structure, morphology and composition. Mainly, three different types of emission are caused by the incident electron beam: Firstly, the beam ionizes atoms in the sample and the so-called secondary electrons (SE) are emitted. Secondly, ionisation of the atoms and deceleration of the electron beam produces X-rays. Furthermore, some of the electrons of the scanning beam are backscattered (BSE). The SEM-detector for the SE, collects electrons for each point, and their signal is then recomposed to produce an image. With the backscatter detector different sample-materials can be distinguished, because elements with heavy nuclei reflect more electrons than lighter elements (called atomic number (Z) contrast) [137].

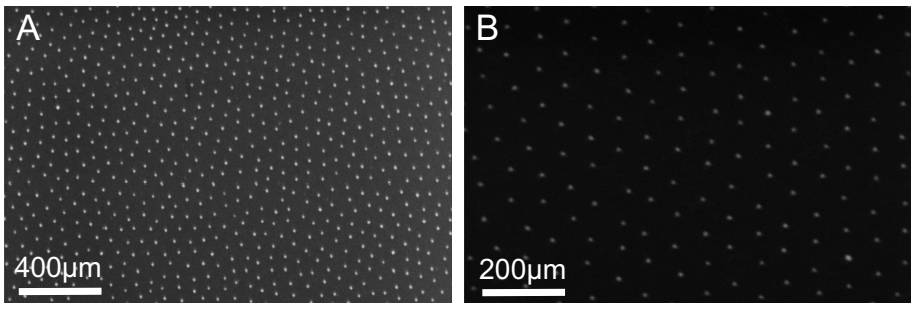

Figure 4.1: Example SEM micrographs of glas slides decorated with gold nano dots.

The electron lenses made of electric and magnetic fields can have lens errors similar to optical lenses. For example spherical aberration is more important for a good resolution and a big magnification as the theoretical limit of diffraction. The latter is defined by the de-Broglie-wavelenth λ of the electron. $\lambda = \frac{h}{\sqrt{2em_0U}} = \frac{h}{p}$ (with Plancks constant h, the elementary charge e, the rest mass m_0 and the momentum p of the electron, as well as the accelerating voltage U) is in the order of magnitude of an atomic radius, when

electrons are accelerated to 0.1 kV [137]. Therefore, the limiting factor of the resolution is the accelerating voltage U, because electron rest mass and charge are constant. In figure 4.1 example SEM images of gold nano dots on glass are depicted.

4.2 Light microscopy

Light microscopy was an essential tool for this thesis, especially for the research with biological cells. The main reasons for this are the properties of the cells, such as their size ($\approx 50\,\mu$m lenght), their complex substructure and their in princple colorless and translucent cytosome. However, with common and modern methods, it is possible to make cells and their internal features visible [1].
In a microscope the effects of two lens systems are multiplied [137]. The total magnification of the microscope v_M can be calculated by multiplying the reproduction scale, $\beta = \frac{t}{f_1}$, of the objective with the magnification of the magnifying glass of the eyepeace, $v_o = \frac{s_0}{f_2}$, ($s_0 \approx 25\,$cm for the human eye): $v_M = \beta v_o$, see [137]. In the microscopes used for this thesis (Zeiss AxioImager, Zeiss AxioVert200, Olympus CK40) objectives were used with correction for spherical and chromatic aberration, typical lens errors. The correction of objectives is mainly achieved by a complex lens system of up to 10 lenses out of different kinds of glass. One distinguishs between 'dry' and immersion systems. The latter can amplify the numerical aperature, and thus, the resolution of an objective by increasing the aperature angle of the optical system [137].
A fundamental limtation of all microscopes (exeption for special cases: 4π and STED microscopy [176]) is that a given type of radiation cannot be used to probe structural details much smaller than its own wavelength. The ultimate limit of resolution of a light microscope is therefore set by the wavelength of visible light, which ranges from about $0.4\,\mu$m (for violet) to $0.7\,\mu$m (for deep red). In practical terms, bacteria and mitochondria, which are about 500 nm wide, are generally the smallest objects whose shape we can clearly discern in the light microscope [1]. Another typical limitation of microscopy, especially for biological samples, is the contrast. Fortunately, most specimens have structural details with different refractive indices, which can be used in phase contrast microscopy. Another possibility to increase the contrast is to stain specific structural features of the specimen.

4.2.1 Phase contrast microscopy for cell phenotype analysis

Phase contrast microscopy is used to visualize the mostly transparent cells. With the help of this technique, the varying refractive index within one cell is used to enhance the contrast inside of a cell. The principle is called amplitude modulation of the transmitted light. A transparent object e.g. a cell, hardly modulates the transmitted light. Staining would increase the amplitude modulation, but is often limited, especially for observation of living cells for a longer period. However, cells have a different refractive index n than their surrounding and thus, they can change the phase of the tranmitted light wave. A spacial phase modulation is obtained, not a temporal modulation. This implies for monochromatic observation the transmission of one carrier wave and its side bands. With additonal optics carrier wave and side bands are seperated. One of them is delayed for $\frac{\pi}{2}$ with the help of a quarter-wave-plate. After overlap of the two signals, an amplitude modulation and thus, a brightness contrast is gained.

4.2.2 Fluorescence for internal cell structure analysis

Fluorescence microscopy requires fluorescent objects of interest. The emission of shorter wavelength light that occurs shortly (nanosecond range) after the absorption of longer wavelength light is called fluorescence. The critical property is the difference between the exciting and emitted wavelengths, known as 'Stokes shift'. To observe the fluorescent objects, the exciting light has to be filtered out completely without blocking the emitted fluorescence [1, 121]. Molecules that can be used for fluorescence observation are called fluorophores. There are several systems developed for labeling biological specimen, live cell staining or anti-immuno staining amongst others. The here used approaches are described in detail in appendix 3.
In a fluorescence microscope the fluorescent specimen is illuminated by one wavelength and the return light is filtered to only obtain the emitted longer wavelength. In this thesis microscopes with epi-illumination (Zeiss AxioImager, Zeiss AxioVert200) were used. In this configuration the microscope objective not only has the role of imaging, but also serves as the condenser that illuminates the specimen. This requires a special kind of beam splitter in the light path of the microscope. A dichroic mirror is utilized to seperate the excitation from the emission. The beamsplitter is used in combination with two filters: the excitation filter, which preselects the exciting wavelengths, and the barrier filter that only allows the longer wavelength to transmit back to the detector [121]. The filter sets used in this thesis were from Zeiss (Germany) or AHF (Germany).

4.3 Data aquisition and processing

Data are aquired analyzing the images of the cells obtained with a CCD camera attached to a microscope, on which the experimental setup is build. To obtain details about several cell responses, different aspects of the cell morphology were analyzed, described in the following paragraphs.

Cell orientation Microscopy images were analyzed using the software ImageJ [165]. For the investigation of the cell orientation the outline of each cell was marked, and an ellipse was fitted to the cell outline, see figure 4.2A.
Thereafter, the angle φ between the major ellipse axis and signal direction (e.g. surface grooves, mechanical stretch, electrical field) was measured. For the controls the angle between major ellipse axis and the image x-axis was measured. The orientation of the cells along the grooves was quantified by the non-polar order parameter, S [106]:

$$S = \langle \cos 2\varphi \rangle = \int f(\varphi) \cos 2\varphi d\varphi \tag{4.1}$$

It follows from the above definition that $S = 0$ if the cells are randomly orientated, $S = 1$ if they are aligned with the signal direction, and $S = -1$ if they are oriented perpendicular to the signal direction.
The orientation angles, φ, are collected in a histogram and the desired angle distribution function, $f(\varphi)$, is obtained after normalization ($\int f(\varphi)d\varphi = 1$).

Cell elongation The elongation, E, was calculated using the lengths of the major (A_{maj}) and minor axes (A_{min}) of the fitted ellipse (figure 4.2A):

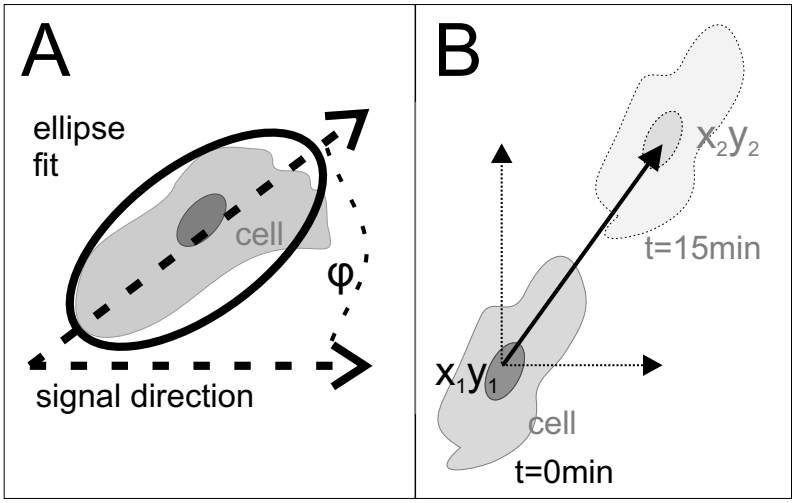

Figure 4.2: A: Schematic representation of the orientation angle φ between the signal direction and the major axis of a cell determined by fitting an ellipse to the cells outer boundary. B: Schematic view of the coordinate and vector definition for the quantification of directed cell migration.

$$E = \frac{(A_{maj} - A_{min})}{(A_{maj} + A_{min})} \tag{4.2}$$

For $E = 0$ the cell shape would be a perfect circle and for $E = 1$ the cell shape would be a thin line.

Directed migration Directional migration was assessed from time-lapse movies using ImageJ software and with the help of the Manual Tracking Plug-in [166]. Directed migration was described by the step direction and step length between every image. The values x_i and y_i are calculated using the coordinates at the center of every tracked cell. The distance traveled by the cell center is measured, as described in figure 4.2B, after every time interval. The index indicates the time steps from 1 to n, where n is the last imaged step of one cell.

For the study described in chapter 6 directed migration was described by the step direction and step length between every image (15 min) and the here defined migration indices M_x and M_y (euqation 4.3 were calculated for each cell as the net movement along the x- and y-direction, respectively (x-axis in direction of the grooves):

$$M_x = \sqrt{x_1^2 + x_2^2 + ...x_n^2}, \quad M_y = \sqrt{y_1^2 + y_2^2 + ...y_n^2} \tag{4.3}$$

In analogy to the chemotactic index [64] the directionality of the migration was quantified by dividing M_y by M_x. This simple parameter is easy to interpret since for $M_y/M_x = 1$ the cells perform a perfect random walk, for $M_y/M_x < 1$ cells migrate preferably along the grooves, and for $M_y/M_x > 1$ they preferentially migrate orthogonal to the grooves.

Directed migration and polar order parameter For further analysis of the directed cell migration, the polar order parameter P was calculated from the measured coordinates as

follows [74] :

$$P = \langle \cos\varphi \rangle = \int g(\varphi) \cos\varphi d\varphi \tag{4.4}$$

It follows from the above definition that $P = 0$ if the cells walk in a random manner, $P = 1$ if they migrate in direction of the positive x-direction (here always signal direction), and $P = -1$ if they migrate in negative x-direction . The orientation angles, φ, are collected in a histogram and the desired angle distribution function, $g(\varphi)$, is obtained after normalization ($\int g(\varphi)d\varphi = 1$). For migration in y-direction (orthogonal to the signal) P becomes also 0, that is way directed migration perpendicular to the applied guiding field is analysed with the described apolar order parameter S, see above.

4.4 Controller model

Phenomena like directed cell migration and cell orientation have different levels of understanding. On the molecular level, research tries to understand the complex machinery and pathways of signal trandsduction that lead to cellular reactions. On the macroscopic or phenomenological level one is just interested in the type of machine involved. The information flux diagram of an automatic controller (see figure 4.3) characterizes the machine on the macroscopic level. The block diagram can be understood without knowing details of the machine. In biological systems the details of the machine are based on chemical reactions and the machine properties can be determined by an input-output analysis [72, 108], which is described in this section. The hallmarks of automatic control are first an element that measures the cellular output, second, a means of feeding back this information into the input in such a way to minimize the deviation of the output from the desired level (set point) (figure 4.3). Such a regulating mechanism is important for many cell functions like cell migration and orientation.

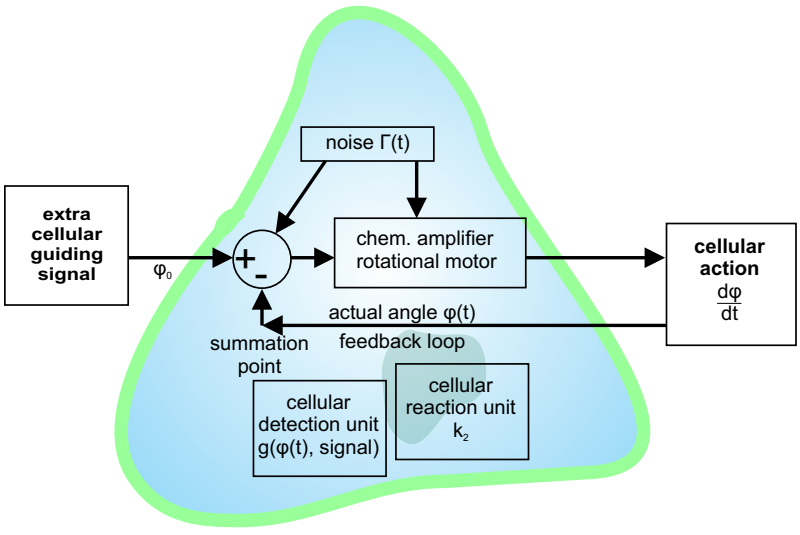

Figure 4.3: Schematic representation of an intracellular automatic controller, with ingoing signals and a measurable response.

The here controlled variable is the angle of orientation, φ towards the direction of the

external guiding signal. Observations in several studies made clear, that the cell must have a means for measuring its actual angle of orientation in respect to the applied extracellular guiding signal [54, 74, 93]. The cellular detection unit acts in addition as a feedback element. In the summation point, the actual angle of orientation, φ, is subtracted from the desired one, φ_0. The angle-dependence and field-dependence of the detection unit will be described by the unknown function $g(\varphi, signal)$ and the strength of the reaction unit by the coefficient k_2. The temporal change of the angle of orientation, $d\varphi/dt$, quantifies the reaction of the cellular automation. Combining these consideration, the predicted machine equation for one cell is:

$$\frac{d\varphi}{dt} = -k_2 g(\varphi, signal) + \Gamma(t) \tag{4.5}$$

This stochastic differential equation ('Langevin equation') describes basically the cellular response. The first term on the right side (deterministic signal) describes the cellular response to an extracellular guiding signal. The second term (stochastic signal $\Gamma(t)$) has to be introduced since random orientation is observed in case of no guiding signal. The unknown detection unit characteristics, $g(\varphi, signal)$, is derived from the symmetry properties of the machine: (1) An apolar symmetry is assumed for the analysis of cell orientation (for the differences in case of directed cell migration see below). It means that the cells cannot register the sign of the guiding field. (2) A mirror symmetry is assumed. This means that the cells cannot distinguish between left and right. The proposed detection characteristics is then, with even n (see appendix 3.5):

$$g(\varphi, signal) = b_0 + (signal)^n sin(2\varphi) + ... \tag{4.6}$$

To proceed further, one has to know some properties of the stochastic signal, Γ. First, its average is zero ($[\Gamma] = 0$). Second, a white noise source is assumed. Its autocorrelation is

$$[\Gamma(t)\Gamma(t')] = q\delta(t - t') \tag{4.7}$$

where q describes the strength of the stochastic signal and $\delta(t-t')$ is Dirac's delta-function. Because of the stochastic properties, the angle of orientation cannot be predicted except by statistical properties. The probability that the angle of orientation falls between φ and $\varphi + \Delta\varphi$ is described by the angle distribution function $f(\varphi)$. The motion equation of the angle distribution function $f(\varphi, t)$ can be obtained from the above derived Langevin equation 4.5. The result is the following, called 'Fokker-Planck equation':

$$\frac{\partial f(\varphi, t)}{\partial t} = \frac{\partial}{\partial \varphi}\left[k_2 g(\varphi, signal) + \frac{q}{2}\frac{\partial}{\partial \varphi}\right] f(\varphi, t) \tag{4.8}$$

This equation is essential since it connects the model predictions with the experiments. In the experiments described in this thesis not only one cell is observed, but several on the same time. Therefore, reliable statements about the cellular reactions can only be given by analysing the distribution function of all cells. The general mathematical procedure for solving the 'Fokker-Planck equation' is given in [174] and [175]. The steady-state angle distribution function has one important predicted result:

$$f(\varphi) = f_0 exp\left[\frac{k_2}{q}(signal)^n \cos(2\varphi) + ...\right] \tag{4.9}$$

where f_0 is determined by the normalization ($\int f(\varphi)d\varphi = 1$). It is assumed that the first nontrivial term in $g(\varphi)$ describes basically the alignment properties of the cell. The sign of the machine coefficient, k_2, determines the set point of the automatic controller: The distribution function is maximum at $\varphi = 0°$ and minimum at $\varphi = \pm 90\,°$ for $(k_2(signal)^n)/q > 0$. In this case the set point is $\varphi_0 = 0°$, but for $(k_2(signal)^n]/q < 0$, the distribution function reaches its maximum at $\varphi = \pm 90\,°$ and its minimum at $\varphi = 0\,°$ and hence the set point, φ_0, is $\pm 90\,°$.

Existence of an automatic controller The existence of a cellular automatic controller for cell orientation can be shown in the following way: a cell, having an automatic controller, will change its alignment if the guiding signal is altered. Therefore, signal-jump experiments should be performed: For $t < 0$ no guiding signal is applied and the cells orient randomly (apolar order parameter $\langle\cos(2\varphi)\rangle = 0$; see chapters 8 and 9). Then, at time $t = 0$ an extracellular guiding signal e.g. uniaxial mechanical strech or an electric field, is switched on. The cells react and align their long axis with respect to the applied guiding signal ($\langle\cos(2\varphi)\rangle \neq 0$). The apolar order parameter decreases in time and approaches a new saturation value. Technical details of the controller can be found in appendix 4.4.

Signal strength characteristics The signal-strength characteristics, $g(signal)$, of the cellular detection unit is again predicted by using the symmetry properties of the cells. This characteristic is basically described by the first nontrivial term: $(signal)^2$. The signal-strength characteristic can be determined by investigating the angle distribution function at different signal strengths after the cellular orientation reached its maximum. Again a plot of the logarithm of the experimentally determined angle distribution function $f(\varphi, t = const)$ is plotted vs $\cos(2\varphi)$ and the slope, $\alpha_2 = \frac{k_2}{q}(signal)^2$, of the straight line is determined. This procedure is repeated for different signal strengths. A plot of the measured slope, α_2, versus the applied signal strength yields the desired characteristics of the detection unit. A parabolic characteristics is obtained for cells in an electrical field, see chapter 9:

$$\alpha_2 = (K_G^E E)^2 \tag{4.10}$$

where the electric guidance coefficient, K_G^E, characterizes the electric field sensitivity. The electric guidance coefficient is an imaginary number since the desired orientation angle (set point) is perpendicular to the direction of the guiding signal.

Steady-state dose-response curve The steady-state dose-response curve is of great physiological importance, since it describes the mean orientation as a function of the applied guiding signal. A dimensionless representation is possible: (1) The extracellular guiding signal is the dose. It is a dimensionless quantity if the applied guiding signal is multiplied by the appropriate guidance coefficient: $K_G^E E$. (2) The cellular response is quantified by the dimensionless apolar order parameter, $\langle\cos(2\varphi)\rangle$. In an according plot the resulting line is a theoretical prediction (appendix 4.4) based on the symmetry properties of the detection unit. This steady state dose-response curve is not dependent on the investigated cell type or the kind of guiding signal, as long as the symmetry requirements of the detection unit are fulfilled. Thus, the theoretical prediction should hold for different cell types and different types of guiding fields.

Apolar order parameter The apolar order can be predicted by taking only the first nontrivial term of $g(\varphi, signal)$. The apolar order parameter is the ratio of two hyperbolic Bessel functions

$$\langle \cos(2\varphi) \rangle = \frac{I_1(\alpha_2)}{I_0(\alpha_2)} \tag{4.11}$$

The argument, α_2, of the Bessel functions is the ratio of the deterministic part of the cellular signal chain, $k_2 b_2(signal)$, and of the stochastic part of the cellular signal chain, q.

Temporal behavior of the controller The stochastic source strength, q, can be determined from signal-jump experiments. At first, no guiding signal is applied and the apolar order parameter is zero. Then at $t = 0$, a guiding signal is switched on and the apolar order parameter decreases in time until the saturation value, $\langle \cos(2\varphi) \rangle^{st}$, is reached. The temporal response can be described by a single exponential function with the characteristic time τ_2

$$\langle \cos(2\varphi) \rangle = \langle \cos(2\varphi) \rangle^{st} (1 - exp(-t - t_0)/\tau_2)) \tag{4.12}$$

This function fits the experimental data, which can be seen in chapters 8 and 9. The characteristic time, τ_2, the lag-time, t_0, and the steady state apolar order parameter, $\langle \cos(2\varphi) \rangle^{st}$, are fitting parameters. The characteristic time, τ_2, can be measured for different electric field strengths. When the inverse of the characteristic time, $\tau(E)$, is plotted versus the square of the applied guiding field, E, the experimental data can be compared with the predictions. The general mathematical procedure for solving the Fokker-Planck equation 4.8 is given in [175, 174]. A straight line is predicted if the deterministic signal is much larger than the stochastic one. This prediction is actually observed for large field strengths. The coefficient, k_2, which characterizes the reaction unit of the controller is given by the slope of this straight line. The strength of the stochastic source can be obtained from the intersection with the y-axis as q. A parabola is predicted if the stochastic signal is large compared with the deterministic one. The absolute value of the electric guidance coefficient, K_G^E, can be calculated by using the values, k_2 and q, see appendix 3.5.

Directed migration In the case of directed migration in direction of the guiding signal, the apolar order paramter $\langle \cos(2\varphi) \rangle$ cannot be used anymore fo analysis. As some cell types seem to be able to sense the sign of the guiding field (e.g. in the case of an applied electrical field), a polar order parameter describes the phenomenon better. In that case the terms with $\sin(\varphi)$ of the generalized guiding signal (eq. 4.6) cannot be neglected and the temporal behavior can be described with the following equation:

$$\langle \cos(\varphi) \rangle = \langle \cos(\varphi) \rangle^{st} (1 - exp(-t - t_0)/\tau_1)) \tag{4.13}$$

Characteristic parameters that describe the cellular migration controller response are equivalent to the description of the orientation controller, as described in [74].
Further statistical analysis (t-test and ANOVA) was performed using Microcal Origin 7.5 software.

Part III

Authentic stent surfaces

5 Cell adhesion, spreading and proliferation on stent surfaces

The current focus of stent (fig.5.1) design is to develop a coating that improves vascular tissue regeneration via increased endothelialization and diminished growth of smooth muscle cells and the following restenosis (see cshapter 1). In this chapter, the *in vitro* performance of authentic stents with various surface coatings is presented. This study was performed in cooperation with Boston Scientific, an established stent designer and producer. The intent was to investigate the effect that the different surface coatings had on adhesion, spreading and proliferation of vascular cells (endothelial, EC, and smooth muscle cells, SMCs).

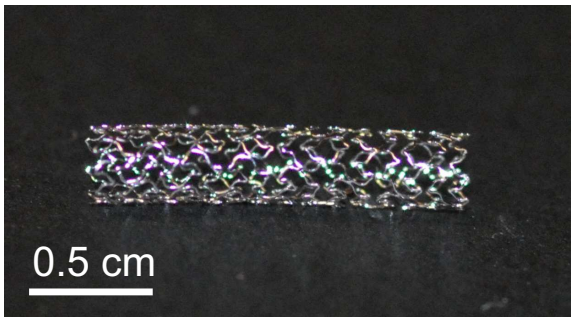

Figure 5.1: Example of an expanded stainless steel stent

Specifically, the investigations were divided as follows:

Observation of initial spreading characteristics and long term proliferation of human primary ECs and SMCs (from several donors) on test surfaces and stents.

Short (4 to 48 hours) and long term cell assays (3 up to 30 days) on flat test surfaes and stents.

EC monolayer formation on expanded, three dimensional stents.

5.1 Additional materials and methods

Stents and flat test samples with several coatings were produced, analyzed and delivered by Boston Scientific [173]. The coating materials were irdium-oxide (IrOxI - IrOxV), stainless steel (SS) or platinum-electropolished stainless steel (PSS). (See table 5.1 for a complete

description of the various configurations.) The five IrOx coatings varied in percentage of oxygen concentration and in surface structure. The dimensions of the surface structures were in the range of a few nanometers.

Sample type	Coating type	Abbrevation
flat test surface	irdidium-oxide	IrOxI
	irdidium-oxide	IrOxII
	irdidium-oxide	IrOxIII
	irdidium-oxide	IrOxIV
	stainless steel	SS
	platinum polished SS	PSS
stent	irdidium-oxide	IrOxI
	irdidium-oxide	IrOxII
	irdidium-oxide	IrOxIII
	irdidium-oxide	IrOxIV
	irdidium-oxide	IrOxV
	stainless steel	SS
	platinum polished SS	PSS

Table 5.1: Overview of coatings on flat test surfaces and stents

PDMS chambers were made to exactly fit the flat test samples. Thus, cell growth on any other surfac was prevented. The stents were fixed into small grooves in a PDMS chamber with KwikSil (World Precision Instruments) so they could not come loose during cell culture procedures (figure 5.2).

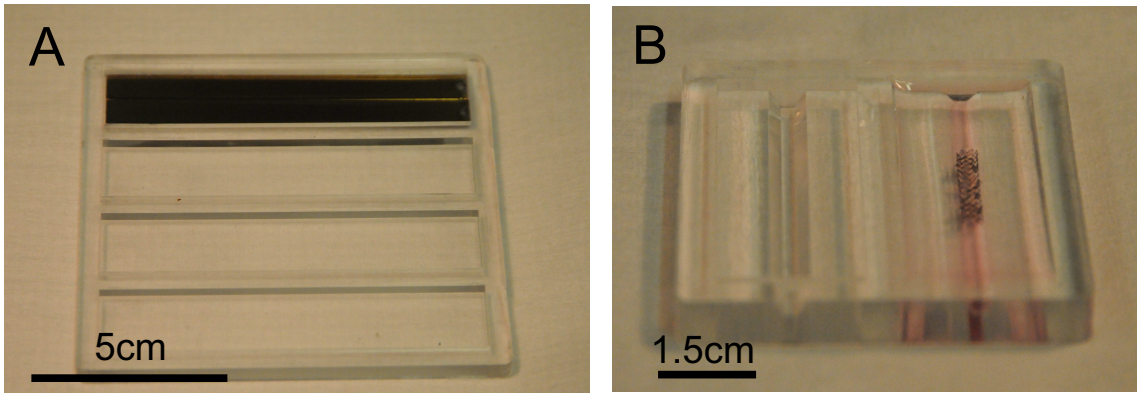

Figure 5.2: PDMS chambers for test strips (A) and stents (B). In A two test strips with IrOx coating are visible. In B a stent with IrOx coating is lying in one side of the chamber sourrounded by red cell medium.

One of the challenges that needed to be addressed in this study was the observation of cells on non-transparent surfaces. Upright fluorescence microscopy and z-stack image acquisition successfully diminshed the effort monitoring of the stained cells. In addition, stents are made of flexible materials [173, 101, 131], which take on different three-dimensional shapes. The observation method used here (fluorescence microscopy) is described in chapter 4.2 in detail. For the short-time assays, cells were fluorescently marked by live cell

staining (see appendix 3). Up to 20 images were taken at random locations on each substrate type for each cell-type to evaluate cell attachment and spreading area. The number of cells was counted after 4, 24 and 48 hours to calculate the cell density per area. For all of the long term cell assays immunostaining was used; ECs were stained with VE-cadherin antibodies, SMCs with α-actin antibodies (for details see appendix 3). Images were taken at eight different focus (z-) positions (see chapter 4.2). The mean values of cellular spreading area were normalized by that of the reference surface: stainless steel. Standard statistical analysis was performed using Microcal Origin 7.5 software. All cell experiments were repeated twice with cells from each donor.

5.2 Short and long term studies on flat model surfaces

5.2.1 Initial cell attachment, spreading and cell adhesion

Initial cell-surface contact, attachment, and adhesion are considered to be important parameters for further re-endothelialization of a stent surface. The first part of this study focused on the observation of initial seeding and adhesion of ECs and SMCs *in vitro* on flat model surfaces by live cell imaging. Cell density and cell area were evaluated for five of the coatings (see table 5.1).

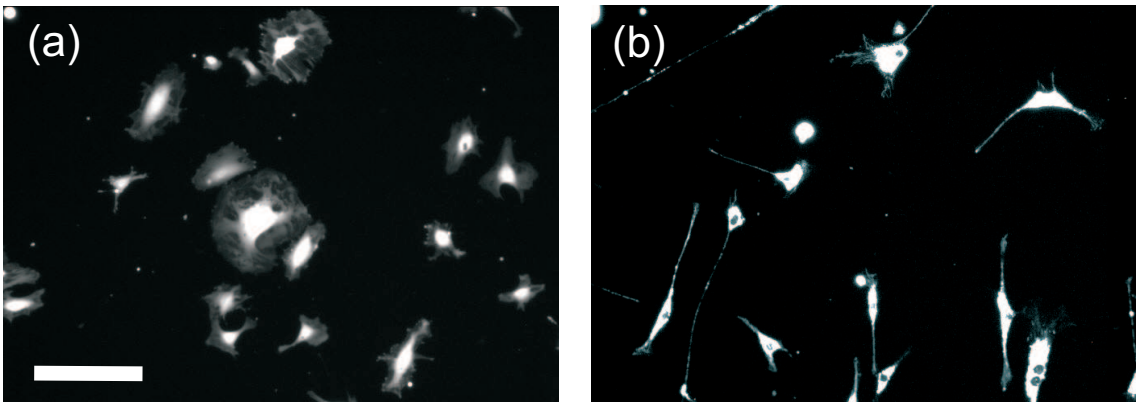

Figure 5.3: (a) Example fluorescence images of endothelial cells (ECs) (a) on SS, 4 h after seeding, and smooth muscle cells (SMCs) (b) on IrOxIV, 4*h* after seeding, both stained with live cell staining 3; the scalebar represents 200 μm.

Cell morphology In figure 5.3, fluorescently stained ECs and SMCs are depicted 4 h after seeding on two different substrates. ECs show typical spreading characteristics, comparable to those on petri dishes. They are mainly round shaped with pronounced lamellipodia. SMCs show their typical elongated shape with thin potrusions.

Cell density The cell density for each coating was measured for ECs and SMCs at 4, 24, and 48 h hours after cell seeding (figures 5.4 a and b). In the first 48 hours, proliferation of ECs was very low on all substrates, a characteristic of human primary endothelial cells under cell culture conditions. The only coating to cause any significant difference on EC behavior was the PSS: it decreased the density of adherent cells at all time points. In

contrast, the initial number of adhering SMCs was comparable on all surfaces (figure 5.4 b) and significant proliferation over the 48-hour-long experiment was measured.

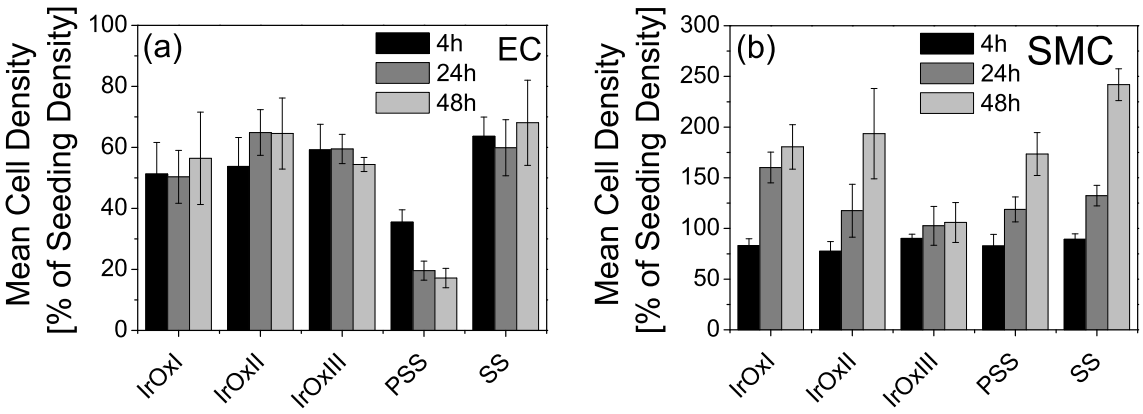

Figure 5.4: Mean cell density of endothelial (ECs) (a) and smooth muscle cells (SMCs) (b) at the 3 time points (4, 24, 48 hours) after cell seeding. Numbers are expressed as percent (%) of initial cell seeding (25 cells/mm^2). Error bars represent Standard Error, indicating intra-strip variability (two runs, two strips each)

5.2.2 Long term cell growth on flat model surfaces

To gather insights into woundhealing behavior of the two cell-types, the cells were monitored on flat surfaces of each coating for up to 30 days. Observable indications of good wound healing in this study included proliferation to confluence (monolayer formation) and mean cell area of ECs and SMCs on the surfaces.

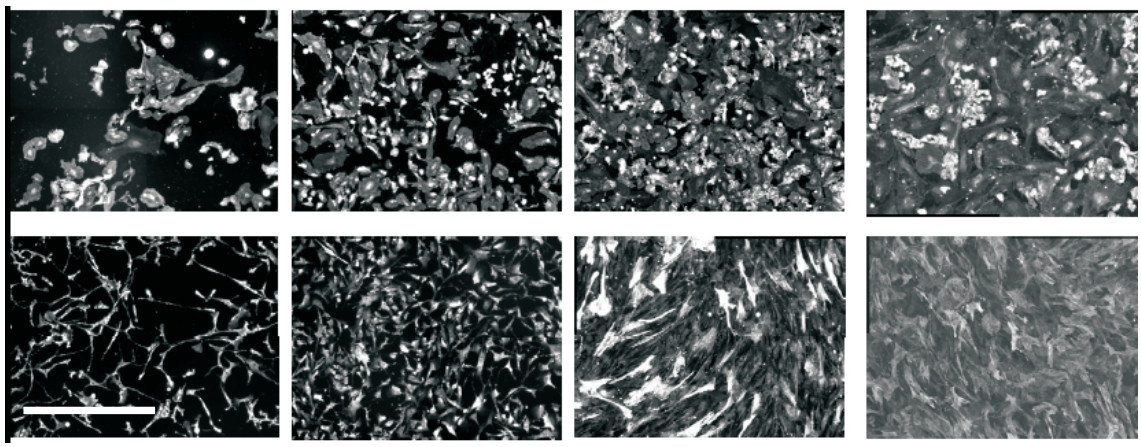

Figure 5.5: Endothelial (upper row) and smooth muscle cells (bottom row) 3, 7, 14 and 30 days after seeding on SS. The last images show a monolayer of ECs after 30 days, and multilayers of SMCs; the scalebar represents 800 μm.

Monolayer formation A typical sequence of images of ECs (top row) and SMCs (bottom row) on SS substrates for time periods of 3, 7, 14 and 30 days can be seen in Figure 5.5. Cells' proliferation and monolayer formation was remarkably good on IrOxIII and

SS coatings. At periods longer than 14 days, complete monolayers and even multilayers (SMCs only) could be observed on all coatings, except PSS. Therefore, only the cell area on images taken in the first 14 days were analyzed further.

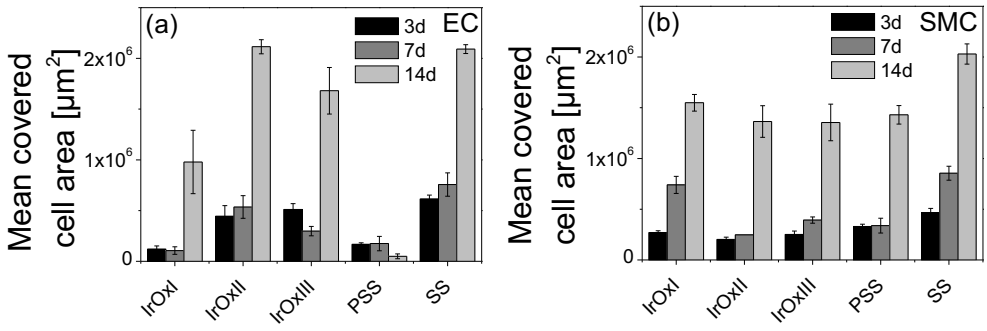

Figure 5.6: Mean of total covered cell area on test strips of endothelial (ECs) (a) and smooth muscle cells (SMCs) (b).

Cell area The analysis of the mean covered area with cells reveals a remarkable low growth of ECs on PSS (figure 5.6), but a very good proliferation on IrOxIII and SS. In figure 5.6 (b) it can be seen that SMCs grow in a very similar way on all substrates. As SMCs showed no remarkable decrease in viability on any of the substrates, further experiments focused on ECs. Further measurements with ECs of three different donors can be seen in appendix 4.1.

5.3 In vitro cell adhesion on stents

After initial studies on flat test surfaces, it was not clear, whether the same conclusions could be drawn for the cell growth on stents. Therefore, the long term tests with cells were also performed on authentic, expanded stents (see section 1.2.1 for a description of a stent). The stent samples contained a further coating called IrOxV. As SMCs proliferated well on all flat surfaces, the investigation on stents focused on ECs only. EC growth and monolyer formation and cell number per area on stents were observed after 14 days.

Monolayer formation In figure 5.7, an overlay of images of antibody-stained cells and nucleus staining (DAPI) is shown. On these images, the presence of VE-cadherins, which form cell-cell-junctions, is visible. (Another example of VE-cadherin staining is depicted in Appendix 4.1.) With the help of these images, the formation of a monolayer could be visualized on all surfaces. The further qualitative analysis of the substrate revealed less cell coverage of IrOxIV stents and partly also of PSS stents.

Cell number per area The DAPI stained cell nuclei were used to quantify the cell number per area on the stents (figure 5.8). The measurements on stents confirmed the results obtained on test strips. The ECs grew very well on IrOxIII stents. As on the test strips, the cell behavior did not differ much on the other IrOx surfaces from the SS. Only on

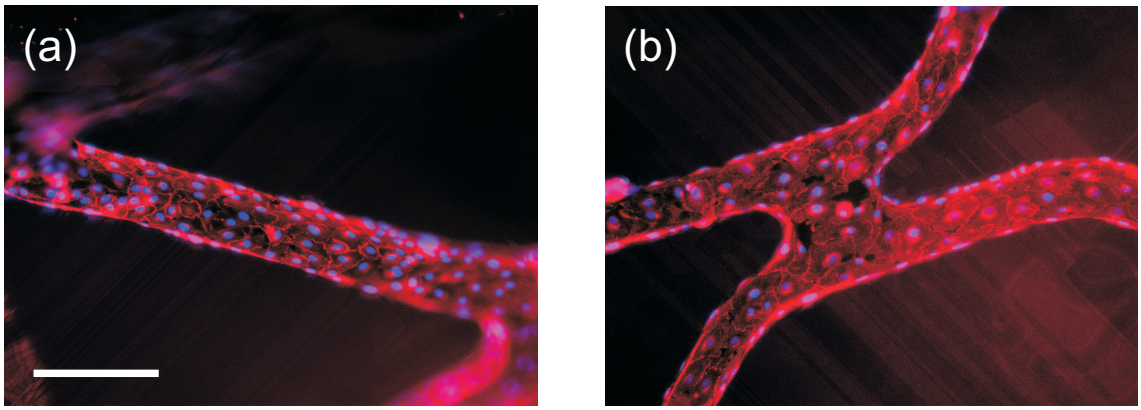

Figure 5.7: Endothelial cells after 14 days on a stent with (a) the IrOxIV-coating and (b) the SS-coating. Antibody staining with anti-VE-cadherin (red color) and DAPI-staining (blue nucleus) is visible; the scalebar represents 200 μm.

IrOxIV do the cells show less viability for all cell donors. PSS stents performed much better than PSS test strips. This gives hints that the coating of flat test strips cannot always be compared to stent coatings.

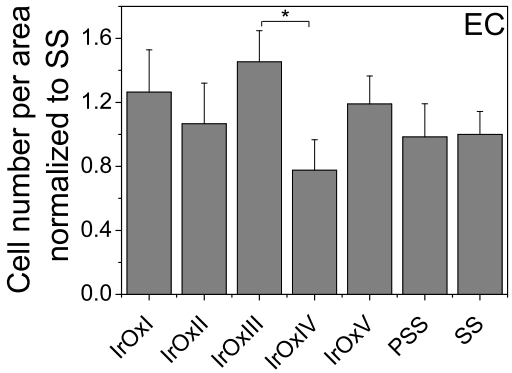

Figure 5.8: Endothelial cell number per area after cell growth on stent struts for 14 days; mean over all experiments. Only the values for IrOxIII and IrOxIV are significantly different (t-test).

5.4 Discussion and conclusions

Summarizing, the data suggest that initial endothelial and smooth muscle cell adhesion and long term behavior on all IrOx substrates are comparable to what is observed on stainless steel. The aim to test and compare cell spreading and proliferation on several different surfaces quantitatively and qualitatively was well achieved. Only the PSS coating partly reduces EC spreading on test strips, which was not observed on stents, giving hints that the preparation of PSS surfaces on stents might induce different characteristics than on flat test samples. In contrast to the behavior of the ECs, similar experiments conducted with SMCs show that this cell type is not as sensitive to the various surface

types when it comes to the initial adhesion and long term behavior. This reduced sensitivity to surface signals leads to the need to introduce further signals e.g. cell type specific drugs to stimulate a cell type specifically. Investigations of short-term adhesive events or long-term adhesion, proliferation and differentiation phases on various surfaces should be pursued. For example Anselme *et al.* used *in vitro* experiments to study the relation between surface properties of metallic materials and their biological activities and developed a statistical model approach [3].
All conclusions can only be drawn for the *in vitro* behavior of ECs and SMCs in culture, since operational, it is very challenging to mimic realistic *in vivo* conditions in the cultured cell assays. Long-term studies on stents reveal a good formation of monolayer in the 3-D environment. In attempt to enhance the *in vivo*-like conditions *in vitro*, cell's behavior could be observed under flow conditions. Given that ECs and SMCs are in contact with blood flow *in vivo*, one could imitate these conditions to gain more holistic information [170].
Furthermore, the exact topological and chemical differences between the various surface coatings could not be determined accurately with the methods currently available. However, it is known that the surface structures of the coatings are on the same order of magnitude as the dimensions of the membrane proteins (nanometer-scale) and cells are known to react to varying nano-topographies [4]. Dalby *et al.* stimulated mesenchymal stem cells to produce bone mineral *in vitro* by disorder of surface topography on the nanometer scale [41]. Additionally, even smallest differences in the chemical composition of a surface may produce local ion distributions that could cause ion channels of a cell to reverse their polarity and respond, thus starting an internal signaling event [33]. Therefore, by analyzing a reasonable amount of images per test sample, differences of cell behavior on the different nanoscale topographies could be gained.
In further studies, a systematic variation of selected surface parameters like surface roughness would be interesting. The influence of either chemistry and/or physical topography on cell functions could be distinguished and direct conclusions about the cell reactions could be drawn, as shown in [41, 201, 94]. That would allow to keep all except one of the surface parameters constant. This could partially be achieved in the studies described in chapter 6 and chapter 7.
The studies of authentic stents and the occurring difficulties in understanding why cells behave differently on one surface rather than on another, made me realise that the topic of implant technology and the interface of materials with blood, extra cellular matrix and cells, is a very complex one. My motivation for further experiments was to simplify the system of cells and their surroundings. The idea was to study singled out influences on the cell that can be precisely controlled. In the following chapters of this thesis, studies about changing single parameters like topography, surface chemistry and external fields are presented.

Part IV

Extracellular signals

6 Vascular cells on nano-micro topographies

After the study with authentic stents, their complex diversity in surface chemistry and topography, the following chapter focusses on a survey of pure topographic stimuli towards cells.
In order to increase the chance of appropriate healing, current research on coronary implants seeks to gain a deeper understanding of the response and function of fibroblasts, endothelial and smooth muscle cells (FCs, EC, and SMCs) and their interaction with the stent surface, see part I, sections 1.2.1 and 2.1.1.
In the following chapter the alignment and migration of cultured human FCs, human ECs, and human SMCs exposed to chemically identical, defined grooved surface topographies with sub-cellular nano-micro dimensions were systematically examined. The cells responded to this input signal by alignment parallel to the grooves. This cell response and the directed migration are quantified in order to elucidate possible differences between the three cell types. The results of this chapter are accepted for publication in the Journal *Acta Biomaterialia*.

6.1 Different sensitivity of human endothelial cells, smooth muscle cells, and fibroblasts to topography in the nano-micro ranges

In this study migration and alignment of human FCs, ECs and SMCs (see appendix 3)with respect to surface structures with sub-celluar dimensions (3 different depths: 50, 100, 200 nm; and 4 different widths: 2, 3, 5 and 10 μm, see section 3.1) were analyzed. Images of cells on the PDMS substrates were taken 24 hours after seeding and analyzed for orientation and elongation, see section 4.3.
In figure 6.1 phase contrast micrographs of FCs, ECs, and SMCs demonstrate cell shape and alignment of the three cell types cultured on the micro-structured surfaces. A significant alignment along the grooves is visible for all cells, in particular for the small spacing (2 μm) of the grooves with a depth of 200 nm (fig. 6.1 A, C, E). Cells are much less aligned along the grooves for the case of 10 μm spacing (fig. 6.1 B, D, F). Quantification of alignment and cell shape was done for more than 100 cells per experiment and results for the order parameter, S, and elongation, E, are given in figure 6.2.
The order parameter increases with decreasing groove width and increasing groove depth. This observation holds true for all three cell types demonstrating an increased sensitivity of the cells to increasing depth of the topography. For non-structured surfaces the order

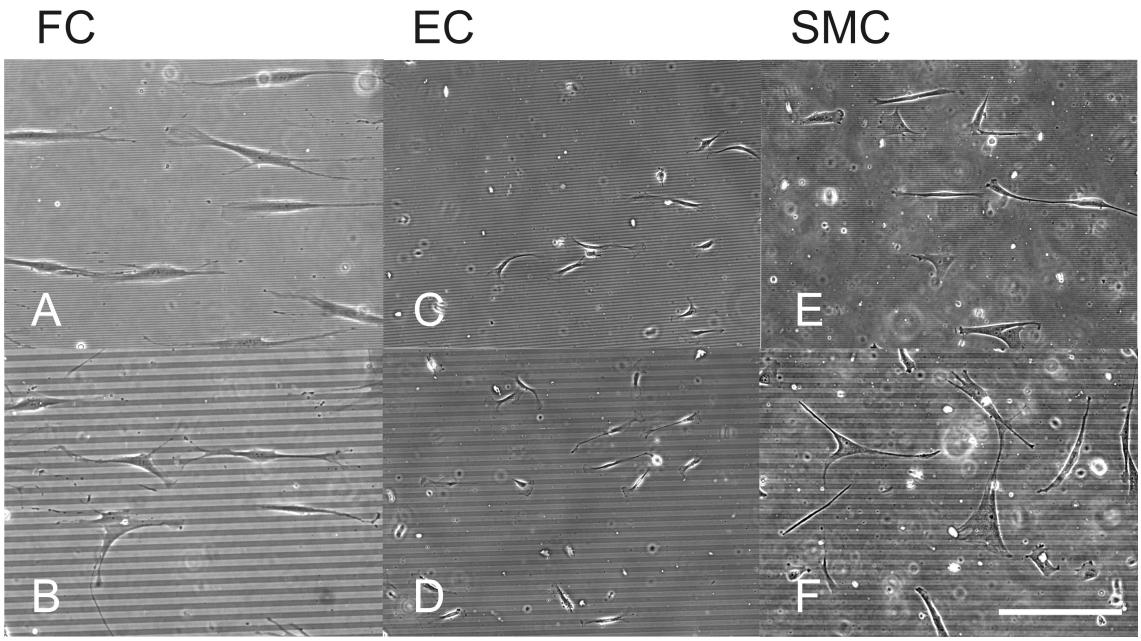

Figure 6.1: Phase contrast images taken 24 h after seeding of aligned human fibroblasts (FCs), human endothelial cells (ECs), and human smooth muscle cells (SMCs) cultured on PDMS substrates with 200 nm deep grooves. A and B: FCs on 2 μm and 10 μm wide grooved substrates; C and D: ECs on 2 μm and 10 μm wide grooved substrates; E and F: SMCs on 2 μm and 10 μm wide grooved substrates, scale bar represents 150 μm.

parameter is $S \approx 0$ as expected. The highest order parameter ($S \approx 0.95$) is measured for FCs cultured on grooves with 2 μm width and 200 nm depth which is near to perfect alignment along the grooves. Fibroblasts align significantly along the grooves even for small groove depths of 50 nm if the spacing is 2 ($S \approx 0.2$; fig. (6.2A)). In contrast, the order parameters for ECs and SMCs are much smaller than for fibroblast and show no significant orientation along the grooves for 50 nm, or even 100 nm, depths. For grooves of 2 μm width and 200 nm depth, the order parameters are $S \approx 0.35$ to 0.4 for ECs and SMCs, respectively, demonstrating a much weaker orientation response than for the FCs ($S \approx 0.95$) and no significant difference between them. Since cell alignment and polarity might be correlated to cell elongation, we analyzed whether the cells showed different elongation behavior on the various substrates; results are given in fig. 6.2.
The FCs shape is increasingly elongated when the cells adhere to the grooved topography. Furthermore, FCs became more elongated for deeper grooves (fig. 6.3). Indeed, the groove depth seems more important than groove width for FCs elongation (fig. 6.1B) due to the fact that there are only minor differences in elongation for the different grooves widths of 2, 3, 5, and 10 μm for one particular depth (t-test). For example, the elongation of FCs was approximately 50% higher on 2 μm wide and 200 nm deep grooves as compared to grooves with the same width but only 50 nm deep (t-test $p < 0.05$). For ECs and SMCs no significant variation of the elongation was measured, either for different widths or depths (t-test shows no significant difference, $p < 0.05$). However, the overall lower elongation of ECs compared to SMCs can be attributed to the natural phenotype of the round ECs compared to the long and thin SMCs shape.

Directed migration of FCs, ECs and SMCs was observed over a time period of 24 h on

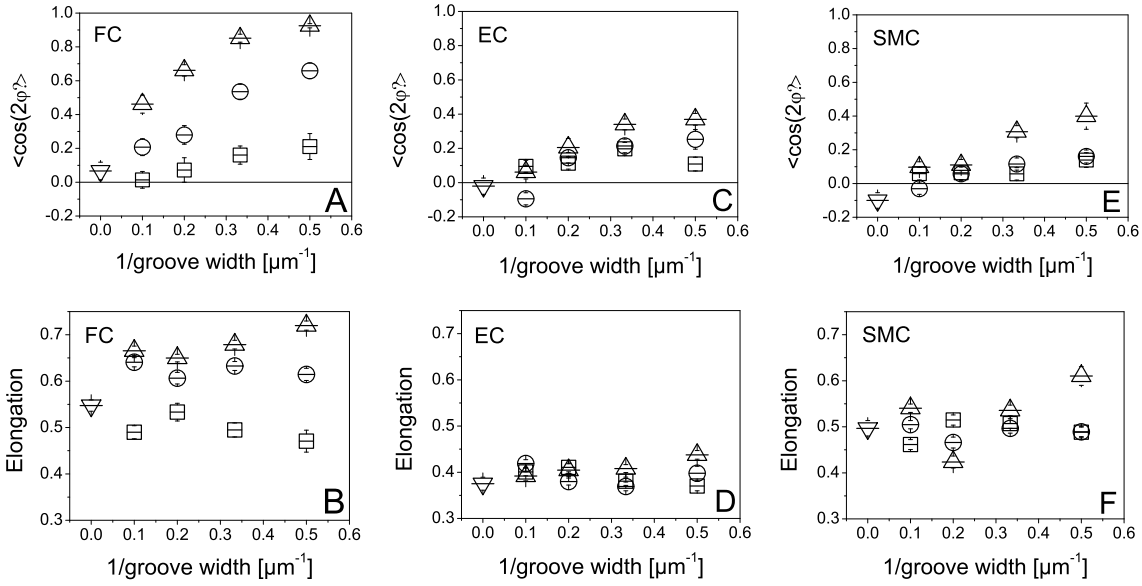

Figure 6.2: Averages of the order parameter $S = \langle\cos(2\varphi)\rangle$ (upper row) and elongation (bottom row) for human fibroblasts (FCs) (A,B), endothelial cells (ECs) (C,D), and smooth muscle cells (SMCs) (E,F). Cell shape and alignment was analyzed after 24 h on substrates with 50, 100 and 200 nm deep grooves (tip-down triangle: control flat surface; square 50 nm depth, circle 100 nm depth, tip-up triangle 200 nm groove depth for different widths of 2, 3, 5 and 10 μm (x-axis shows 1/width, for flat control substrates $1/\infty = 0$).

200 nm deep and 2 μm wide grooves. All three cell types were seeded at a low density (25 cells/mm^2) as compared to the first experiments to decrease the possibility of mutual disturbance during their migration. Images were taken every 15 minutes and cell migration was analyzed as described. A characteristic example for a time-lapse video of the directed migration of FCs along the grooves is provided in supplemental material.

The results of the analysis of directed migration of the three cell types is presented in figure 6.4. The data were taken from four movies and normalized by the number of analyzed cells (30 per cell type). All three cell types migrated in the direction of the grooves (x-direction) since the mean value of M_y/M_x for the cells on the grooves was significantly less than in the control experiments which were conducted on flat surfaces ($M_y/M_x \approx 1$). The largest directionality is found for FCs with a preferred direction along the grooves ($M_y/M_x \approx 0.4$). ECs and SMCs also show a distinct migration in the groove direction as compared to the flat PDMS surface but less significant than FCs (t-test $p < 0.05$) and not significantly different from each other (t-test, ECs: $M_y/M_x \approx 0.56$ and SMCs: $M_y/M_x \approx 0.63$).

6.2 Discussion and conclusions

It is well known that cells can align along microgrooves or similar topographical features on a surface [19, 198, 207, 39]. Many of these studies used structures in the range of several micrometers in lateral distance as well as depth and measured the response of one cell type only. However, cell-type-specific responses, such as different thresholds in directed migration or contact guidance, are interesting observations that could be explored for different

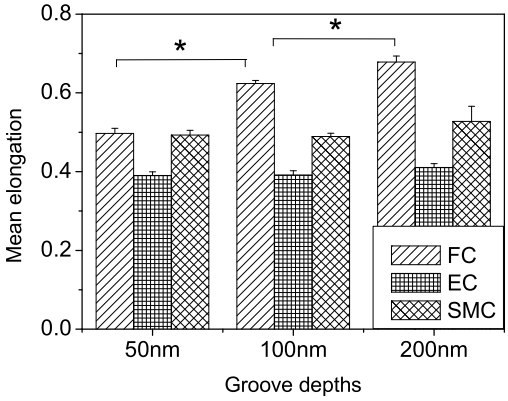

Figure 6.3: Mean elongation averaged over all groove widths for the three different groove depths (50, 100, 200 nm). The mean values for FCs are significantly different for each depth (t-test $p < 0.05$). Mean values of endothelial cells (ECs) and smooth muscle cells (SMCs) are not significantly different within each cell type for the various depths. Mean values for the three cell types are significantly different (*t-test $p < 0.05$) considering the same groove depth, except for SMCs and FCs on 50 nm depth (no significant difference).

applications. It could, for example, be helpful in the design of cell-type-specific implant surfaces which would facilitate specific healing processes by the desired cell types. To address the question of cell-type-specific responses, the response of human FCs, ECs and SMCs to grooved substrates was compared. These cell types are important for healing processes in the cardiovascular system and thus are likely to be in contact with implant surfaces such as those of stents after engrafting. Using common micro-fabrication techniques and plasma treatment we produced chemically identical but differently grooved substrates with systematically varied depths and widths in the nanometer and micrometer scale, respectively. It is worth mentioning that the topographical features should be of appropriate dimension to induce a measurable response on one hand but should be small enough to avoid saturation in the cellular response on the other hand. Using these substrates, we demonstrated that all three cell types responded with a significant directed migration and partial orientation along the grooves. All three cell types respond more strongly if exposed to grooves of smaller width or greater depth. This seems to be a general behavior since many other systematic studies revealed a similar dependence of cell orientation or migration on these groove dimensions [19, 125, 122, 18]. In fact, the square of the aspect ratio of groove width and groove depth was found to be the important feature for cell alignment along grooves [106].

Despite that common behavior of the three cell types cell-specific differences were found. The sensitivity, if defined as the degree of cell orientation along the grooves, is different between the three cell types. FCs are the most sensitive cell type and they respond with a strong alignment, elongation, and migration along the grooves. They react significantly to groove depths of 50 nm if the groove width is below 5 μm. This confirms other studies, which found that topography of depths even as small as a few tenths of nanometer, can induce a cellular response [43, 94, 232, 38]. In fact a lower threshold in groove depth of 35 nm was found to induce fibroblast alignment [125]. This step height is in the size range

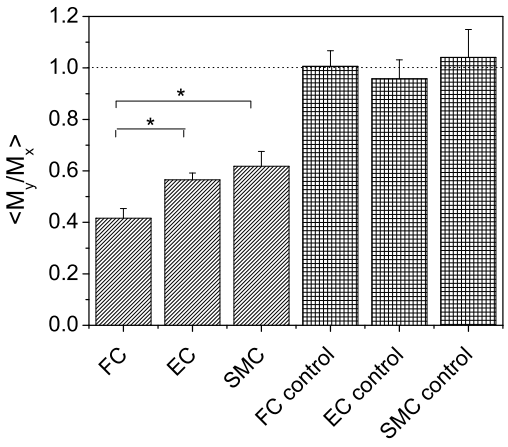

Figure 6.4: Directed migration of human fibroblasts (FCs), endothelial cells (ECs), and smooth muscle cells (SMCs) over 200 nm deep and 2 μm wide grooved substrates. The mean value for the migration $\langle M_y/M_x \rangle$ of FCs is significantly less than those of ECs and SMCs (*t-test $p < 0.05$). The values for ECs and SMCs are not significantly different to each other. The data from the control movies on flat substrates reveal the expected random walk (dotted line; $\langle M_y/M_x \rangle = 1$). Migration of the cells is demonstrated in time-lapse movies (supplement 1 to 3, see appendix 4).

of the diameter of collagen fibrils and may indicate the relevance of such topographical features in the cells' native environment. ECs and SMCs were less sensitive to the provided surface topography.

The observed difference in sensitivity may be due to the different tasks of the three cell types in the vascular system leading to different sensitiveness towards structured substrates. Important for this issue is the mechanism by which a cell senses the topography, which might be the alignment of cytoskeleton elements and focal contacts [208, 151, 219] and the probing of the topography by protrusions and filopodia [42]. ECs *in vitro* usually take on a rounded shape whereas the natural phenotype of the SMCs more closely resembles that of the FCs, an elongated shape, with abundant protrusions and filopodia which are sometimes directed in many different directions. Since the SMCs and ECs exhibited similar behaviors, while having different natural cell shapes and number of protrusions, cell shape controlling mechanisms cannot be a sufficient explanation for the contact guidance behavior of cells. Accordingly, this conclusion is supported by the finding that the cell shape of mouse mammary epithelial cells is dependent on topography [2], whereas Kaiser *et al.* found only small changes in the shape of NIH3T3 fibroblasts [95] due to topography. Investigations of cytoskeleton structures such as the ratio of G- and F-actin or the different intermediate filament systems might help to give a better understanding of the cell type specific differences in contact guidance.

Conclusions The microtopography of a substrate is an important feature for controlling responses of cells in contact with an implant or biomaterials. Therefore, the responses of three different cell types which are important for healing and maintenance in the cardiovascular system were systematically investigated. All three cell types demonstrated a general behavior: cell orientation increased with smaller lateral spacing and with in-

creasing depth of the grooves. Specifically, human FCs aligned and migrated along the grooved surface structures much more strongly than ECs and SMCs. Furthermore, no significant difference was measured in the response between ECs and SMCs. It was clearly demonstrate that all three cell types align and migrate along the grooves, an effect which might be used in the design of surface coatings of implants. The strong alignment and directed migration of FCs might be used for specific selection and guidance of these cells to attract them towards a wound. However, the relatively weak alignment and directed migration along the grooves is not sufficient to direct ECs and SMCs by such surface structures. Additional signals might therefore be required to trigger cell-type-specific directed migration or alignment responses from some types of cells. To determine the appropriate signals, future studies to examine how ECs and SMCs respond to a combination of chemical and topographical signals would be interesting. Cell stimulation by other signals such as biochemsitry, electric fields with physiological relevant amplitudes [228] or mechanical strain [80] is shown in the follwing chapters of this thesis.

7 Behavior of vascular cells on biofunctionalized gold nanostructures

Cell-cell and cell-extracellular matrix (ECM) adhesion are involved in fundamental cellular functions including motility, proliferation, differentiation, and apoptosis. They are complex, highly regulated processes, investigated in various studies [15, 227, 66](see also section 2.1.2). In this chapter endothelial (ECs) and smooth muscle cells (SMCs) are tested on biofunctionalized gold nanostructures decorated with three linker systems (for details see sections 3.2 and 3.3). Peptide sequences of the extracellular matrix (RGD and REDV) and VE-cadherins (VE-Cad) typical for endothelial cell-cell contacts are bound to gold nano structures with defined distances. These surfaces are used to observe specific ligands and/or distance dependence of the spreading and adhesion characteristics of the two cell types. The here presented data in comparison with recent studies [4, 5], indicate a universal distance dependence for integrin clustering and focal adhesion formation. This finding will be helpful in the future to stimulate vascular cells for vessel formation (angiogenesis) and wound healing.

7.1 Additional materials

Cell culture was performed as described in appendix 3.1. In all experiments medium containing 1% serum was used to avoid excessive ECM production, as it would prevent specific ligand binding on the surfaces. Every condition was tested three times, each time with two samples.
The ordering parameter of the nanostructures was tested with SEM directly after production of the substrates, as well as randomly after some cell experiments, see sections 3.2 and 4.1.

7.2 Universal integrin clustering distance for vascular cells

ECs and SMCs were seeded on glass and examined after one day by optical phase contrast microscopy. Only three-quarters of the glass substrate area were patterned with Au nanodots presenting different spacings between the dots. The Au dots were functionalized either by RGD-peptides, REDV-peptides or VE-Cad and the inter-particle regions were passivated by PEG. A line of cells marks the borderline of the nano-patterned area, see figure 7.1. The unpatterned area of the substrates (corresponding to the upper part in the figure) was hence entirely passivated against cell adhesion, consequently cell adhesion and attachment is only observed on the patterned part of each sample.

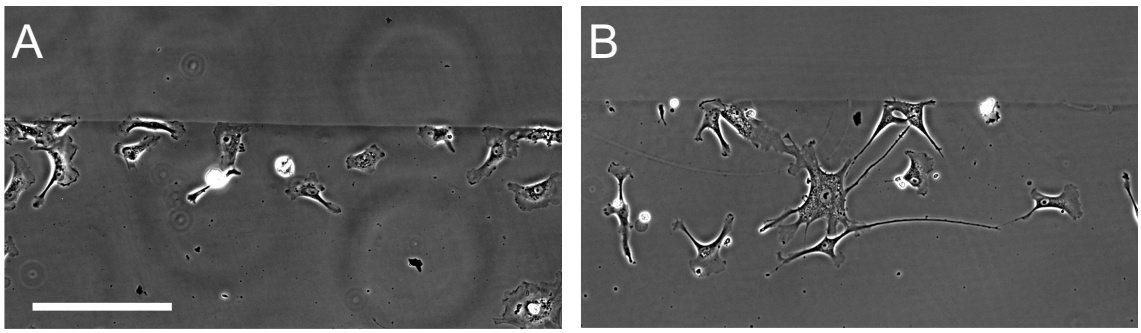

Figure 7.1: Endothelial (A) and smooth muscle cells (B) at the dipping line on glass slides decorated with gold nano dots (here distance of 40 nm) and biofunctionalization, here RGD; scalebar represents 200 μm.

When plated on Au-nanodot patterns with various spacings and functionalized by various linker systems, ECs and SMCs show different adhesion behaviors (figure 7.2, two columns on the left). It can be seen that both cell types spread very well on the 40 nm patterns (figure 7.2, 40 nm patterns indicated at the side: rows 1, 3 and 5), showing a spreading behavior comparable to that seen on uniformly glass surfaces. On the other hand, hardly any cell spreading is observed on substrates with 90 nm spaced nanodots (figure 7.2, rows 2, 4 and 6). Quiescent cells, presenting a rounded shape that causes string scattering of light, and migrating cells with extended filopodia can be noted. Cell spreading on the 90nm patterned surfaces is rather poor. Only a few cells remain attached after 1 day of incubation.

In an attempt to quantitatively understand the different adhesion properties of cells on these interfaces the spreading area and cell number density of essentially attached cells were plotted in figures 3 and 4. The analysis of the spreading area reveals significant differences for the two tested nanodot distances 40 nm and 90 nm. For all linker systems and both cell types, the spreading area is significantly higher (between 20 and 50%) on the 40nm patterns compared to the 90nm patterns. On all tested linker systems and nanodot distances the cells spread to a lesser extent than on uniform glass, except for the case of SMCs seeded on the 40 nm distance and decorated with RGD-peptides (see figures 7.2 and 7.3). For the 40 nm distances ECs and SMCs spreading area is about 20 to 30% decreased on VE-Cad decorated surfaces compared to those with RGD and REDV peptides (significance confirmed by t-test). Spreading area is in general smaller on the 90 nm distances than on the 40 nm distances, but is not significantly different for the different linker systems, except again for the SMCs, whose spreading area is significantly smaller on VE-Cad than on RGD and REDV (confirmed by t-test). The analysis of number of cells counted per mm^2 (see figure 7.4 shows that the 3 linker systems can attract ECs and SMCs in different ways. On the VE-Cad functionalized surfaces cell attachment is reduced in more than a 40% in comparison to the other linkers for the same nano-dot distances (significance confirmed with t-test). On RGD and REDV decorated surface, both cell types seeded on the 40 nm inter-particle distances show similar attachment behaviors as on the glass controls. Furthermore, it is clearly shown that significant differences in cell number exist for the same linker systems between the two tested nano-dot distances (confirmed with t-test, see figure 7.4). On the 40 nm pattern cell number is for all linker systems about 50% higher than on the 90 nm pattern.

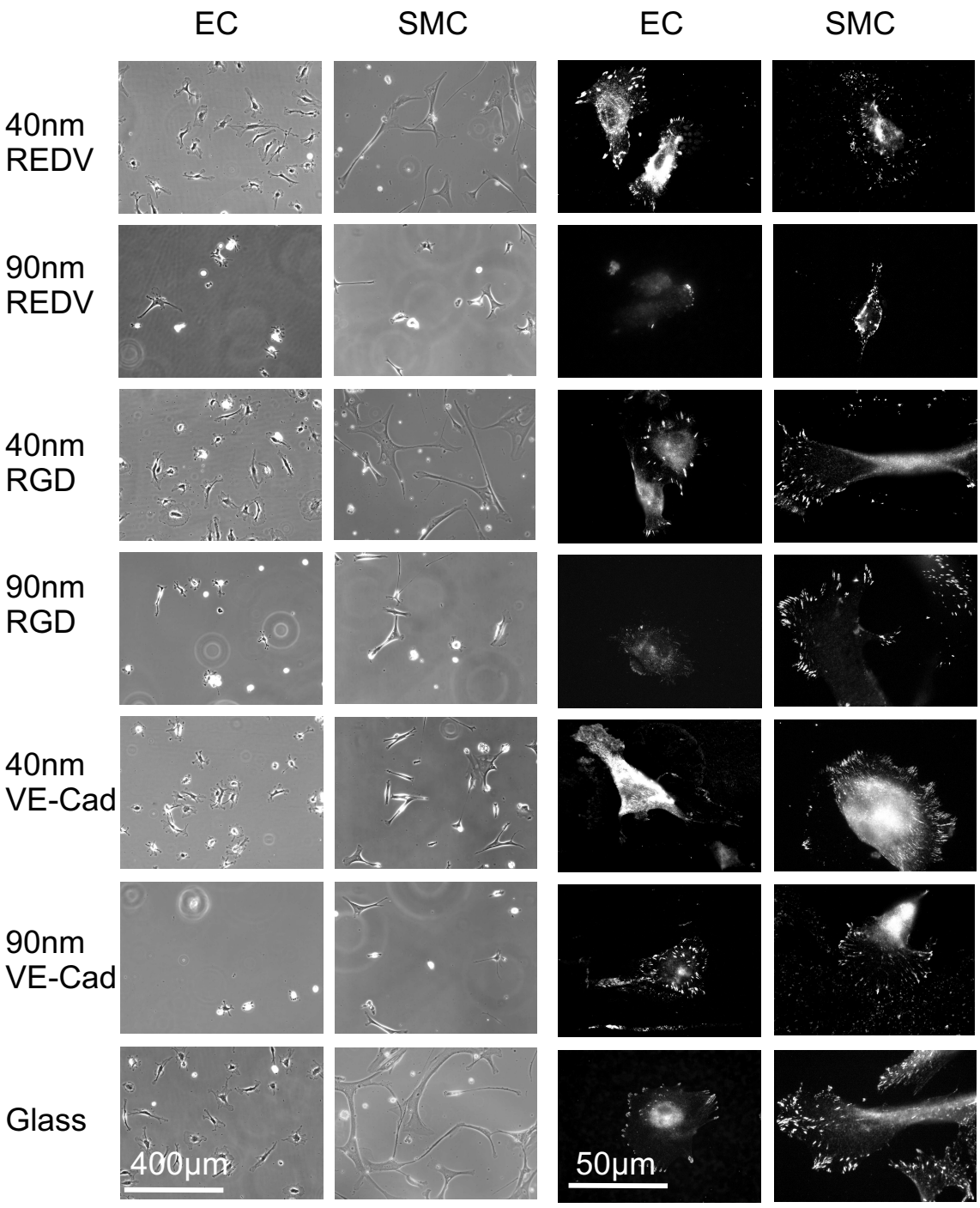

Figure 7.2: Left two columns: phase contrast images of endothelial (ECs) and smooth muscle cells (SMCs) on various surfaces. Right two columns: fluorescence images of the two cell types stained with anti-paxillin marker. Rows 1, 3 and 5: 40 nm distances of gold nano dots. Rows 2, 4 and 6: 90 nm distances. Row 7: glasss control. Rows 1 and 2: REDV-linker; rows 3 and 4: RGD linker and rows 5 and 6: VE-Cadherin decoration.

In figure 7.2 (two columns on the right) fluorescent images of cells with their focal adhesions immunostained with focal-adhesion-marker (paxillin) are depicted. On small dis-

tances both cell types build visible focal adhesions, whereas on long distances many cells were washed away during the procedure and those left on the surface showed only poorly recognizable focal adhesions. In general SMCs, if attached to a 90 nm-distance-pattern, build clearly focal adhesions, see an example for the RGD-linker in figure 7.2, right column, row 4. As most of the cells were washed from the surfaces during anti-body-staining procedure, not many examples could be found.

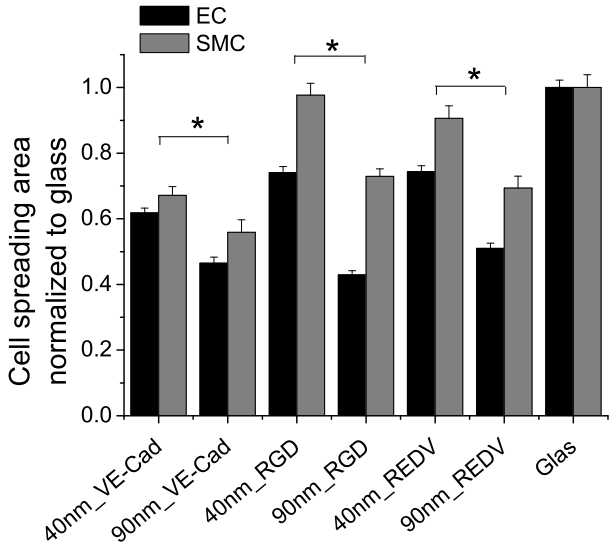

Figure 7.3: Cell spreading area of endothelial (ECs) and smooth muscle cells (SMCs) on gold nanostructures with several linker systems: VE-Caderine, RGD, REDV and glass as control (normalizing reference); two different gold dot distances per linker system were tested, 40 nm and 90 nm. The spreading areas of ECs and SMCs is significant different for the two distances for all linker systems (indicated with *).

7.3 Discussion and conclusions

The complex interaction between the intracellular and the extracellular machinery allows cells to perform their particular functions in a multicellular organism [194]. Cellular functions such as cell differentiation, growth, adhesion, motion are controlled by the properties of the extracellular machinery. In return, cells structure and secrete their own environment. Extracellular factors of the surrounding tissue preferentially stimulate growth of cell types relative to others. Thus, in addition to the influence of the cell environment onto cell function, the extracellular matrix (ECM) is able to discriminate between different cell types [1]. The ECM is composed of a variety of macromolecules e.g. collagen and fibronectin [102]. Its properties (mechanics, structure, and chemical composition) determine the particular cell types embedded, which in turn control the organization of the ECM. The ECM protein, which was interesting for this study, was fibronectin. It is a non-collagen representative of the fibrillar ECM proteins and belongs to the group of multi-adhesion proteins [1]. It consists of multiple domains, each with specific binding

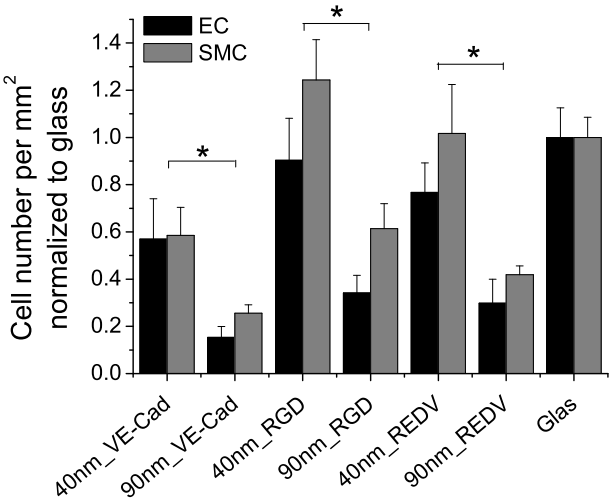

Figure 7.4: Cell number of endothelial (ECs) and smooth muscle cells (SMCs) on gold nanostructures with several linker systems: VE-Caderine, RGD, REDV and glass as control (normalizing reference); two different gold dot distances per linker system, 40 nm and 90 nm. Cell number per area of ECs and SMCs is significant different for the two distances for all linker systems (indicated with *).

sites for both other matrix molecules, and for cell surface receptors. Fibronectin contains several adhesion motifs, such as the RGD and REDV sequences [160, 134]. Cells adhere to the surrounding ECM via integrin-mediated adhesions [169]. Transmembrane integrin molecules are associated to a huge complex of proteins, including vinculin, talin, paxillin, tensin and many others [30, 65], all of them involved in the dynamic interactions with the cytoskeleton [14, 102]. Cells can also adhere to other adjacent cells via cell-cell junctions mediated by cadherins. Cadherins play important roles in cell adhesion and in tissue formation in the body and VE-cadherins in the formation of the endothelium in the blood and lymph vessels [202].

Aiming to gain a better understanding of vascular cell types, the spreading and focal adhesion properties of ECs and SMCs were compared on nanopatterned ECM-mimicking surfaces. The array of nanodots on these surfaces had interparticle spacings of 40 nm or 90 nm and were conjugated to RGD- , REDV peptide, or VE-Cad. These particles have a diameter of 8 nm allowing each particle to interact with only one ligand receptor [4]. In previous studies it was shown that functionalization with RGD and specific ligand spacing on the surface is essential for the successful assembly of focal adhesions and stress fibers, since non-functionalized surfaces or surfaces with spacings larger than 73 nm failed to induce the formation of such structures [4, 22]. One of the main conclusions was that nanoscale differences in ligand density are, indeed, sensed by living cells. However, the nature of the molecular detector that is sensitive to the critical nanoscale spacing between ligands is still unclear and, similarly, the cellular mechanisms responsible for the spacing dependent cellular response were not defined. It is shown here that when adhesive dots are separated by 90 nm, cell adhesion and spreading, as well as the formation of focal adhesions, are aberrant, whereas separation of 40 nm between the dots

allows effective adhesion. Thus, this length scale appears to be a universal spacing for effective adhesion mediated by integrins. This can be explained through the theories already developed on previous studies [4, 22, 23]. It appears that there is a critical ligand (RGD) density (interligand spacing of 70 nm) that is essential for the formation of stable integrin-mediated adhesions. At larger spacings, integrin adhesion can still take place, yet the adhesions formed fail to develop into focal adhesions and to induce stress fiber assembly. Interestingly, cell-reorganized fibronectin fibrils were shown to form assemblies with a characteristic spacing of 71 nm, as given by the spatial arrangements of the protein interaction sites [162]. This finding indicates that nanoscale periodic patterns play a crucial role in molecular assemblies of focal adhesion sites. Here is shown that the previously drawn conclusions hold also true for the REDV-peptide and the associated integrin ($\alpha_4\beta_1$). The universal distance-dependence for focal contact formation and cell adhesion shown previously for other cell types (e.g. MC3T3-osteoblasts, REF52-fibroblasts, 3T3-fibroblasts, and B16-melanocyte [4]) hold also true for the two vascular cell types (ECs and SMCs) investigated here. A distance-dependent behavior for ECs and SMCs on VE-Cad decorated nano-patterns was also demonstrated here. Although both cell types adhere equally poor on the VE-Cad compared to the RGD and REDV peptides, a universally characteristic cell adhesion behavior depending on the ligand spacing was indicated. This behavior is worth more profound investigation.

Conclusions The universal distance dependence for integrins binding to ECM-peptides was further expanded for the particular cases of REDV motif and vascular cells (previously observed for RGD and other cell types). We have demonstrated that spreading behavior and focal adhesion formation of vascular cells is similar to other cell types. VE-Cad-ligands in the first place, decrease cellular adhesion significantly on the tested ligand distances, but also induce a distance-dependent adhesion behavior in the cells. Together with ligand-distance gradients, new approaches for tissue engineering are currently pursued [79]. In further studies a possible cell separation with the help of surface modifications could help to accelerate the wound healing and endothelialization after (stent) implantation. Deeper knowledge of the cell-adhesion mechanisms will one day fulfill the requirements for the castomized modification of implant surfaces.

8 Cyclic stretched membranes and mechanical forces

The physiology of vascular cells is dependent on the stimulating mechanical forces caused by pulsatile flow and shear stress. Cells adherent on a cyclically stretched substrate with a periodically varying uniaxial strain are known to dynamically reorient nearly perpendicular to the strain direction (for details see section 2.2.1). Here we investigate the dynamic reorientation of human endothelial (ECs) and smooth muscle cells (SMCs) over a range of stretching frequency from 0.01 to 1Hz and strain amplitude of 8%. In the observed time frame of 6h ECs show a clear frequency dependence in reorientation response, whereas SMCs show almost no reorientation. Stained stress fibres (actin) and focal adhesions (paxilin) demonstrate that cytoskeleton reorientation takes place before the whole cell body is aligned. The study indicates significant differences in reaction times of the two cell types, which are promising results for future tissue engineering and implant wound healing improvements.

8.1 Different time and frequency dependence of endothelial and smooth muscle cells on cyclically stretched substrates

Before application of stretch, ECs and SMCs adhering to fibronectin coated elastomeric substrates (see section 3.4), were randomly oriented. This corresponds to an initial order parameter (see section 4.3) of around $S = 0 \pm 0.2$, see figures 8.1 and 8.3. Deviation from $S = 0$ result from the restricted number of cell which could be observed and from random migrations of cells. Upon application of cyclic stretching, several cell responses could be observed. In figure 8.1 phase contrast image series for the two cell types are depicted. One can obtain a tendency of cell elongation and orientation perpendicular to the stretch direction. Averages of cell orientation of at least three time lapses for each measured frequency are shown in figure 8.2 and 8.3, where mean cell elongation E and the mean order parameter S are plotted as a function of time to demonstrate the dynamic evolution of the shape and the orientation of the cells.

Elongation After the cyclic strain is switched on ($f = 0.01$, 0.1 or 1 Hz, $A = 8\%$), mean elongation of the cells changed only for ECs at a stretching frequency of 1 Hz, see figure 8.2. After a mean elongation (see section 4.3) of $E \approx 0.25$ without stretch, corresponding to rather round-shaped cells, ECs became slightly elongated ($E \approx 0.35$). For SMCs the average elongation is higher ($E \approx 0.5$) than for ECs, and does not further increase upon application of stretch with the frequencies used. SMC elongation shows typical broad

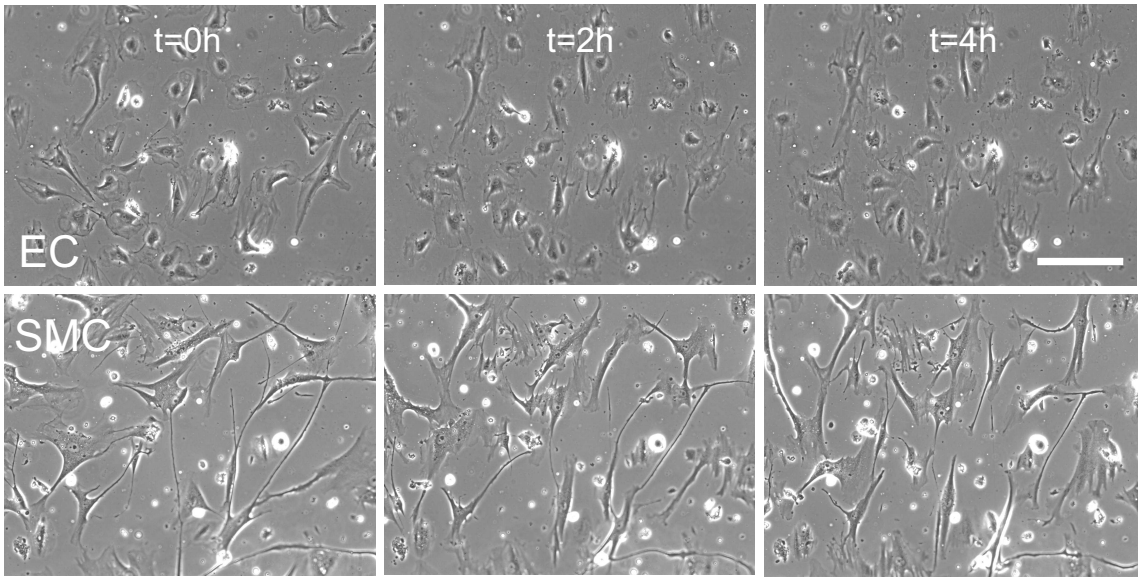

Figure 8.1: Endothelial cells (ECs) and smooth muscle cells (SMCS) in phase contrast movies before stretching ($t = 0$) and after 2 and 4 h cyclic stretch, (frequency 1 Hz, amplitude 8%); scale bar represents 200 μm.

variations, due to their irregular cell shape, see figures 8.1 and 8.2.

Orientation For ECs the cells change their orientation perpendicular to the applied strain at 0.1 Hz and 1 Hz stretching frequency, see figure 8.3. Correspondingly, S changes exponentially from an initial value of $S \approx 0$ to a new steady state order parameter between $S \approx -0.4$ (for 0.1 Hz) and $S \approx -0.8$ (for 1 Hz), depending on the stretching frequency. SMCs show almost no reorientation for the measured frequencies and time period.

Time and frequency dependence Dynamic cell reorganization at cyclic stretch was quantified by the characteristic time τ_2 (see section 4.4) for strain frequencies from 0.01 to 1 Hz for ECs. The orientation of SMCs was not significantly altered after 6 hours to evaluate τ_2 for all frequencies, see figure 8.3. At 0.01 Hz τ_2 was not measurable for ECs, since there was no significant deviation form the control situation with no application of stretch ($S \approx 0$). At 0.1 Hz the mean value for three experiments is $\tau_2 = 91.68 \pm 50.24$ min (mean value of three time lapse movies with standart error of the mean) and at 1 Hz $\tau_2 = 37.60 \pm 4.79$ min. This demonstrates the dependence of cell reorientation dynamics on the stretching frequency. Remarkable is the big variation of τ_2 at 0.1 Hz. This enhances the suggestion that the lower threshold frequency for EC is around 0.1 Hz, see below. It can be stated that the higher the frequency, the faster the cells reaction.

Threshold frequency Below a certain threshold frequency f depending on the cell type, cell reorientation perpendicular to the stretch direction can no longer be observed and the mean cell orientation fluctuates around $S = 0$. Only at frequencies higher than the threshold value ($f > f_t$) do cells change to a perpendicular orientation with time. The observed threshold frequency appeared to be cell-type dependent: For ECs the threshold frequency was found to be between 0.01 Hz and 0.1 Hz, as ECs show significant differences

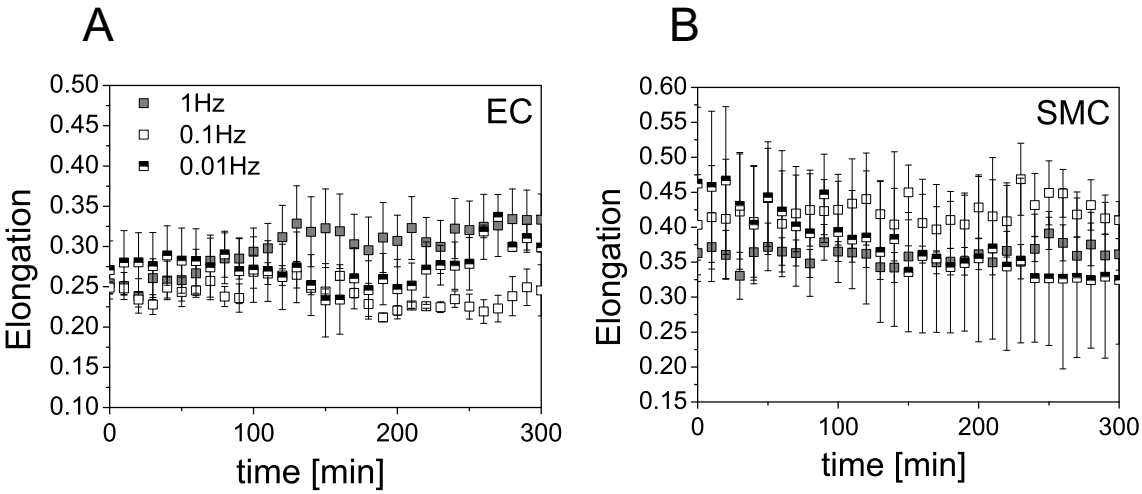

Figure 8.2: Time development of elongation $E = \frac{(A_{maj}-A_{min})}{(A_{maj}+A_{min})}$ (see section 4.3) for endothelial cells (ECs) (A) and smooth muscel cells (SMCs) (B) for the three different frequencies: 1 Hz (grey), 0.1 Hz (white), 0.01 Hz (black-white). ECs change their shape measurable only at 1 Hz. SMCs nearly do not change their elongation state and typically show great variations for all frequencies.

in orientation for the two frequencies (see figure 8.3A). The threshold frequency for SMC is speculated to be approximately 1 Hz, since, in our measurements, a slight reorientation response can be observed after 5 hours at the highest frequency (see figure 8.3B).

Stress fibers and focal adhesions For further analysis of the cells' orientation response to cyclic stretching, the intracellular actin stress fibres and paxillin in focal adhesion were stained after stretching and compared with those of non-stretched cells. In figure 8.4, representative images of actin stress fibers and focal adhesions are shown for both cell types at different stretching frequencies, including control condition (no stretching). For both cell types actin stress fibers and focal adhesions are obviously not orientated for the frequency of 0.01Hz and the control (fig. 8.5). For 0.1 Hz and 1 Hz actin fibers and focal adhesions are orientated. The quantification of the mean orientation (for details see appendix 3.4) demonstrates generally stronger perpendicular alignment for ECs than for SMCs, see figure 8.5. Actin stress fibers orient almost perpendicular in ECs at frequencies of 0.1 Hz and 1 Hz ($S \approx -0.9$, t-test states no significant difference of the mean values of 0.1 Hz and 1 Hz). In SMCs the actin stress fibre orientation is less pronounced, but also around the same value for 0.1 Hz and 1 Hz ($S \approx -0.5$, t-test states no significant difference of the mean values of 0.1 Hz and 1 Hz). Focal adhesions show a slightly different behavior. In SMCs the overall focal adhesion orientation is weaker than in ECs, but for SMCs the maximum orientation can be observed at 1 Hz ($S \approx -0.45$), whereas the focal adhesion orient in a not significant manner for 0.1Hz ($S \approx -0.15$) and below. For ECs the focal adhesion orientation is at its maximum at 0.1 Hz ($S \approx -0.7$) and is smaller at 1 Hz ($S \approx -0.55$).

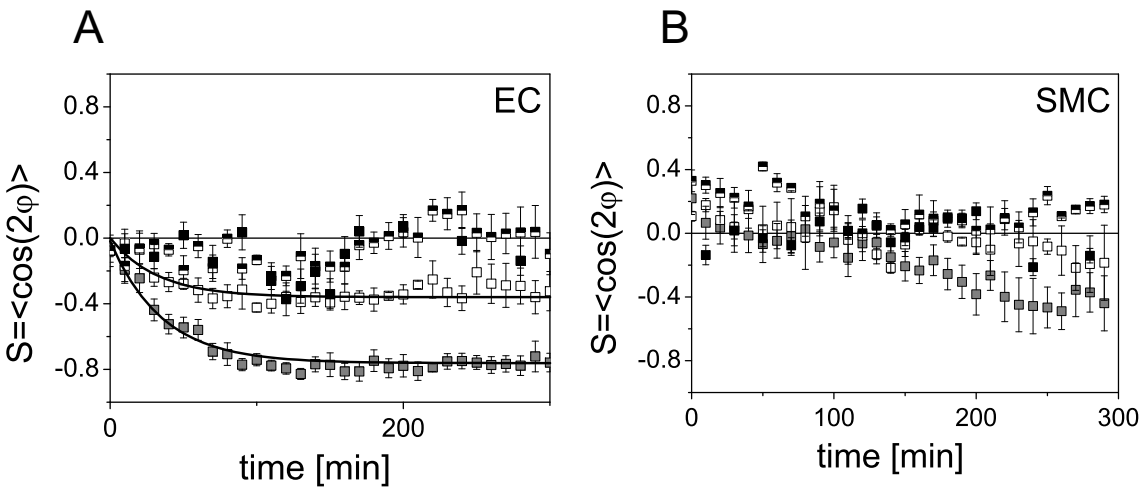

Figure 8.3: Time development of orientation (order parameter $S = \langle\cos(2\varphi)\rangle$) (see sections 4.3 and 4.4) for endothelial cells (ECs) (A) and smooth muscle cells (SMCs) (B) for three different frequencies: 1 Hz (grey), 0.1 Hz (white), 0.01Hz (black-white), control=no stretch (black). In A fitting lines for 0.1 Hz and 1 Hz are included (black curves).

8.2 Discussion and conclusions

Arterial wall cells are permanently subjected to mechanical stress induced by pulsatile flow. The mechanical stress is composed of two major elements. One is hydrodynamic shear stress parallel to the longitudinal axis of the vessel. The other is pressure induced periodic stretch in the circumferential direction. In arteries with sufficiently high shear rate and little flow turbulence, ECs respond to shear stress by aligning themselves parallel to the direction of flow. Many studies have shown that ECs, cultured in a flow-regulated chamber, orient parallel to the direction of flow [167, 231, 130]. Thus, it has been widely accepted that the flow shear stress is a major factor responsible for EC orientation. On the other hand, in native arteries SMCs exhibit a spiral orientation with a small pitch; an almost circumferential orientation [177]. Since SMCs normally grow in the vessel wall and form it, they are not directly exposed to the blood flow. Therefore, their circumferential orientation is probably caused by mechanical stimulation derived from the periodic strain of the arterial wall. Along with this hypothesis, investigators analyzed the behavior of vascular cells such as ECs and SMCs [97, 141, 183, 143, 86, 45, 124] cultured on stretchable substrates which were periodically stretched and relaxed. These studies have shown that vascular cells tended to align perpendicular to the direction of stretch. This suggests that, irrespective of the cellular species, mechanical stress-induced cellular alignment is a common behavior of adhesive cells *in vitro*, which may operate to induce cellular orientation in tissues *in vivo*. A lot of researchers have studied the effects of magnitude and exposure time of cyclic stretch on many cell types. They investigated various parameters such as changes in cell orientation, cytoskeleton modification, cell proliferation, and alteration in mRNA levels and protein synthesis [210, 46, 213, 149, 108, 148]. Above all, the effect of strain amplitude on cell reorientation has been studied but only a few investigated the frequency dependence of cell orientation response. Kaspar *et al.* [100] reported that the proliferation rate of human-derived osteoblast-like cells increased with the increasing number of stretch cycles applied until a certain maximum number of cycles was reached, and

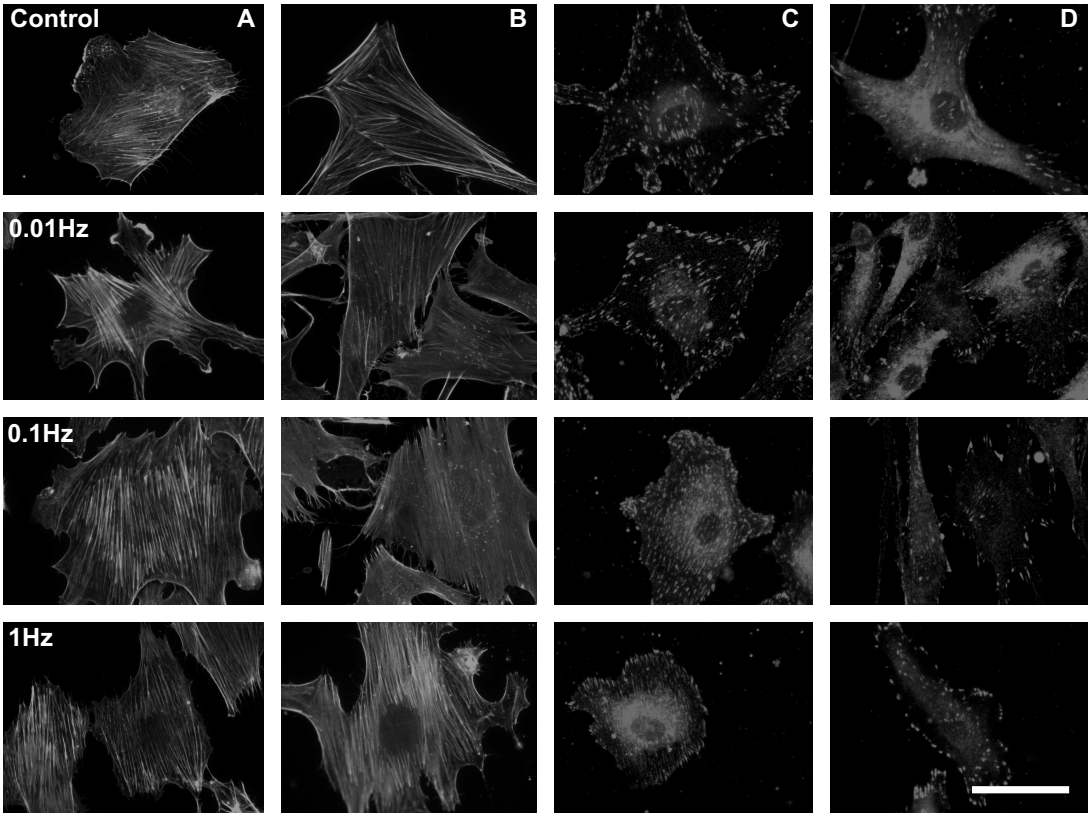

Figure 8.4: Fluorescence microscopy images of phalloidin-stained F-actin (columns A and B) and focal adhesions (marker protein is paxilin, columns C and D) in endothelial cells (columns A and D) and smooth muscle cells (columns B and D) at control conditions and after 6 h of cyclic stretch at frequencies of 0.01 Hz, 0.1 Hz and 1 Hz (amplitude 8%); scale bar represents 30 μm.

they concluded that the effect of frequency on cell proliferation was only small when the number of cyclic strains reached a constant. In combination with an appropriate number of cycles they found an optimal frequency (1 Hz) as stimulus for bone cell proliferation. Liu *et al.* noted that smooth muscle cells (SMC) stretched with the same amplitude showed changes in alignment depending on the frequencies tested, which were 0.5, 1, 1.5 and 2 Hz [123]. They concluded that the frequency was an important regulatory factor for SMC alignment and served as an independent signal from amplitude and duration. In their studies, however, the time course of reorientation could not be measured in detail as they used rather crude time steps of several hours. Jungbauer *et al.* systematically studied the influence of amplitude and frequency on fibroblast cells and examined their temporal behavior with regard to theoretical modeling [93, 48]. In the presented study human primary ECs and SMCs were stretched at a specific duration of cyclic strain (approximately 6 h, amplitude 8%), and at different stretching frequency. A very high time resolution of 100 sec intervals was achieved here by performing the experiments on top of an automated microscope. In contrast to that, other studies typically observe only one time point at the end of the experiments [210, 149] or performed experiments with low temporal resolution of many minutes [148]. Thus, the present study is a detailed analysis

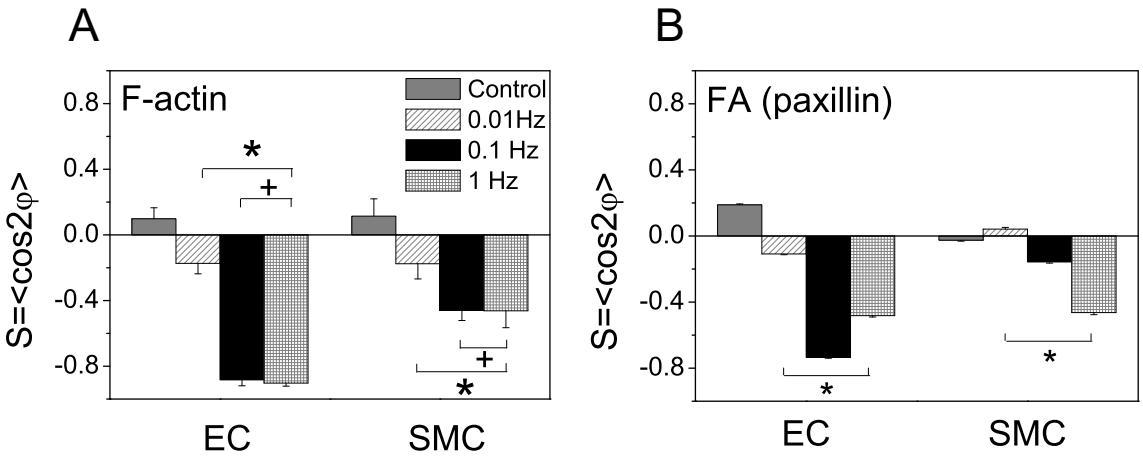

Figure 8.5: Analysis of F-actin-orientation (A) and paxillin-marked focal adhesion (FA) orientation (B) after 6h and different frequencies (1 Hz, 0.1 Hz, 0.01 Hz and control) for the two cell types. Stars (*) indicate significant differences of the means (t-test), crosses (+) represent no significance. In addition in figure B all three means of frequencies are significant different to each other, whereas in figure A only the mean for 0.01Hz is significant different to those for 0.1 Hz and 1 Hz.

of the effects of frequency on the temporal dynamics of ECs reorientation in comparison to SMCs reorientation on a cyclic stretched substrate.

Orientation and frequency dependence With the help of an order parameter to quantify the cell orientation it is shown here that the dynamic orientation of ECs perpendicular to the stretch direction depends on the frequency. It can be demonstrated clearly that ECs react faster and enhanced at 1 Hz stretching frequency than at 0.1 Hz. It is remarkable, that the dependency on frequency is measurable in two different responses: the reaction time and the level of reorientation. In the frequency regime used in this study, SMCs' reorientation does not show a clear frequency dependence. For the SMCs used the lower frequency threshold for orientation seems to be around 1 Hz. This can be explained by the outcome of other studies, which showed, that SMCs need up to 10 h to react to cyclic stretching [123, 124], which was beyond the timescale of this study. Nevertheless, it is shown that within a frequency region of 0.1 Hz to 1 Hz ECs reorientate significantly quicker and more pronounced than SMCs.

Orientation and elongation Differences in reorientation and elongation time might result from the use of different cell types from different donors. That can be supported by the slower response of the different cell types in other studies [123, 93]. Kanda et al. showed differences in the time scale of cell orientation responses of ECs, SMCs and fibroblasts (all from bovine origin) [97]. In our experiments only the ECs became slightly elongated during application of cyclic stretch. For the ECs this process is visible within 100 and 200 min when cells reached a new steady state in the cell orientation.

The mechanisms of the cellular orientation response are not well understood, yet. Buck *et al.* [21] regarded the response as a cellular avoidance reaction to stretch in the direction of their long axes. This may be derived from cellular response of reducing stress or strain energy exerted on cells. Accordingly, the cells adhering parallel to the direction of stretch

were subjected to the maximum distortion in the direction of their longitudinal axes, while the cells adhering perpendicularly were exposed to minimal distortion. As a result, all cells might align perpendicularly to avoid the stretch.

Cytoskeleton It is speculated that after adjusting themselves to a new orientation, the cells start to rebuild the cytoskeleton and elongate along the new orientation. The essential features of reorientation are the same for all cell types; however, the threshold frequency f_{t1} and the characteristic time of reorientation are significantly different for the here presented measurements. The results show that ECs have at least a ten times lower frequency threshold (0.1 Hz) of reorientation than the SMCs (1 Hz). The reorientation of ECs already starts measurably after 30-50 min (see figure 8.3) and reaches its maximum after 100 min, whereas SMCs start to reorientate after more than 100 min of applied stretch (only for 1 Hz). One possible explanation could be the different structure or amount of the two cell types' stress fibres. Measurements of F- and G-Actin content could reveal if and how much the cells differ in their cytoskeleton constitution [123]. Alternatively, a similar approach as performed by Na *et al.* [146] could clarify the differences in initial cell mechanical properties and stiffening and actin filament turnover at cyclic strain by AFM indentation measurements. In this study, further hints of cellular behavior under the stretching conditions used could be found in the analysis of the orientation of the actin stress fibres and focal adhesions. Fuerthermore, cell reorientation requires a continuous remodeling of focal adhesions and the actin cytoskeleton [146, 105]. The actin stress fibers need to be depolymerized and polymerized or turned in a new direction to establish a new equilibrium after an adaptive process. Similar processes are required for the focal adhesions. In cell migration, reorientation and shape changes a continuous remodeling of focal adhesion sites is needed. The temporal dynamics of these processes should correspond with the exponential time course of reorientation observed in our experiments. The analysis of the actin stress fibres and focal adhesion orientation fits into the evaluation of the EC and SMC shape reorientation. The biological reorganization mechanism in the SMCs observed in this study is much weaker for the low frequency range of 0.01 Hz to 1 Hz than in ECs and results in a less pronounced orientation, visible for cell shape and cellular cytoskeleton. Furthermore, it can be stated that the reorientation of internal cell structures is much more rapid than the whole cell body orientation. Already after 6 hours SMC actin stress fibres show a clear orientation at 0.1Hz and they do not increase their perpendicular alignment at 1Hz, whereas the whole SMCs show an only weak orientation after 6h at 1 Hz. This is consistent with the study of Liu *et al.*, who show cell body and actin stress fibres reorientation after more than 10h [123]. Yamada *et al.* analyzed pork EC actin stress fibres at one frequency and found dependencies on cell density and cell-cell contacts [222]. Yano *et al.* showed that β_1 integrin reorganized in a pattern along the axis of elongated cells, creating a fusion of focal adhesions in ECs after 4 h strain exposure [224]. This corresponds to the findings presented, which show the reorientation of focal adhesions for both cell types, which are comprise clustered integrins. The results presented here indicate that the actin filament system should be one of the critical points in the chain of cyclic strain-induced signal transduction of cells. It is shown that the effect of frequency on ECs and SMCs alignment depends on the integrity of the actin filament system. However, further studies are still needed to elucidate the signal transduction induced by the frequency of cyclic strain, especially the link between the filament system

and EC and SMC reorientation. Speculating about the mechanisms that are involved in interaction between the two cell types, cyclic strain studies in co-culture of the two cell types seem to be promising. Smith *et al.* demonstrated e.g. that vascular SMCs exposed to physiological levels of stretch increase their vascular endothelial growth factor (VEGF) secretion and may provide an arterial stimulus for maintenance of steady state levels of VEGF essential for EC survival [184].

It is very important to correlate the repetitive strain-induced cellular orientation *in vitro* with pulsatile-induced orientation in native arteries. In arteries, the principal direction of strain due to pulsatile pressure is circumferential. Therefore, if the periodic stretch-induced orientation response seen in cultured cells operated *in vitro*, vascular cells in native arteries should align longitudinally. However, it is generally observed that SMCs *in vivo* align almost circumferentially, as described previously [50]. Accordingly, the alignment of SMCs subjected to directional stress observed *in vitro* is in marked contrast to that observed *in vivo*. Since SMCs grow three dimensionally (3D) in the extracellular matrix *in vivo*, the avoidance reaction *in vitro* might be due to the nonphysiological experimental conditions in 2D culture.

Conclusion In short, our results demonstrate a frequency-dependent response of ECs and SMCs for the applied cyclic strain and frequencies. We observed a cell-type dependent lower threshold frequency below which no reorientation occurred (0.1 Hz for ECs, 1 Hz for SMCs). In this study SMCs seem to react much weaker and slower than the ECs. For ECs the exponential reorientation characteristic expected could be measured. This is a result which can be pursued in finding strategies for tissue engineering and wound healing after implantation. Further studies could include the investigation of protein concentration of known pathways for mechanotransduction in ECs and SMCs from the same donor, to understand cellular differences on a molecular level. Our results may provide a basis for further approaches in tissue engineering and post-implantation wound healing.

9 Static and pulsed electrical fields

Endogenous direct current electrical fields (dcEFs) exist in and around the vasculature and are also present in all developing and regenerating animal tissues, and are important for wound healing [168, 136]. Electrical fields may be involved in maintaining a healthy state at the endothelial cell (EC) interface, which is a common interest in recent research [172]. In addition to having an effect in the health of established blood vessels, electrical stimulation has emerged as an approach to induce the formation of new blood vessels (angiogenesis) *in vivo* [99, 158, 37, 61](see also section 2.2.2). In this thesis, ECs and smooth muscle cells (SMCs) were observed under dcEFs and extremely low frequency pulsed electrical fields (ELFP-EFs). Differences in their orientation and migration characteristics could be measured and analyzed in detail with the controller model of Kemkemer *et al.* [108, 74], which extracts important information from the raw data (see also section 4.4).

9.1 Vascular cells in direct current and pulsed physiological electrical fields

9.1.1 Automatic controller model of cell orientation and migration in direct current electrical fields

ECs and SMCs show two observable reactions to an applied dcEF: cell orientation and directed migration.

Existence of an automatic controller for cell orientation The existence of a cellular automatic controller (see chapter 4.4 for a description) was shown by altering the guiding signal (here an electrical field) and observing changes in cell orientation. The following signal-jump experiments were performed: For $t < t_0$ no guiding signal is applied and the cells orient randomly (apolar order parameter $\langle\cos(2\varphi)\rangle = 0$). Then, at time $t = t_0$ the dcEF is switched on. The cells react to the dcEF and align their long axis perpendicular to the applied guiding signal ($\langle\cos(2\varphi)\rangle \neq 0$). Example images of ECs and SMCs before and after alignment are shown in figure 9.1. Observation over time revealed that the apolar order parameter decreased in time and approached a new saturation value, see figures 9.2A and 9.3 for several electrical field strengths (from 50 mV/mm to 530 mV/mm). ECs and SMCs probably have an automatic controller for aligning their long axis with respect to an external electrical field. An overview over the time development of all experiments performed with the two cell types and different electrical field strengths is shown in figures 5 and 6, appendix 4.4.
The assumed mathematical structure of the machine equation (equation 4.5, see section

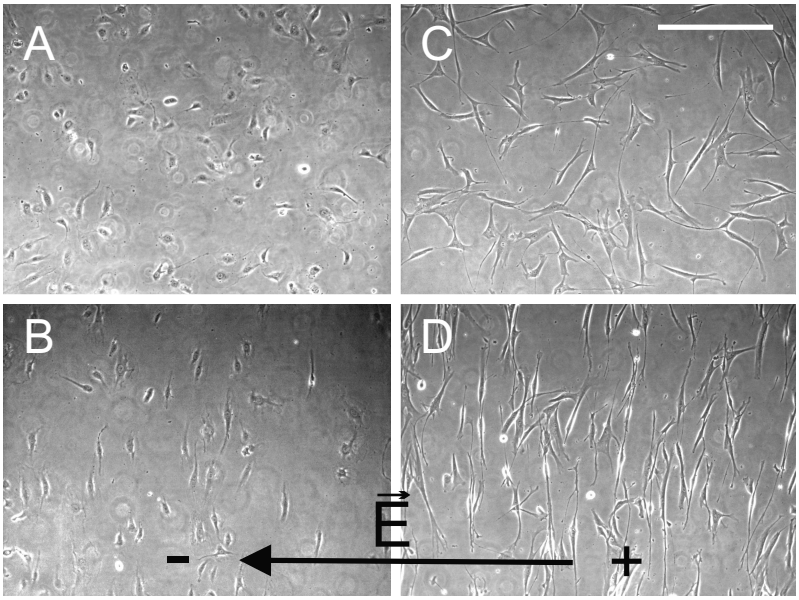

Figure 9.1: Endothelial (ECs) (A, B) and smooth muscle cells (SMCs) (C, D) before and after 6 h of electrical field application (200 mV/mm). Before application ECs and SMCs are orientated randomly (A, C), after E-field application, they align perpendicular to streamlines of the E-field (B, D); scalebar represents 400 μm.

4.4) is verified: the cellular response (here the cell reorientation after switching on the dcEF) depends on the guiding signal, which demonstrates the existence of a deterministic cellular signal. Furthermore, the random oriented cells, as long as no guding field is applied, show the existence of a stochastic signal.

Angle characteristics The angle characteristics, $g(\varphi)$, of the cellular detection unit were predicted by using the symmetry properties of the cells. This characteristic is basically described by the first nontrivial term: $sin(2\varphi)$ (see equation 4.6 section 4.4). A straight line is predicted (equation 4.9, section 4.4) if the logarithm of the measured angle distribution function is plotted versus $\cos(2\varphi)$. One example is shown in figure 9.2B. The signal-strength characteristic can be determined by analyzing the angle distribution function at different dcEF strengths. The logarithm of the experimentally found angle distribution function is plotted versus $\cos(2\varphi)$ and the slope, $\alpha_2 = \frac{k_2}{q} E^2$, of the straight line is determined. This procedure was repeated for different signal strengths (dcEF from 50 mV/mm to 533 mV/mm). A plot of the measured slope, α_2, versus the applied signal strength yields the desired characteristics of the detection unit, depicted in figure 9.4. A parabolic characteristic is obtained ($\alpha_2 = (K_G^E E)^2$, see chapter 4.4) where the electric guidance coefficient, K_G^E, characterizes the electric field sensitivity. ECs as well as SMCs reach saturation in response at $\approx$ 0.2 V/mm, see figures 9.3 and 9.4. Thus, the parabolic fit can only be applied for the first four data points. The obtained value is $K_G^E = \mathrm{i}\,4.69 \pm 0.18$ mm/V for ECs and $\mathrm{i}\,6.90 \pm 0.3$ mm/V for SMCs. The electric guidance coefficient K_G^E is an imaginary number since the desired orientation angle (set point) is perpendicular to the direction of the guiding signal.

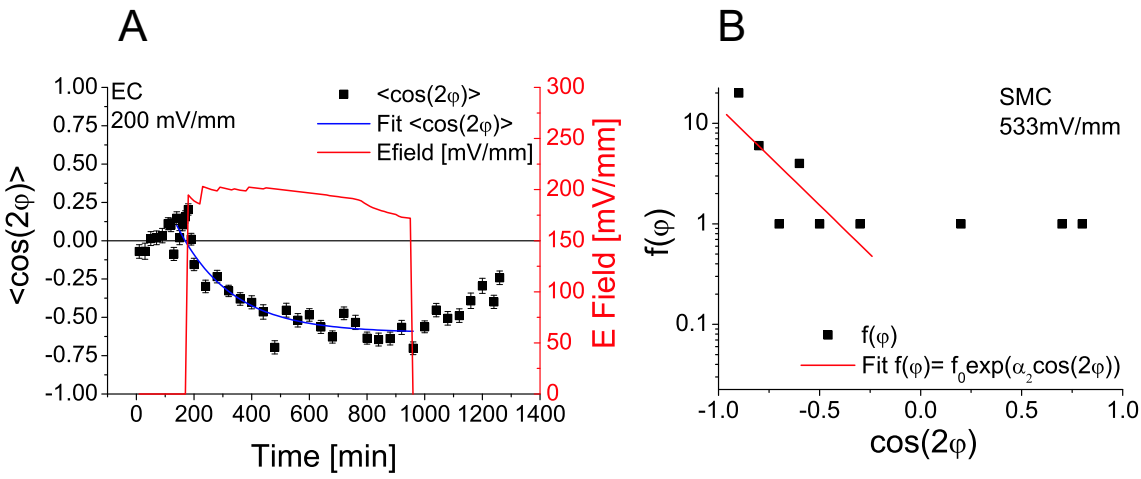

Figure 9.2: A: Example of the time development of $\langle\cos(2\varphi)\rangle$ of endothelial cells (ECs) in an electrical field of 200 mV/mm; blue line: fit of $\langle\cos(2\varphi)\rangle = \langle\cos(2\varphi)\rangle^{st}(1 - exp(-t - t_0)/\tau_2))$; B: Steady state distribution $f(\varphi)$ of $\cos(2\varphi)$ of smooth muscle cells (SMCs), with fit of $f(\varphi) = f_0 exp\,[\alpha_2 \cos(2\varphi)]$;

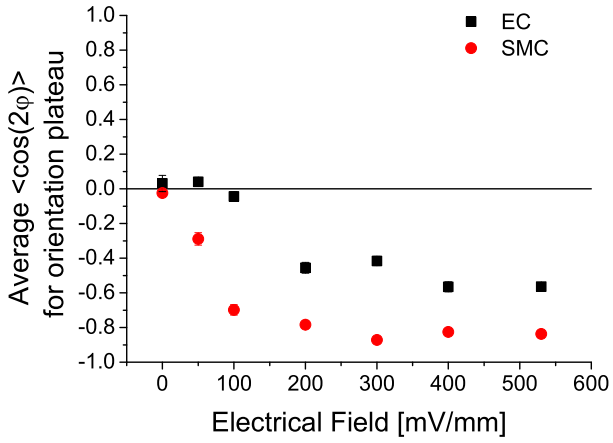

Figure 9.3: Summary of average oder parameter $\langle\cos(2\varphi)\rangle$ of endothelial (ECs) and smooth muscle cells (SMCs) in various electrical fields, measured after reaching saturation.

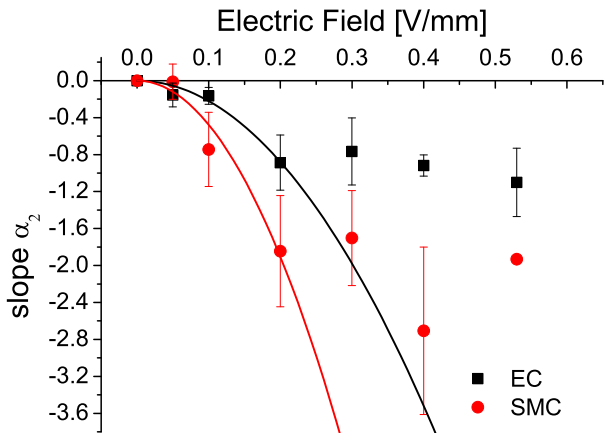

Figure 9.4: Parabolic fit of slope $\alpha_2 = (K_G^E E)^2$, which is plot vs the electrical field for endothelial (ECs) and smooth muscle cells (SMCs).

Steady-state dose-response curve The steady-state dose-response curve is of great physiological importance since it describes the mean orientation as a function of the applied guiding signal. A dimensionless representation is depcited in figure 9.5. The resulting line is a theoretical prediction (see equation 7 in appendix 3.5) based on the symmetry properties of the detection unit $g(\varphi, signal)$. The data points in figure 9.5 represent actual measurements. The experimentally determined values of ECs and SMCs orientation in electrical fields are according to the theoretical prediction (see section 4.4).

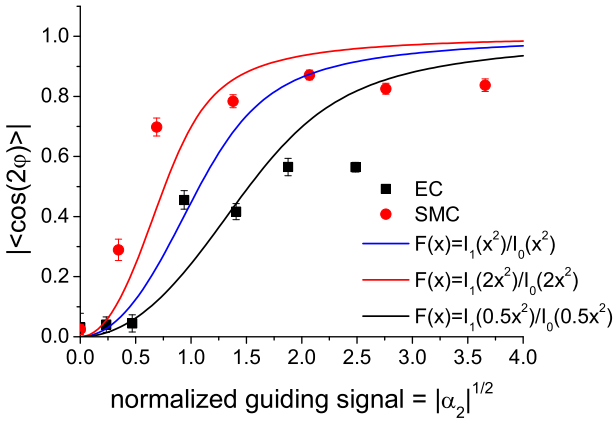

Figure 9.5: Steady-state dose-response curve for normalized order paramter $|\langle\cos(2\varphi)\rangle|$ and normalized guiding signal $|\alpha_2|^{1/2}$ of the two cell types (ECs and SMCs), fit: Bessel-functions

Temporal behavior of the automatic controller The stochastic source strength, q (see chapter 4.4), can be determined from signal-jump experiments. First, no dcEF is applied and the apolar order parameter is zero. At $t = 0$, a dcEF is switched on and the apolar

order parameter decreases in time until the saturation value, $\langle \cos(2\varphi) \rangle_{st}$, is reached. The temporal response can be described by a single exponential function with the characteristic time τ_2, see section 4.4, equation 4.12. A typical response curve and corresponding fit is shown in figure 9.2A.

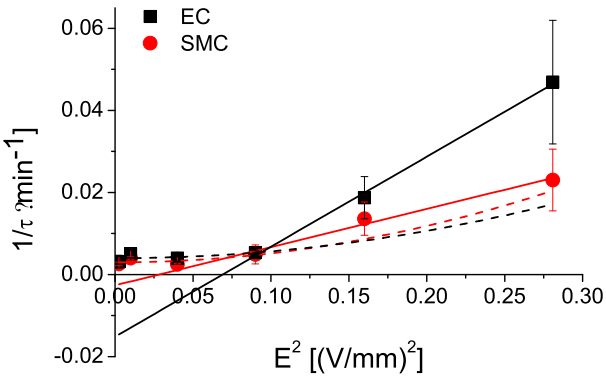

Figure 9.6: The inverse of the characteristic time τ_2 vs the square of the applied guiding field E, measured for endothelial (ECs) and smooth muscle cells (SMCs), linear (straight lines) and parabolic fit (dashed curves).

The characteristic time, τ_2, was measured for different electric field strengths. The results are shown in figure 9.6 where the inverse of the characteristic time, τ_2, is plotted versus the square of the applied guiding field, E. The experimental data can be compared with the predictions (see section 4.4, equation 4.8). The values obtained by the linear fit for the two investigated cell types are presented in tabel 9.1. The small (parabolic fit), as well as the large signal (straight line fit) approximation is in accordance with the experimentally determined values for ECs and SMCs, see figure 9.6. The absolute value of the electric guidance coefficient, K_G^E, can be calculated for ECs and SMCs by using the values, k_2 and q. The direct measured K_G^E of the steady-state dose-response curve is displayed in tabel 9.1.

cell type	k_2 $[mm^2/V^2/min]$	q $[min^{-1}]$	$K_G^E = \sqrt{\frac{k_2}{q}}$ $[mm/V]$	K_G^E**(*)** $[mm/V]$
EC	0.21 ± 0.01	-0.0151 ± 0.0021	$\mathrm{i}\,3.72 \pm 0.27$	$\mathrm{i}\,4.69 \pm 0.18$
SMC	0.08 ± 0.01	-0.0012 ± 0.0012	$\mathrm{i}\,8.16 \pm 4.11$	$\mathrm{i}\,6.90 \pm 0.3$

Table 9.1: Electric guiding coefficient K_G^E for endothelial (EC) and smooth muscle cells (SMC) calculated from time development (see figure 9.6: q is given by the intersection with the y-axis of the straight line fit; k_2 is the slope of the straight line, see also section 4.4) and steady-state dose-response curve(*).

Migration of endothelial and smooth muscle cells in dc electrical fields

ECs' and SMCs' migrational behavior was observed with and without the application of dcEFs. In figure 9.7 path plots are depicted, which show the random walk of ECs and

SMCs in the control experiments. From the graphs clearly different migration directions for each tracked cell can be obtained.

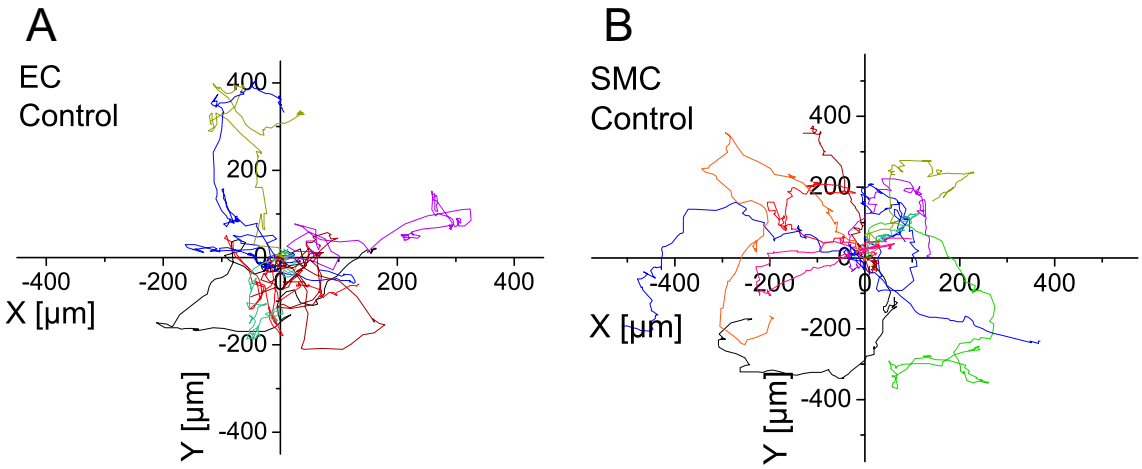

Figure 9.7: Path plot of ECs (A) and SMCs (B) under control conditions (no EF application). Cells show a random walk during 20 hours of observation.

During application of a dcEF, ECs start to migrate towards the cathode (negative x-direction, see figure 9.8A). Apart from the directed migration in negative x-direction, the cells' paths still show a statistical noise (random walk) in y-direction, see figure 9.8 for an example. Contrarily, SMCs migrate after EF-application in y-direction on equipotential lines (see figure 9.9A), in the same direction as their cell shape orientation (see paragraphs above).

Temporal behavior As the directed migration of the ECs along the direction of the electrical field cannot be described with a nonplar order parameter, the single cell steps per time period (10min) were analyzed with the help of the polar order parameter $\langle\cos(\varphi)\rangle$, see figure 9.8B (for the description and explanation of the polar order paramter, see section 4.4). The polar order parameter shows clearly a time dependence after switching on the EF, which can be described with a similar function as for the cell orientation, shown in figure 9.8B (temporal behavior function 4.13). The characteristic time, τ_1 for the depicted example of ECs (figure 9.8) is 60.24 ± 12.18 min. Contrary to the orientation controller, ECs' automatic controller for migration can distinguish between the sign of the EF.
An example path-plot and the time development of the order parameter of SMCs are depicted in figure 9.9. The response of SMCs is significant different to that of the ECs. SMCs migrate on equipotential lines, perpendicular to the applied EF. This behavior can be described with the apolar order parameter $\langle\cos(2\varphi)\rangle$. The time development can again be fit with equation 4.12 like in the orientation analysis. The characterisic time τ_2 for the depicted SMC example (figure 9.9B) is 268 ± 94 min. The detection unit and controller mechanism of migration of SMCs seems to function similarly to their orientation controller. In contrast to the ECs, SMCs give no measurable response to the sign of the applied EF. Most of the obtained time-lapse data for this study show a high signal-to-noise ratio or have no statistic relevance, as too few cell paths could be tracked. Therefore, no steady-state analysis and no electric field time-dependence can be presented so far. Further analysis of the steady-state and the time-dependence was not possible for the migration data due

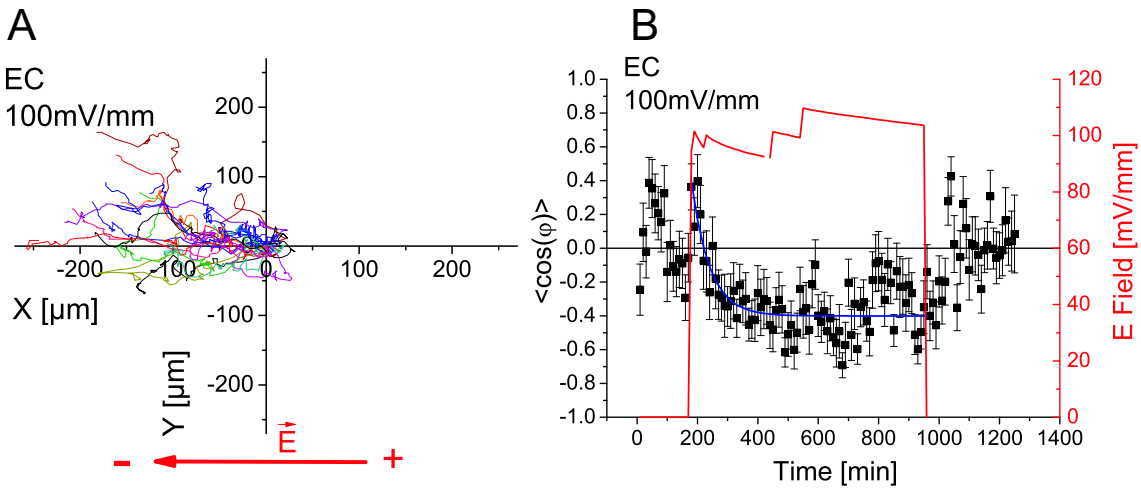

Figure 9.8: A: One example of a path plot of directed migration of endothelial cells (ECs) in a dcEF of 100 mV/mm, observed for 10 hours. The arrow indicates the direction of the dcEF. B: Order paramter $\langle\cos(\varphi)\rangle$ with time development fit $\langle\cos(\varphi)\rangle = \langle\cos(\varphi)\rangle^{st}\,(1 - exp(-t - t_0)/\tau_1))$ and applied dcEF for the same example as in A.

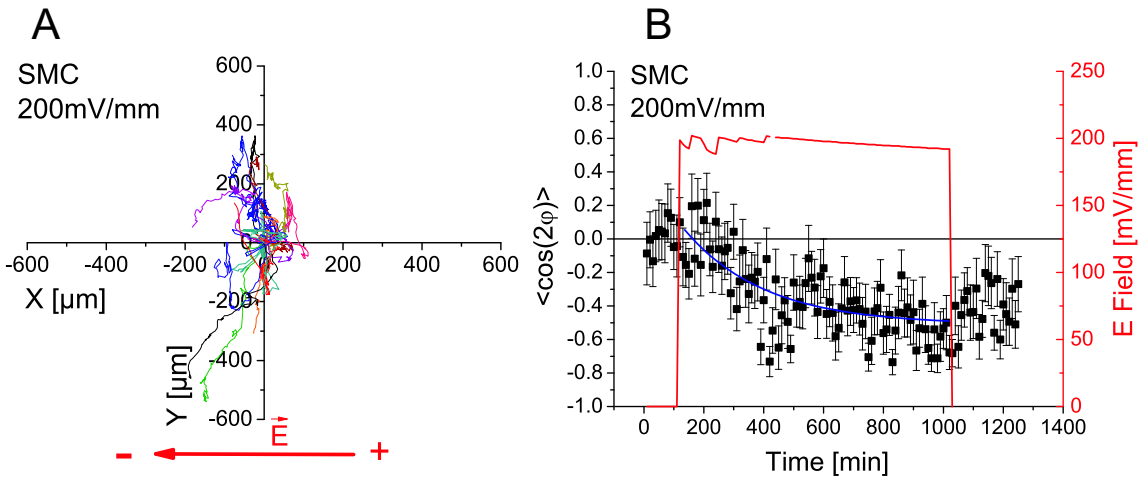

Figure 9.9: A: One example of a path plot of directed migration of smooth muscle cells (SMCs) in a dcEF of 200 mV/mm, observed for 10 hours. The arrow indicates the direction of the dcEF. B: Order paramter $\langle\cos(2\varphi)\rangle$ with time development fit $\langle\cos(2\varphi)\rangle = \langle\cos(2\varphi)\rangle^{st}\,(1 - exp(-t - t_0)/\tau_2))$ and applied dcEF for the same example as in A.

to a high signal-to-noise level of the polar and apolar order parameters and the lack of statistical relevant data. However, from the examples in figures 9.8 and 9.9 and the other data (not shown) no tendency of EF strength dependency for the temporal behavior of migration could be found.

9.1.2 Vacular cells in pulsed electrical fields

Extreme low frequency pulsed electrical fields (ELFP-EFs) from 3.5 to 20 pulses per minute (PpM) and 1 sec long pulses ($\approx 1\,\mathrm{V/mm}$) were applied to observe the behavior of ECs and SMCs.

Orientation of cells in ELFP-EFs The cellular responses can be compared to those after application of dcEFs and images before and after the application of ELFP-EFs were similar to those depicted in figure 9.1. Observation of cellular orientation over time made clear that the apolar order parameter decreased in time and approached a new saturation level, see figure 9.10 and figures 7 and 8 in appendix 4.4 for several pulse doses. However, the analysis of the characteristic time τ_2 did not yield a pulse frequency dependence for the used parameters. Accordingly, the steady state analysis of α_2 revealed no clear frequency or dose dependence, so that it was not possible to calculate an 'electric frequency guiding coefficient'.

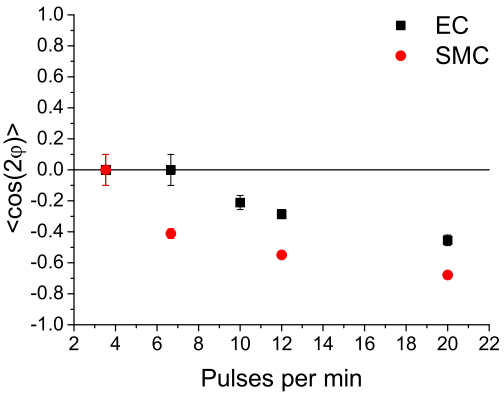

Figure 9.10: Summary of average order parameter $\langle\cos(2\varphi)\rangle$ of endothelial (ECs) and smooth muscle cells (SMCs) in various ELFP-EFs, measured after reaching saturation.

Migration in ELFP-EFs The migration response of ECs and SMCs in ELFP-EFs can clearly be compared to the one in dcEFs. In figure 9.11, example path plots of tracked ECs and SMCs are depicted. ECs migrate clearly in direction of the cathode (here negative x-direction) and SMCs on equipotential lines in $\pm y$-direction. In contrast to the experiments of ECs and SMCs in dcEFs, it was not possible to analyze the polar or apolar parameter with the described controller model because the signal-to-noise ratio was too high to fit the data and to gain any characteristic parameters.

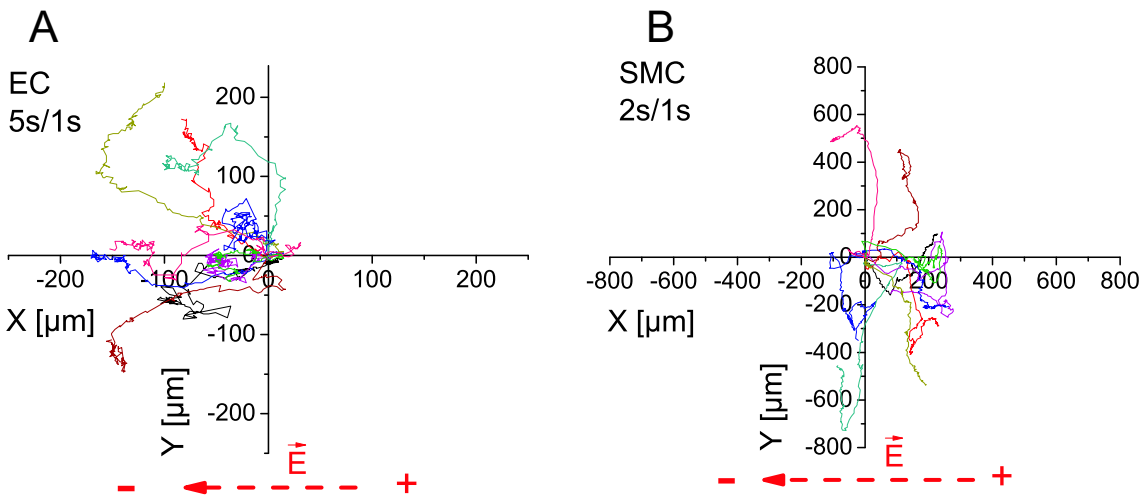

Figure 9.11: Examples of directed migration of ECs and SMCs under ELFP-EFs. ECs migrate in direction of the cathode (negative x-direction) (A), SMCs migrate mainly on equipotential lines in the $\pm y$-direction (B).

9.2 Discussion and conclusions

Electrical fields induce oriented alignment and directional migration in ECs and SMCs. Migration and orientation of vascular cells are important cellular behaviors underlying angiogenesis and vascular remodeling. It was observed in the course of this work that applied electrical fields (direct current and pulsed) induced distinct heterogeneous responses in different vascular cells and understanding this behavior is important for the potential control of angiogenesis by endogenous or exogenously applied electrical stimulation.

Automatic controller As there are different levels of understanding of biological phenomena, an automatic controller model was used to fit the data and to gain quantitative characteristic details of the different cell responses. In the case of cellular orientation and migration the single molecular steps of the signal transduction pathways are not yet fully understood. However, at the phenomenological level, a given response can be thought of as being controlled by a machine or automatic controller: The properties of this controller can then be studied and modeled, providing some insight into the nature of the response mechanism, without knowing all of the molecular steps involved [108, 74]. The existence of an automatic controller could be verified for both cell types regarding their orientation. For migration the tendency towards automatic control mechanisms could be observed but not further quantified.

Orientation Although both cell types orient perpendicular to an applied dcEF, the data reveal that ECs and SMCs react differently in the presence of increasing electrical field strengths. The orientation of SMCs is more pronounced than that of ECs for all field strengths. The steady-state analysis (figures 9.3 and 9.4) indicated that the cells reached a saturated response level at around 200mV/mm. For further studies it would be interesting to find a threshold field strength for the two cell types above which cells do not react anymore and whether the two cell types could be separated by this. The different values

of the electric guidance coefficient K_G^E, depending on the analysis approach (steady state or temporal), can be explained by the saturation level, which is reached at 200 mV/mm and gives not enough values for fitting the data accurately. Nevertheless, a general tendency was recognized: ECs have a electric guiding coefficient, about 35 to 65% smaller than that for SMCs, which indicates that SMCs have a higher electric field sensitivity than ECs. The cellular orientation response in pulsed electrical fields seemed to be dose dependent (see also images in appendix 4.4). Further studies, however, are required to find a frequency, pulse length, or pulse-amplitude dependence and to determine if this could enhance new blood vessel formation *in vivo* (angiogenesis).

Migration Although the data obtained were statistically not relevant for further analysis with the controller model, the experiments performed using dcEFs and ELFP-EFs on ECs and SMCs yielded several interesting observed trends in their migration behavior. ECs have a different migration response than SMCs under a polar guiding signal like an EF. Intriguingly, ECs migrate in a perpendicular direction to their orientational axis and to the migration direction of SMCs (which align in the same direction as ECs). The human coronary artery ECs, observed here, do sense the sign of the EF and migrate towards the negative pole (cathode) along the field direction. This is in contrast to umbilical vein ECs investigated by Bai *et al.* [7]. Bai *et al.* also observed human microvascular ECs, which also migrate towards the negative pole. It can be concluded that, in the context of migration in an EF, the response of coronary and microvascular ECs can be compared. The human coronary artery SMCs, observed here, behave differently than the murine aorta SMCs investigated by Bai *at al.* [7]. In their study, SMCs migrated mainly in the anodal direction, which was not observed in the case presented here. Here, SMCs migrated along eqipotential lines, perpendicular to the electric guiding field. The presented findings are not surprising: Different types of cells respond to electrical fields by migration toward different poles [168]. Some cells migrate cathodally, for instance, neural crest cells, corneal epithelial cells, epidermal keratinocytes, pigmented retinal epithelium, embryonic fibroblasts, osteoblasts, and bovine aortic endothelial cells [119, 195, 54, 34, 128, 186]. Other cells migrate anodally, such as fibroblasts, osteoclasts, and peritoneal macrophages [186, 223, 154]. Intriguingly, lens epithelial cells migrate either cathodally or anodally, depending on EF strength [209]. How cells sense and transduce electric signals remains largely unknown. Some explanations speculate that Ca^{2+} ion concentrations are present at the leading edge of the migrating cell [145]. The exact molecular pathway can be neglected and analyzed if the cell response is with the theory of an automatic controller. In the case of directed response, a proportional controller is also used by different cell types to correct their angle of migration [108]. The ECs investigated here show an automatic controller tendency, which can be described with the analysis of the temporal development of a polar order parameter ($< \cos(\varphi) >$). The response of the SMCs can be described with the same controller as the orientation, because their migration direction satisfies mirror-symmetry as it neither indicates a recognition of the sign of the E-field, nor a preferred direction ($\pm y$-direction).

Pulsed versus dc electrical field In general, it can be concluded that the migration and the orientation response in ELFP-EFs is too weak to make quantitative statements. More statistical relevant data has to be obtained to be able to calculate orientation character-

istics as was performed for cells in dcEFs. Signs for an automatic controller mechanism of cells in pulsed fields were found in other studys. Under uniform pulsed fields, neurites showed a preferential orientation toward the cathode pole of the field in a manner similar to that previously found for dc fields. The extent of neurite orientation depended upon the duration, amplitude, and frequency of the pulse, but appeared to be similar to that produced by a uniform dc field of an equivalent time-averaged field intensity [157]. In further studies with vascular cells, different pulse frequency, amplitudes and lengths should be tested to determine the machine characteristics of a possible automatic controller mechanism.

Conclusion Small dcEFs and ELFP-EFs of a size equivalent to those that arise immediately at a wound induced significant directional migration and orientation responses of vascular endothelial cells and SMCs. Distinct heterogeneity in the responses existed between the two types of vascular cells tested. For the orientation response the difference could be quantified with the help of an automatic controller model. For migration it can be stated that ECs can sense the sign of the electric guiding field, migrating toward the cathode, whereas SMC do not sense the sign and migrate along equipotential lines. This may have potential physiological and clinical implications in areas where electrical stimulation is used to promote angiogenesis or vasculature remodeling. Furthermore, in the context of after implantation wound healing, it would be interesting to study the electrical impact of different metallic implant coatings on their vascular surrounding.

Summary

Vascular diseases and the associated problems with wound healing after stent implantation are still a major health threat in modern society. Understanding the regulation and functions of the vasculature could lead to substantial improvements in the treatment of these costly, widespread diseases. Furthermore, results which help to shed some light to the intricate signaling pathways responsible for angiogenesis could help to increase healing chances of cancer and other tumors. In the regulation and function of vascular cells a multitude of extracellular signals is involved, such as messenger molecules, extracellular matrix, pulsatile blood flow and endogenous electrical fields. Consequently, the research conducted in this thesis was focused on the investigation of the interaction of some of the aforementioned extracellular signals and vascular cells, namely endothelial cells (ECs) and smooth muscle cells (SMCs). Moreover, the final intention was to find cell-specific differences in the two cell types that would allow to separately stimulate ECs and SMCs. This process could promote divergent behaviors of the two cell types that will bring developments in tissue engineering and improvements in intravascular wound healing.

In a first phase of the project, cell spreading and proliferation was tested and compared on different stent coatings. The quantitative and qualitative analysis made clear that in contrast to the behavior of the SMCs, ECs showed a more sensitive response to the various surface types, when it comes to the initial adhesion and long term behavior. The stent-study revealed that cellular responses are influenced by a combination of several surface characteristics, which could not be distinguished within this experimental setup. Therefore, the following set of experiments aimed to investigate the effects of topographic or chemical stimulating factors independently.

To understand the role played by the microtopography of a substrate, which is an important feature for controlling cell response upon contact with an implant or with biomaterials, vascular cells were observed on biologically inert, well defined micro-nano grooves. The behavior of ECs and SMCs was systematically investigated regarding morphology and compared with human fibroblast cells (FCs), which are also important for healing and maintenance in the vascular system. All three cell types demonstrated a general behavior: cell orientation was more pronounced with smaller lateral spacing and with increasing depth of the grooves. Specifically, FCs aligned and migrated along the grooved surface structures to a larger extend than ECs and SMCs. Furthermore, no significant difference was measured in the response between ECs and SMCs to the grooves.

As topography alone was not sufficient to provoke divergent behavioral responses, the influence of biofunctionalized nanostructured surfaces on ECs and SMCs was examined.

The gold nanostructures on glass slides were decorated with different ligands of extracellular matrix (ECM) motifs (RGD and REDV) and specific cell-cell-contact proteins, like vascular endothelial cadherins (VE-Cad). The nanostructures consisted of arrays of gold nano-dots with defined, tunable spacings. In between these anchoring points, the surface was passivated. As a result of the cell assays on these surfaces, the relevant distance (between 40 and 90nm) for integrin clustering and binding to ECM-peptides was confirmed for vascular cells on REDV compared to the previous investigated RGD on other cell types. The integrin clustering starts a cascade of signaling pathways that ultimately lead to successful spreading. Spreading behavior and focal adhesion formation of vascular cells was found to be similar to other cell types. VE-Cad-ligands decreased cellular adhesion significantly on the tested ligand distances, but also induced a distance-dependent behavior, which could be observed in less adhesion of the cells on wider ligand distances. Furthermore, no significant differences between ECs and SMCs behaviors on these nanopatterned and biofunctionalized surfaces could be found.

In addition to investigate the influence of surface properties on cells, the reaction of vascular cells upon application of external guiding fields like uniaxial cyclic strain and directed electrical fields was observed. The cyclic strain with several frequencies was applied to the cells via a stretchable membrane on which the cells were seeded. A cell specific frequency-dependent orientation response of ECs and SMCs was demonstrated. Additionally, a cell-type dependent lower threshold frequency was found, below which no reorientation occurred (0.1Hz for ECs, 1Hz for SMCs). The SMCs' orientation response was less pronounced and slower than that of the ECs. Immunohistochemistry stainings of actin fibers and focal adhesion markers in fixed cells could further confirm reorientation of the cytoskeleton. For ECs, the reorientation has a temporal, exponential characteristic, which was quantified by an automatic-controller model.

Another extracellular guiding signal, whose influence on cells was investigated in this thesis, was the electrical field. Direct current electrical fields (dcEFs) and extremely-low frequency pulsed electrical fields (ELF-EFs) of a magnitude equivalent to those that arise immediately at a wounding event, induced significant directional migration and orientation responses of ECs and SMCs. Distinct heterogeneity in the responses existed between the two types of vascular cells tested. The difference in orientation response was quantified with the help of an automatic-controller model. For migration it could be observed that ECs can sense the sign of the electric guiding field, migrating toward the cathode, whereas SMC migrate along equipotential lines.

In conclusion, ECs and SMCs show cell-type specific responses towards several extracellular signals. The herein investigated surface modifications by topography or bionanopatterning, could not stimulate significant differences in the responses of the two vascular cell types under discussion. Upon application of cyclic stretch and electrical fields, significant differences in the cellular responses of ECs and SMCs could be found and quantitatively described with an automated controller model. To deepen the understanding of the crucial functions of biochemical processes in ECs and SMCs, further studies could include the investigation of molecular signal transduction pathways in vascular cells. Furthermore, the results of the investigations with electrical fields may have potential physiological and clinical applications in areas where electrical stimulation is used to promote angiogenesis or vasculature remodeling. To determine the appropriate mixture of signals, future studies to examine how ECs and SMCs respond to a designed combination of extracellular stimuli would be of great interest. This limited sensitivity to surface signals means that

it's necessary to introduce further signals (e.g. cell type specific drugs) to stimulate cell-type-specific spreading behavior, directed migration or proliferation responses. Hopefully, deeper insight into the mechanisms of cell-signal interactions will help to develop future surface coatings for implants and increase wound healing after (stent) implantation.

List of Figures

Bibliography

[1] B. Alberts, A. Johnson, P. Walter, J. Lewis, M. Raff, and K. Roberts. *Molecular Biology of the Cell*. Tayler and Francis, London, 2008.

[2] A.-S. Andersson, P. Olsson, U. Lidberg, and D. Sutherland. The effects of continuous and discontinuous groove edges on cell shape and alignment. *Experimental Cell Research*, 288:177–188, 2003.

[3] K. Anselme and M. Bigerelle. Modelling approach in cell/material interactions studies. *Biomaterials*, 27(8):1187–1199, 2006.

[4] M. Arnold, E.A. Cavalcanti-Adam, R. Glass, J. Blümmel, W. Eck, M. Kantlehner, H. Kessler, and J.P. Spatz. Activation of integrin function by nanopatterned adhesive interfaces. *ChemPhysChem*, 5(3):383–388, 2004.

[5] M. Arnold, V.C. Hirschfeld-Warneken, T. Lohmüller, P. Heil, J. Blümmel, E.A. Cavalcanti-Adam, M. López-García, P. Walther, H. Kessler, B. Geiger, and J.P. Spatz. Induction of cell polarization and migration by a gradient of nanoscale variations in adhesive ligand spacing. *Nano Lett*, 8(7):2063–2069, 2008.

[6] H. S. Badeer. *Cardiovascular Physiology*. Karger, Basel, New York, 1984.

[7] H. Bai, C.D. McCaig, J.V. Forrester, and M. Zhao. Dc electric fields induce distinct preangiogenic responses in microvascular and macrovascular cells. *Arterioscler Thromb Vasc Biol*, 24(7):1234–1239, 2004.

[8] N. Q. Balaban, U. S. Schwarz, D. Riveline, P. Goichberg, G. Tzur, I. Sabanay, D. Mahalu, S. Safran, A. Bershadsky, L. Addadi, and B. Geiger. Force and focal adhesion assembly: a close relationship studied using elastic micropatterned substrates. *Nat Cell Biol*, 3(5):466–472, 2001.

[9] E. Baldi, D. Baldi, and B.J. Lithgow. A pilot investigation of the effect of extremely low frequency pulsed electromagnetic fields on humans' heart rate variability. *Bioelectromagnetics*, 28(1):64–68, 2007.

[10] A. Banes, J. Gilbert, D. Taylor, and O. Monbureau. A new vacuum-operated stress-providing instrument that applies static or variable duration cyclic tension or compression to cells in vitro. *Journal of Cell Science*, 75:35–42, 1985.

[11] G. Bao and S. Suresh. Cell and molecular mechanics of biological materials. *Nature Materials*, 2:715–25, 2003.

[12] C. A. Bassett, R.J. Pawluk, and R.O. Becker. Effects of electric currents on bone in vivo. *Nature*, 204:652–654, 1964.

[13] A. Benbrahim, G.J. L'Italien, C.J. Kwolek, M.J. Petersen, B. Milinazzo, J.P. Gertler, W.M. Abbott, and R.W. Orkin. Characteristics of vascular wall cells subjected to dynamic cyclic strain and fluid shear conditions in vitro. *Journal of Surgical Research*, 65:119–127, 1996.

[14] A.D. Bershadsky, C. Ballestrem, L. Carramusa, Y. Zilberman, B. Gilquin, S. Khochbin, A.Y. Alexandrova, A. B. Verkhovsky, T. Shemesh, and M.M. Kozlov. Assembly and mechanosensory function of focal adhesions: experiments and models. *Eur J Cell Biol*, 85:165–173, 2006.

[15] H.M. Blau and D. Baltimore. Differentiation requires continuous regulation. *J Cell Biol*, 112(5):781–783, 1991.

[16] J. Blümmel, N. Perschmann, D. Aydin, J. Drinjakovic, T. Surrey, M. López-García, H. Kessler, and J.P. Spatz. Protein repellent properties of covalently attached peg coatings on nanostructured sio2-based interfaces. *Biomaterials*, 28:4739–4747, 2007.

[17] M. Boltau, S. Walheim, J. Mlynek, G. Krausch, and U. Steiner. Surface-induced structure formation of polymer blends on patterned substrates. *Nature*, 391(6670):877–879, 1998.

[18] S. Britland, H. Morgan, B. Wojiak-Stodart, M. Riehle, A. Curtis, and C. Wilkinson. Synergistic and hierarchical adhesive and topographic guidance of bhk cells. *Experimental cell research*, 228(2):313–325, 1996.

[19] D.M. Brunette. Fibroblasts on micromachined substrata orient hierarchically to grooves of different dimensions. *Experimental cell research*, 164(1):11–26, 1986.

[20] D.M. Brunette and B. Chehroudi. The effects of the surface topography of micromachined titanium substrata on cell behavior in vitro and in vivo. *Journal of biomechanical engineering*, 121:49–57, 1999.

[21] R.C. Buck. Behavior of vascular smooth muscle cells during repeated stretching of the substratum in vitro. *Atherosclerosis*, 46:217–223, 1983.

[22] E.A. Cavalcanti-Adam, A. Micoulet, J. Blümmel, J. Auernheimer, H. Kessler, and J.P. Spatz. Lateral spacing of integrin ligands influences cell spreading and focal adhesion assembly. *Eur J Cell Biol*, 85(3-4):219–224, 2006.

[23] E.A. Cavalcanti-Adam, P. Tomakidi, M. Bezler, and J.P. Spatz. Geometric organization of the extracellular matrix in the control of integrin-mediated adhesion and cell function in osteoblasts. *Prog Orthod*, 6(2):232–237, 2005.

[24] E.A. Cavalcanti-Adam, T. Volberg, A. Micoulet, H. Kessler, B. Geiger, and J.P. Spatz. Cell spreading and focal adhesion dynamics are regulated by spacing of integrin ligands. *Biophys J*, 92(8):2964–2974, 2007.

[25] J. L. Charest, M.T. Eliason, A.J. Garcia, and W.P. King. Combined microscale mechanical topography and chemical patterns on polymer cell culture substrates. *Biomaterials*, 27:2487–2494, 2006.

[26] C. S. Chen, J. Tan, and J. Tien. Mechanotransduction at cell-matrix and cell-cell contacts. *Annu Rev Biomed Eng*, 6:275–302, 2004.

[27] M.-C. Chen, Y. Chang, C.-T. Liu, W.-Y. Lai, S.-H. Peng, Y.-W. Hung, H.-W. Tsai, and H.-W. Sung. The characteristics and in vivo suppression of neointimal formation with sirolimus-eluting polymeric stents. *Biomaterials*, 30:79–88, 2009.

[28] H.H. Cho, D.-W. Han, K. Matsumura, S. Tsutsumi, and S.-H. Hyon. The behavior of vascular smooth muscle cells and platelets onto epigallocatechin gallate-releasing poly(l-lactide-co-epsilon-caprolactone) as stent-coating materials. *Biomaterials*, 29(7):884–893, 2008.

[29] S. Choudhary, K. Haberstroh, and T.J. Webster. Enhanced functions of vascular cells on nanostructured ti for improved stent applications. *Tissue Engineering*, 13, 2007.

[30] M. Chrzanowska-Wodnicka and K. Burridge. Rho-stimulated contractility drives the formation of stress fibers and focal adhesions. *J Cell Biol*, 133(6):1403–1415, 1996.

[31] T.-Z. Chung, D.-Z. Liu, S.-Y. Wang, and S.-S. Wang. Enhancement of the growth of human endothelial cells by surface roughness at nanometer scale. *Biomaterials*, 24:4655–4661, 2003.

[32] J.D. Cohen. Overview of physiology, vascular biology, and mechanisms of hypertension. *J Manag Care Pharm*, 13:6–8, 2007.

[33] M. Cohen, D. Joester, B. Geiger, and L. Addadi. Spatial and temporal sequence of events in cell adhesion: from molecular recognition to focal adhesion assembly. *ChemBioChem*, 5(10):1393–1399, 2004.

[34] M.S. Cooper and M. Schliwa. Motility of cultured fish epidermal cells in the presence and absence of direct current electric fields. *J Cell Biol*, 102(4):1384–1399, 1986.

[35] R. Coronel, F.J. Wilms-Schopman, T. Opthof, F.J. van Capelle, and M.J. Janse. Injury current and gradients of diastolic stimulation threshold, tq potential, and extracellular potassium concentration during acute regional ischemia in the isolated perfused pig heart. *Circ Res*, 68(5):1241–1249, 1991.

[36] D.R. Critchley. Focal adhesions - the cytoskeletal connection. *Curr Opin Cell Biol*, 12(1):133–139, 2000.

[37] P. Cuevas and E. Asin-Cardiel. Electromagnetic therapeutic angiogenesis: the next step. *Neurol Res*, 22(4):349–350, 2000.

[38] A. Curtis and C. Wilkinson. Nantotechniques and approaches in biotechnology. *Trends Biotechnol*, 19(3):97–101, 2001.

[39] A.S. Curtis, M. Dalby, and N. Gadegaard. Cell signaling arising from nanotopography: implications for nanomedical devices. *Nanomedicine*, 1(1):67–72., 2006.

[40] A.S. Curtis and C.D. Wilkinson. Reactions of cells to topography. *Journal of biomaterials science*, 9:1313–1329, 1998.

[41] M.J. Dalby, N. Gadegaard, R. Tare, A. Andar, M.O. Riehle, P. Herzyk, C.D.W. Wilkinson, and R.O.C. Oreffo. The control of human mesenchymal cell differentiation using nanoscale symmetry and disorder. *Nat Mater*, 6(12):997–1003, 2007.

[42] M.J. Dalby, M.O. Riehle, H. Johnstone, S. Affrossman, and A.S. Curtis. Investigating the limits of filopodial sensing: a brief report using sem to image the interaction between 10 nm high nano-topography and fibroblast filopodia. *Cell biology international*, 28:229–236, 2004.

[43] M.J. Dalby, M.O. Riehle, D.S. Sutherland, H. Agheli, and A.S. Curtis. Use of nanotopography to study mechanotransduction in fibroblasts–methods and perspectives. *European journal of cell biology*, 83:159–169, 2004.

[44] M.J. Dalby, M.O. Riehle, D.S. Sutherland, H. Agheli, and A.S. Curtis. Morphological and microarray analysis of human fibroblasts cultured on nanocolumns produced by colloidal lithography. *European cells & materials*, 9:1–8, 2005.

[45] P. C. Dartsch and H. Hämmerle. Orientation response of arterial smooth muscle cells to mechanical stimulation. *Euopean Journal of Biology*, 41:339–346, 1986.

[46] P. C. Dartsch, H. Hämmerle, and E. Betz. Orientation of cultured arterial smooth muscle cells growing on cyclically stretched substrates. *Acta Anat*, 125:108–113, 1986.

[47] P.F. Davies. Flow-mediated endothelial mechanotransduction. *Physiol Rev.*, 75:519–560, 1995.

[48] R. De, A. Zemel, and S.A. Safran. Dynamics of cell orientation. *Nature Physics*, 3:655–659, 2007.

[49] G. De Luca, H. Suryapranata, G. Gregorio, H. Lange, and M. Chiariello. Homocysteine and its effects on in-stent restenosis. *Circulation*, 112(19):e307–e311, 2005.

[50] S. Dhein, F.W. Mohr, and M. Delmar. *Practical Methods in Cardiovascular Research*. Spinger, Heidelberg, New York, 2005.

[51] D. E. Discher, P. Janmey, and Y. L. Wang. Tissue cells feel and respond to the stiffness of their substrate. *Science*, 310(5751):1139–1143, 2005.

[52] D.L. Elbert and J.A. Hubbell. Conjugate addition reactions combined with free-radical cross-linking for the design of materials for tissue engineering. *Biomacromolecules*, 2(2):430–441, 2001.

[53] E.M. Erb, K. Tangemann, B. Bohrmann, B. Müller, and J. Engel. Integrin $\alpha_{IIb}\beta_3$ reconstituted into lipid bilayers is nonclustered in its activated state but clusters after fibrinogen binding. *Biochemistry*, 36(24):7395–7402, 1997.

[54] C.A. Erickson and R. Nuccitelli. Embryonic fibroblast motility and orientation can be influenced by physiological electric fields. *J Cell Biol*, 98(1):296–307, 1984.

[55] D.S. Faber and H. Korn. Electrical field effects: their relevance in central neural networks. *Physiol Rev*, 69(3):821–863, 1989.

[56] H.M. Finlay, P. Whittaker, and P.B. Canham. Collagen organization in the branching region of human brain arteries. *Stroke*, 29:1595–1601, 1998.

[57] A.V. Finn, G. Nakazawa, M. Joner, F.D. Kolodgie, E.K. Mont, H.K. Gold, and R. Virmani. Vascular responses to drug eluting stents: importance of delayed healing. *Arterioscler Thromb Vasc Biol*, 27(7):1500–1510, 2007.

[58] I. Fishbein, I.S. Alferiev, O. Nyanguile, R. Gaster, J.M. Vohs, G.S. Wong, H. Felderman, I.-W. Chen, H. Choi, R.L. Wilensky, and R.J. Levy. Bisphosphonate-mediated gene vector delivery from the metal surfaces of stents. *PNAS*, 103(1):159–164, 2006.

[59] R.J. Fitzsimmons, D.D. Strong, S. Mohan, and D.J. Baylink. Low-amplitude, low-frequency electric field-stimulated bone cell proliferation may in part be mediated by increased igf-ii release. *J Cell Physiol*, 150(1):84–89, 1992.

[60] J.T. Flaherty, J.E. Pierce, V.J. Ferrans, D.J. Patel, W.K. Tucker, and D.L. Fry. Endothelial nuclear patterns in the canine arterial tree with particular reference to hemodynamic events. *Circulation Research*, 30:23–33, 1972.

[61] J. Folkman. Angiogenesis in cancer, vascular, rheumatoid and other disease. *Nat Med*, 1(1):27–31, 1995.

[62] J. Folkman. Angiogenesis: an organizing principle for drug discovery? *Nat Rev Drug Discov*, 6(4):273–286, 2007.

[63] M. Frick and F. Weidinger. Endothelial function: a surrogate endpoint in cardiovascular studies? *Current pharmaceutical design*, 13:1741–1750, 2007.

[64] R. H. Gavin, editor. *Methods in Molecular Biology: Cytoskeleton Methods and Protocols, Vol. 161.* Humana Press Inc., Totowa, NJ, 2000.

[65] B. Geiger, A. Bershadsky, R. Pankov, and K. M. Yamada. Transmembrane crosstalk between the extracellular matrix–cytoskeleton crosstalk. *Nat Rev Mol Cell Biol*, 2(11):793–805, 2001.

[66] B. Geiger, J.P. Spatz, and A.D. Bershadsky. Environmental sensing through focal adhesions. *Nat Rev Mol Cell Biol*, 10(1):21–33, 2009.

[67] P. Girard and J.P. Blümmel, J. Spatz. Mimicking cadherin-mediated cell-cell adhesion. *European Biophysics Journal*, 34(6):556, 2005.

[68] R. Glass, M. Arnold, J. Blümmel, A. Küller, M. Möller, and J.P. Spatz. Micro-nanostructured interfaces fabricated by the use of inorganic block copolymer micellar monolayers as negative resist for electron-beam lithography. *Adv Funct Mater*, 13(7):569–575, 2003.

[69] R. Glass, M. Möller, and J.P. Spatz. Block copolymer micelle nanolithography. *Nanotechnology*, 14:1153–1160, 2003.

[70] J.D. Glawe, J.B. B. Hill, D.K. Mills, and M.J. McShane. Influence of channel width on alignment of smooth muscle cells by high-aspect-ratio microfabricated elastomeric cell culture scaffolds. *Journal of Biomedical Materials Research*, 75A:106114, 2005.

[71] A.S. Gobin and J.L. West. Val-ala-pro-gly, an elastin-derived non-integrin ligand: smooth muscle cell adhesion and specificity. *J Biomed Mater Res A*, 67(1):255–259, 2003.

[72] H. Gruler. New insights into directed cell migration: characteristics and mechanisms. *Nouv Rev Fr Hematol*, 37(5):255–265, 1995.

[73] H. Gruler and R. Nuccitelli. Neural crest cell galvanotaxis: new data and a novel approach to the analysis of both galvanotaxis and chemotaxis. *Cell Motil Cytoskeleton*, 19(2):121–133, 1991.

[74] H. Gruler and R. Nuccitelli. The galvanotaxis response mechanism of keratinocytes can be modeled as a proportional controller. *Cell Biochem Biophys*, 33(1):33–51, 2000.

[75] P. Hanefeld, U. Westedt, R. Wombacher, T. Kissel, A. Schaper, J.H. Wendorff, and A. Greiner. Coating of poly(p-xylylene) by pla-peo-pla triblock copolymers with excellent polymer-polymer adhesion for stent applications. *Biomacromolecules*, 7:2086–2090, 2006.

[76] H. Hara, M. Nakamura, J.C. Palmaz, and R.S. Schwartz. Role of stent design and coatings on restenosis and thrombosis. *Adv Drug Deliv Rev*, 58(3):377–386, 2006.

[77] R. Haubner, D. Finsinger, and Kessler H. Stereoisomeric peptide libraries and peptidomimetics for designing selective inhibitors of the $\alpha_v\beta_3$ integrin for a new cancer therapy. *Angen, Chem Int Ed Engl*, 36:1374–1389, 1997.

[78] U. Hersel, C. Dahmen, and H. Kessler. Rgd modified polymers: biomaterials for stimulated cell adhesion and beyond. *Biomaterials*, 24(24):4385–4415, 2003.

[79] V.C. Hirschfeld-Warneken, M. Arnold, A. Cavalcanti-Adam, M. López-García, H. Kessler, and J.P. Spatz. Cell adhesion and polarisation on molecularly defined spacing gradient surfaces of cyclic rgdfk peptide patches. *Eur J Cell Biol*, 87(8-9):743–750, 2008.

[80] G.R. Houtchens, M.D. Foster, T.A. Desai, E.F. Morgan, and J.Y. Wong. Combined effects of microtopography and cyclic strain on vascular smooth muscle cell orientation. *Journal of biomechanics*, 41(4):762–769, 2008.

[81] Y.-C. S. Hsieh, S.-J. Hsieh, Y.-S. Chang, C.-M. Hsueh, and S.-L. Hsu. The lipoxygenase inhibitor, baicalein, modulates cell adhesion and migration by up-regulation of integrins and vinculin in rat heart endothelial cells. *Br J Pharmacol*, 151(8):1235–1245, 2007.

[82] H. Huang, R. D. Kamm, and R. T. Lee. Cell mechanics and mechanotransduction: pathways, probes, and physiology. *Am J Physiol Cell Physiol*, 287(1):C1–11, 2004.

[83] A. Hultgårdh-Nilsson and M. Durbeej. Role of the extracellular matrix and its receptors in smooth muscle cell function: implications in vascular development and disease. *Curr Opin Lipidol*, 18(5):540–545, 2007.

[84] H.-S. Hung, C.-C. Wu, S. Chien, and S.-H. Hsu. The behavior of endothelial cells on polyurethane nanocomposites and the associated signaling pathways. *Biomaterials*, 30(8):1502–1511, 2009.

[85] J.E. Hungerford and C.D. Little. Developmental biology of the vascular smooth muscle cell: building a multilayered vessel wall. *J Vasc Res*, 36(1):2–27, 1999.

[86] T. Iba and B.E. Sumpio. Morphological response of human endothelial cells subjected to cyclic strain in vitro. *Microvascular Research*, 42:245–254, 1991.

[87] R.K. Jain. Molecular regulation of vessel maturation. *Nat. Med.*, 9:685–693, 2003.

[88] P.A. Janmey and C.A. McCulloch. Cell mechanics: integrating cell responses to mechanical stimuli. *Annu Rev Biomed Eng*, 9:1–34, 2007.

[89] P.A. Janmey and D.A. Weitz. Dealing with mechanics: mechanisms of force transduction in cells. *TRENDS in Biochemical Sciences*, 29(7):364–370, 2004.

[90] C.M. Jewell, J. Zhang, N.J. Fredin, M.R. Wolff, T.A. Hacker, and D.M. Lynn. Release of plasmid dna from intravascular stents coated with ultrathin multilayered polyelectrolyte films. *Biomacromolecules*, 7:2483–2491, 2006.

[91] J.P. Jung, A.K. Nagaraj, E.K. Fox, J.S. Rudra, J.M. Devgun, and J.H. Collier. Co-assembling peptides as defined matrices for endothelial cells. *Biomaterials*, 30(12):2400–2410, 2009.

[92] S. Jungbauer. *Mechanical stimulation of cells : Dynamic behavior of cells on cyclical stretched substrates*. PhD thesis, University of Heidelberg, 2008.

[93] S. Jungbauer, H. Gao, J. P. Spatz, and R. Kemkemer. Two characteristic regimes in frequency-dependent dynamic reorientation of fibroblasts on cyclically stretched substrates. *Biophysical Journal*, 95(7):3470–3478, 2008.

[94] S. Jungbauer, R. Kemkemer, H. Gruler, D. Kaufmann, and J.P. Spatz. Cell shape normalization, dendrite orientation, and melanin production of normal and genetically altered (haploinsufficient nf1)-melanocytes by microstructured substrate interactions. *ChemPhysChem*, 5(1):85–92, 2004.

[95] J.P. Kaiser, A. Reinmann, and A. Bruinink. The effect of topographic characteristics on cell migration velocity. *Biomaterials*, 27:5230–5241, 2006.

[96] L. Kam, W. Shain, J.N. Turner, and R. Bizios. Selective adhesion of astrocytes to surfaces modified with immobilized peptides. *Biomaterials*, 23(2):511–515, 2002.

[97] K. Kanda and T. Matsuda. Behavior of arterial wall cells cultured on periodically stretched substrates. *Cell Transplantation*, 2:475–484, 1993.

[98] K. Kanda, T. Matsuda, and T. Oka. Two-dimensional orientational response of smooth muscle cells to cyclic stretching. *ASAIO Journal*, 38:M382–M385, 1992.

[99] S. Kanno, N. Oda, M. Abe, S. Saito, K. Hori, Y. Handa, K. Tabayashi, and Y. Sato. Establishment of a simple and practical procedure applicable to therapeutic angiogenesis. *Circulation*, 99(20):2682–2687, 1999.

[100] D. Kaspar, W. Seidl, C. Neidlinger-Wilke, A. Beck, L. Claes, and A. Ignatius. Proliferation of human-derived osteoblast-like cells depends on the cycle number and frequency of uniaxial strain. *Journal of Biomechanics*, 35:873–880, 2002.

[101] Y.P. Kathuria. The potential of biocompatible metallic stents and preventing restenosis. *Materials Science and Engineering*, A 417:40–48, 2006.

[102] B.Z. Katz, E. Zamir, A. Bershadsky, Z. Kam, K.M. Yamada, and B. Geiger. Physical state of the extracellular matrix regulates the structure and molecular composition of cell-matrix adhesions. *Mol Biol Cell*, 11(3):1047–1060, Mar 2000.

[103] D. Kaufmann, B. Bartelt, M. Wolf, K. Kunzi-Rapp, C.O. Hanemann, R. Fahsold, C. Hein, W. Vogel, and G. Assum. Spinal neurofibromatosis without caf-au-lait macules in two families with null mutations of the nf1 gene. *Am J Hum Genet*, 69:1395–1400., 2001.

[104] S. Kaul, P.K. Shah, and G.A. Diamond. As time goes by. *Journal of the American College of Cardiology*, 50:128–137, 2007.

[105] R. Kaunas, P. Nguyen, S. Usami, and S. Chien. Cooperative effects of rho and mechanical stretch on stress fiber organization. *PNAS*, 102(44):15895–15900, 2005.

[106] R. Kemkemer, S. Jungbauer, D. Kaufmann, and H. Gruler. Cell orientation by a microgrooved substrate can be predicted by automatic control theory. *Biophysical journal*, 90:4701–4711, 2006.

[107] R. Kemkemer, D. Kling, D. Kaufmann, and H. Gruler. Elastic properties of nematoid arrangements formed by amoeboid cells. *Eur Phys J E*, 1(2-3):215–225, 2000.

[108] R. Kemkemer, C. Neidlinger-Wilke, L. Claes, and H. Gruler. Cell orientation induced by extracellular signals. *Cell biochemistry and biophysics*, 30:167–192, 1999.

[109] A.L. Kindzelskii and H.R. Petty. Extremely low frequency pulsed dc electric fields promote neutrophil extension, metabolic resonance and dna damage when phase-matched with metabolic oscillators. *Biochim Biophys Acta*, 1495(1):90–111, 2000.

[110] M.L.W. Knetsch, Y.B.J. Aldenhoff, and L.H. Koole. The effect of high-density-lipoprotein on thrombus formation on and endothelial cell attachement to biomaterial surfaces. *Biomaterials*, 27:2813–2819, 2006.

[111] S. A. Kontulainen, J. M. Hughes, H. M. Macdonald, and J. D. Johnston. The biomechanical basis of bone strength development during growth. *Medicine and sport science*, 51:13–32, 2007.

[112] L.Y. Koo, D.J. Irvine, A.M. Mayes, D.A. Lauffenburger, and L.G. Griffith. Co-regulation of cell adhesion by nanoscale rgd organization and mechanical stimulus. *J Cell Sci*, 115(Pt 7):1423–1433, 2002.

[113] M. Kryszewski. Fifty years of study of the piezoelectric properties of macromolecular structural biological materials. *Acta Phys. Pol. A*, 105:389–408, 2004.

[114] M.E. Kutcher and I.M. Herman. The pericyte: Cellular regulator of microvascular blood flow. *Microvascular Research*, online publication:12, 2009.

[115] K.-W. Lau, A. Johan, U. Sigwart, and J.-S. Hung. A stent is not just a stent: Stent construction and design do matter in its clinical performance. *Singapore Med J*, 45(7):305–11, 2004.

[116] K.-W. Lau, K.-H. Mak, J.-S. Hung, and U. Sigwart. Clinical impact of stent construction and design in percutaneous coronary intervention. *American Heart Journal*, 147:764–773, 2004.

[117] A.A. Lee, T. Delhaas, L.K. Waldmann, D.A. MacKenna, F.J. Villarreal, and A.D. McCulloch. An equibiaxial strain system for cultured cells. *A. J. Physiology*, 271:1400–1408, 1996.

[118] T. Lee and B.E. Sumpio. Cell signalling in vascular cells exposed to cyclic strain: the emerging role of protein phosphatases. *Biotechnol. Appl. Biochem.*, 39:129–139, 2004.

[119] X. Li and J. Kolega. Effects of direct current electric fields on cell migration and actin filament distribution in bovine vascular endothelial cells. *J Vasc Res*, 39(5):391–404, 2002.

[120] A. Lichtenberg, I. Tudorache, S. Cebotari, S. Ringes-Lichtenberg, G. Sturz, K. Hoeffler, C. Hurscheler, G. Brandes, A. Hilfiker, and A. Haverich. In vitro re-endothelialization of detergent decellularized heart valves under simulated physiological dynamic conditions. *Biomaterials*, 27:4221–4229, 2006.

[121] J.W. Lichtman and J.-A. Conchello. Fluorescence microscopy. *Nat Methods*, 2(12):910–919, Dec 2005.

[122] X. Lin and B.P. Helmke. Micropatterned structural control suppresses mechanotaxis of endothelial cells. *Biophysical journal*, 95(6):3066–3078, 2008.

[123] B. Liu, M.J. Qu, K.R. Qin, H. Li, Z.K. Li, B.R. Shen, and Z.L. Jiang. Role of cyclic strain frequency in regulating the alignment of vascular smooth muscle cells in vitro. *Biophysical Journal*, 94:1497–1507, 2008.

[124] W.H. Liu, C.M. Nelson, J.L. Tan, and C.S. Chen. Cadherins, rhoa, and rac1 are differentially required for stretch-mediated proliferation in endothelial versus smooth muscle cells. *Circ Res.*, 101:e44–e52, 2007.

[125] W.A. Loesberg, J. te Riet, F. van Delft, P. Schon, C.G. Figdor, and S. Speller. The threshold at which substrate nanogroove dimensions may influence fibroblast alignment and adhesion. *Biomaterials*, 28:3944–3951, 2007.

[126] W.A. Loesberg, X.F. Walboomers, J.J.W.A. van Loon, and J.A. Jansen. The effect of combined hypergravity and microgrooved surface topography on the behaviour of fibroblasts. *Cell Motility and the Cytoskeleton*, 63:384–394, 2006.

[127] T.F. Lüscher. *Endothelial Vasoactive Substances and Cardiovascular Disease*. Karger, Basel, New York, 1988.

[128] P. W. Luther, H. B. Peng, and J. J. Lin. Changes in cell shape and actin distribution induced by constant electric fields. *Nature*, 303(5912):61–64, 1983.

[129] G. Maheshwari, G. Brown, D.A. Lauffenburger, A. Wells, and L.G. Griffith. Cell adhesion and motility depend on nanoscale rgd clustering. *J Cell Sci*, 113 (Pt 10):1677–1686, 2000.

[130] A. M. Malek and S. Izumo. Mechanism of endothelial cell shape change and cytoskeletal remodeling in response to fluid shear stress. *Journal of cell science*, 109 (Pt 4):713–726, 1996.

[131] G. Mani, M.D. Feldman, D. Patel, and C.M. Agrawal. Coronary stents: A materials perspective. *Biomaterials*, 28:1689–1710, 2007.

[132] V.G. Manolopoulos and P.I. Lelkes. Caclic strain and forskolin differentially induce camp production in phenotypically diverse endothelial cells. *Biochemical and Biophysical Research Communications*, 191(3):1379–1385, 1993.

[133] A. Marino and R. O. Becker. Piezoelectric effect and growth control in bone. *Nature*, 228(5270):473–474, 1970.

[134] S.P. Massia and J.A. Hubbell. Vascular endothelial cell adhesion and spreading promoted by the peptide redv of the iiics region of plasma fibronectin is mediated by integrin $\alpha_4\beta_1$. *J Biol Chem*, 267(20):14019–14026, 1992.

[135] C.D. McCaig, A.M. Rajnicek, B. Song, and M. Zhao. Controlling cell behavior electrically: current views and future potential. *Physiol Rev*, 85(3):943–978, 2005.

[136] C.D. McCaig and M. Zhao. Physiological electrical fields modify cell behaviour. *Bioessays*, 19(9):819–826, 1997.

[137] D. Meschede, editor. *Gerthsen Physik*. Springer Verlag, Berlin, Heidelberg, New York, 2004.

[138] D.C. Miller, A. Thapa, K.M. Haberstroh, and T.J. Webster. Endothelial and vascular smooth muscle cell function on poly(lactic-co-glycolic acid) with nano-structured surface features. *Biomaterials*, 25:53–61, 2004.

[139] M. Minary-Jolandan and M.-F. Yu. Nanoscale characterization of isolated individual type i collagen fibrils: polarization and piezoelectricity. *Nanotechnology*, 20:085706(6pp), 2009.

[140] S. Miyamoto, S.K. Akiyama, and K.M. Yamada. Synergistic roles for receptor occupancy and aggregation in integrin transmembrane function. *Science*, 267(5199):883–885, 1995.

[141] J.E. Moore, E. Bürki, A. Suciu, S. Zhao, M. Burnier, H.R. Brunner, and J.J. Meister. A device for subjecting vascular endothelial cells to both fluid shear stress and circumferential cyclic stretch. *Annals of Biomedical Engineering*, 22:416–422, 1994.

[142] M.M. Moore, J. Goldman, A.R. Patel, S. Chien, and S.Q. Liu. Role of tensile stress and strain in the induction of cell death in experimental vein grafts. *Journal of Biomechanics*, 34:289–297, 2001.

[143] M. Moretti, A. Prina-Mello, A.J. Reis, V. Barron, and P.J. Prendergast. Endothelial cell alignment on cycically-stretched silicone surfaces. *Journal of Materials Science: Materials in Medicine*, 15:1159–1164, 2004.

[144] T.L. Morkved, M. Lu, A.M. Urbas, E.E. Ehrichs, H.M. Jaeger, P. Mansky, and T.P. Russell. Local control of microdomain orientation in diblock copolymer thin films with electric fields. *Science*, 273(5277):931–933, 1996.

[145] M.E. Mycielska and M.B.A. Djamgoz. Cellular mechanisms of direct-current electric field effects: galvanotaxis and metastatic disease. *J Cell Sci*, 117(Pt 9):1631–1639, 2004.

[146] S. Na, G.A. Meininger, and J.D. Humphrey. A theoretical model for f-actin remodeling in vascular smooth muscle cells subjected to cyclic stretch. *Journal of Theoretical Biology*, 246:87–99, 2007.

[147] A. R. Naylor, Z. Mehta, and P.M. Rothwell. A systematic review and meta-analysis of 30-day outcomes following staged carotid artery stenting and coronary bypass. *Eur J Vasc Endovasc Surg*, 37(4):379–387, 2009.

[148] C. Neidlinger-Wilke, E. Grood, L. Claes, and R. Brand. Fibroblast orientation to stretch begins within three hours. *Journal of Orthopaedic Research*, 20:953–956, 2002.

[149] C. Neidlinger-Wilke, H.-J. Wilke, and L Claes. Cyclic stretching of human osteaoblasts affects proliferation and metabolism: A new experimental method and its application. *Journal of Orthopaedic Research*, 12:70–78, 1994.

[150] K.Y. Nishimura, R.R. Isseroff, and R. Nuccitelli. Human keratinocytes migrate to the negative pole in direct current electric fields comparable to those measured in mammalian wounds. *J Cell Sci*, 109 (Pt 1):199–207, 1996.

[151] C. Oakley and D.M. Brunette. Topographic compensation: guidance and directed locomotion of fibroblasts on grooved micromachined substrata in the absence of microtubules. *Cell motility and the cytoskeleton*, 31:45–58, 1995.

[152] B. O'Brien and W. Carroll. The evolution of cardiovascular stent materials and surfaces in response to clinical drivers: A review. *Acta Biomaterialia*, 5:945–958, 2009.

[153] A.T.L. Ong, J. Aoki, M.J. Kutryk, and P.W. Serruys. How to accelerate the endothelialization of stents. *Archives des Maladies du Coeur et des Vaisseaux*, n 2:tome 98, 2005.

[154] N. Orida and J. D. Feldman. Directional protrusive pseudopodial activity and motility in macrophages induced by extracellular electric fields. *Cell Motil*, 2(3):243–255, 1982.

[155] J.C. Palmaz, S. Bailey, D. Marton, and E. Sprague. Influence of stent design and material composition on procedure outcome. *Journal of Vascular Surgery*, 36:1031–1039, 2002.

[156] M. Park, C. Harrison, P.M. Chaikin, R.A. Register, and D.H. Adamson. Block copolymer lithography: Periodic arrays of similar to 10(11) holes in 1 square centimeter. *Science*, 276(5317):1401–1404, 1997.

[157] N.B. Patel and M.M. Poo. Perturbation of the direction of neurite growth by pulsed and focal electric fields. *J Neurosci*, 4(12):2939–2947, 1984.

[158] C. Patterson and M.S. Runge. Therapeutic angiogenesis: the new electrophysiology? *Circulation*, 99(20):2614–2616, 1999.

[159] M. Peuster, C. Hesse, T. Schloo, C. Fink, P. Beerbaum, and C. von Schnakenburg. Long-term biocompatibility of a corrodible peripheral iron stent in the porcine descending aorta. *Biomaterials*, 27:4955–4962, 2006.

[160] K. Pfaff, M.and Tangemann, B. Müller, M. Gurrath, G. Müller, H. Kessler, R. Timpl, and J. Engel. Selective recognition of cyclic rgd peptides of nmr defined conformation by $\alpha_{IIb}\beta_3$, $\alpha_v\beta_3$, and $\alpha_5\beta_1$ integrins. *J Biol Chem*, 269(32):20233–20238, 1994.

[161] B.D. Plouffe, D.N. Njoka, J. Harris, J. Liao, N.K. Horick, M. Radisic, and S.K. Murthy. Peptide-mediated selective adhesion of smooth muscle and endothelial cells in microfluidic shear flow. *Langmuir*, 23(9):5050–5055, 2007.

[162] T. Pompe, L. Renner, and C. Werner. Nanoscale features of fibronectin fibrillogenesis depend on proteinsubstrate interaction and cytoskeleton structure. *Biophys. J.*, 88:527–534, 2005.

[163] M. Prunotto, C. Isaia, M.A. Gatti, E. Monari, E. Pasquino, and M. Galloni. Nitinol carbofilm coated stents for peripheral applications: study in the porcine model. *J Mater Sci Mater Med*, 16(12):1231–1238, 2005.

[164] S. Ramcharitar, A.L. Gaster, J. Daemen, and P. Serruys. Drug-eluting stents, restenosis and revascularization. *Herz*, 32(4):287–295, 2007.

[165] U. S. National Institutes of Health Bethesda Maryland USA Rasband, W. S. Imagej. *http://rsb.info.nih.gov/ij/.*, 1997-2008.

[166] U. S. National Institutes of Health Bethesda Maryland USA Rasband, W. S. Imagej manual tracking plugin. *http://rsb.info.nih.gov/ij/plugins/track/track.html*, 2008.

[167] N. Resnick, H. Yahav, A. Shay-Salit, M. Shushy, S. Schubert, L.C.M. Zilberman, and E. Wofovitz. Fluid shear stress and the vascular endothelium: for better and for worse. *Progress in Biophysics & Molecular Biology*, 81:177–199, 2003.

[168] K.R. Robinson. The responses of cells to electrical fields: a review. *Journal of Cell Biology*, 101:2023–2027, 1985.

[169] E. Ruoslahti and M.D. Pierschbacher. New perspectives in cell adhesion: Rgd and integrins. *Science*, 238:491–497, 1987.

[170] N. Sakamoto, T. Ohashi, and M. Sato. Effect of fluid shear stress on migration of vascular smooth muscle cells in cocultured model. *Annals of Biomedical Engineering*, DOI: 10.1007/s10439-005-9043-y:tome 98, 2006.

[171] G. Sangiorgi, G. Melzi, P. Agostoni, C. Cola, F. Clementi, P. Romitelli, R. Virmani, and A. Colombo. Engineering aspects of stents design and their translation into clinical practice. *Ann Ist Super Sanita*, 43(1):89–100, 2007.

[172] P.N. Sawyer, E. Himmelfarb, I. Lustrin, and H. Ziskind. Measurement of streaming potentials of mammalian blood vessels, aorta and vena cava, in vivo. *Biophys J*, 6(5):641–651, Sep 1966.

[173] Boston Scientific Technologie Zentrum GmbH Munich Scheuermann, T. Technical report, Boston Scientific Corp., Maple Grove, MN, 2007.

[174] M. Schienbein and H. Gruler. Langevin equation, fokker-planck equation and cell migration. *Bull Math Biol*, 55(3):585–608, 1993.

[175] M. Schienbein and H. Gruler. Chemical amplifier, self-ignition mechanism, and amoeboid cell migration. *Phys Rev E Stat Phys Plasmas Fluids Relat Interdiscip Topics*, 52(4):4183–4197, 1995.

[176] R. Schmidt, C.A. Wurm, S. Jakobs, J. Engelhardt, A. Egner, and S.W. Hell. Spherical nanosized focal spot unravels the interior of cells. *Nature Methods*, 5(6):539–544, 2008.

[177] R.F. Schmidt, F. Lang, and G. Thews. *Physiologie des Menschen*. Spinger, Heidelberg, New York, 2005.

[178] M.H. Shamos, L.S. Lavine, and M.I. Shamos. Piezoelectric effect in bone. *Nature*, 197:81, 1963.

[179] F. Sharif, S.O. Hynes, R. Cooney, L. Howard, J. McMahon, K. Daly, J. Crowley, F. Barry, and T. O'Brien. Gene-eluting stents: adenovirus-mediated delivery of enos to the blood vessel wall accelerates re-endothelialization and inhibits restenosis. *Mol Ther*, 16(10):1674–1680, 2008.

[180] T. Sharkawi, F. Cornhill, A. Lafont, P. Sabaria, and M. Vert. Intravascular bioresorbable polymeric stents: A potential alternative to current drug eluting metal stents. *Journal of Pharmaceutical Sciences*, 96:2829–2837, 2007.

[181] A. Shukla, A.R. Dunn, M.A. Moses, and K.J. Van Vliet. Endothelial cells as mechanical transducers: enzymatic activity and network formation under cyclic strain. *Mech Chem Biosyst*, 1(4):279–290, 2004.

[182] M.D. Silverman, C.R. Waters, G.T. Hayman, J. Wigboldus, M.M. Samet, and P.I. Lelkes. Tissue factor activity is increased in human endothelial cells cultured under elevated static pressure. *Am J Physiol Cell Physiol*, 277:233–242, 1999.

[183] P. Sipkema, P.J.W. van der Linden, N. Westerhof, and F.C.P. Yin. Effect of cyclic axial stretch of rat arteries on endothelial cytoskeletal morphology and vascular reactivity. *Journal of Biomechanics*, 36:653–659, 2003.

[184] J.D. Smith, N. Davies, A.I. Willis, B.E. Sumpio, and P. Zilla. Cyclic stretch induces the expression of vascular endothelial growth factor in vascular smooth muscle cells. *Endothelium*, 8(1):41–48, 2001.

[185] B. Song, M. Zhao, J.V. Forrester, and C.D. McCaig. Electrical cues regulate the orientation and frequency of cell division and the rate of wound healing in vivo. *Proc Natl Acad Sci U S A*, 99(21):13577–13582, 2002.

[186] H.K. Soong, W.C. Parkinson, S. Bafna, G.L. Sulik, and S.C. Huang. Movements of cultured corneal epithelial cells and stromal fibroblasts in electric fields. *Invest Ophthalmol Vis Sci*, 31(11):2278–2282, 1990.

[187] M. Sotoudeh, S. Jalali, S. Usami, J.Y.J. Shyy, and S. Chien. A strain device imposing dynamic and uniform equi-biaxial strain to cultured cells. *Annals of Biomedical Engineering*, 26:181–189, 1998.

[188] J.P. Spatz, S. Mössmer, C. Hartmann, M. Möller, T. Herzog, M. Krieger, H.-G. Boyen, P. Ziemann, and Kabius B. Ordered deposition of inorganic clusters from micellar block copolymer films. *Langmuir*, 16:407–415, 2000.

[189] J.P. Spatz, S. Mößmer, and M. Möller. Mineralization of gold nanoparticles in a block copolymer microemulsion. *Chem Eur J*, 2(12):1552–1555, 1996.

[190] D. Stamenovic and N. Wang. Cellular responses to mechanical stress invited review: Engineering approaches to cytoskeletal mechanics. *J Appl Physiol*, 89:2085–2090, 2000.

[191] P.R. Standley, A. Camaratta, B.P. Nolan, C.T. Purgason, and M.A. Stanley. Cyclic stretch induces vascular smooth muscle cell alignment via no signaling. *Am J Physiol Heart Circ Physiol*, 283:1907–1914, 2002.

[192] J. Steffel and F.C. Tanner. Biological effects of drug-eluting stents in the coronary circulation. *Herz*, 32:268–273, 2007.

[193] J.P. Stegemann, H. Hong, and R.M. Nerem. Mechanical, biochemical, and extracellular matrix effects on vascular smooth muscle cell phenotype. *J Appl Physiol*, 98:2321–2327, 2005.

[194] C.H. Streuli and M.J. Bissell. Expression of extra cellular matrix components is regulated by substratum. *J. Cell Biol*, 110:1405–1415, 1990.

[195] G.L. Sulik, H.K. Soong, P.C. Chang, W.C. Parkinson, S.G. Elner, and V.M. Elner. Effects of steady electric fields on human retinal pigment epithelial cell orientation and migration in culture. *Acta Ophthalmol*, 70(1):115–122, 1992.

[196] T. Takemasa, K. Sugimoto, and K. Yamashita. Amplitude-dependent stress fiber reorientation in early response to cyclic strain. *Experimental Cell Research*, 230:407–410, 1997.

[197] A.I. Teixeira, G.A. Abrams, P.J. Bertics, C.J. Murphy, and P.F. Nealey. Epithelial contact guidance on well-defined micro- and nanostructured substrates. *Journal of cell science*, 116:1881–1892, 2003.

[198] R.G. Thakar, F. Ho, N.F. Huang, D. Liepmann, and S. Li. Regulation of vascular smooth muscle cells by micropatterning. *Biochemical and biophysical research communications*, 307(4):883–890, 2003.

[199] R.T. Tranquillo, T.S. Girton, B.A. Bromberek, T.G. Triebes, and D.L. Mooradian. Magnetically orientated tissue-equivalent tubes: application to a circumferentially orientated media-equivalent. *Biomaterials*, 17:349–357, 1996.

[200] T.A. Trikalinos, A.A. Alsheikh-Ali, A. Tatsioni, B.K. Nallamothu, and D.M. Kent. Percutaneous coronary interventions for non-acute coronary artery disease: a quantitative 20-year synopsis and a network meta-analysis. *Lancet*, 373(9667):911–918, 2009.

[201] R. Tsaryk, M. Kalbacova, U. Hempel, D. Scharnweber, R.E. Unger, P. Dieter, C.J. Kirkpatrick, and K. Peters. Response of human endothelial cells to oxidative stress on ti6al4v alloy. *Biomaterials*, 28(5):806–813, 2007.

[202] E. Tzima, M. Irani-Tehrani, W.B. Kiosses, E. Dejana, D.A. Schultz, B. Engelhardt, G. Cao, H. DeLisser, and M.A. Schwartz. A mechanosensory complex that mediates the endothelial cell response to fluid shear stress. *Nature*, 437(7057):426–431, 2005.

[203] A.N. Veleva, D.E. Heath, S.L. Cooper, and C. Patterson. Selective endothelial cell attachment to peptide-modified terpolymers. *Biomaterials*, 29(27):3656–3661, 2008.

[204] D. Versari, L.O. Lerman, and A. Lerman. The importance of reendothelialization after arterial injury. *Current pharmaceutical design*, 13:1811–1824, 2007.

[205] V. Vogel and M. Sheetz. Local force and geometry sensing regulate cell functions. *Nat Rev Mol Cell Biol*, 7(4):265–275, 2006.

[206] N. Von Offenberg Sweeney, P.M. Cummins, E.J. Cotter, P.A. Fitzpatrick, Y. A. Birney, E.M. Redmond, and P.A. Cahill. Cyclic strain-mediated regulation of vascular endothelial cell migration and tube formation. *Biochemical and Biophysical Research Communications*, 329:573–582, 2005.

[207] X.F. Walboomers, H.J. Croes, L.A. Ginsel, and J.A. Jansen. Contact guidance of rat fibroblasts on various implant materials. *J Biomed Mater Res*, 47(2):204–212., 1999.

[208] X.F. Walboomers, L.A. Ginsel, and J.A. Jansen. Early spreading events of fibroblasts on microgrooved substrates. *J Biomed Mater Res*, 51:529–534, 2000.

[209] E. Wang, Y. Yin, M. Zhao, J.V. Forrester, and C.D. McCaig. Physiological electric fields control the g1/s phase cell cycle checkpoint to inhibit endothelial cell proliferation. *FASEB J*, 17(3):458–460, 2003.

[210] H. Wang, W. Ip, R. Boissy, and E.S. Grood. Cell orientation response to cyclically deformed substrates: Experimental validation of a cell model. *Journal of Biomechanics*, 28(12):1543–1552, 1995.

[211] H.Q. Wang, L. Bai, B.R. Shen, Z.Q. Yan, and Z.L. Jiang. Coculture with endothelial cells enhances vascular smooth muscle cell adhesion and spreading via activation of beta1-integrin and phosphatidylinositol 3-kinase/akt. *European journal of cell biology*, 86:51–62, 2007.

[212] J.H.C. Wang, P. Goldschmidt-Clermont, N. Moldovan, and F.C.-P. Yin. Leukotrienes and tyrosine phosphorylation mediate stretching-induced actin cytoskeletal remodeling in endothelial cells. *Cell Motility and the Cytoskeleton*, 46:137–145, 2000.

[213] J.H.C. Wang, P. Goldschmidt-Clermont, J. Wille, and F.C.P. Yin. Specificity of endothelial cell reorientation in response to cyclic mechanical stretching. *Journal of Biomechanics*, 34:1563–1572, 2001.

[214] R.L.C Wang, H.J. Kreuzer, and M. Grunze. Molecular conformation and solvation of oligo(ethylene glycol)-terminated self-assembled monolayers and their resistance to protein adsorption. *J Phys Chem B*, 101(47):9767–9773., 1997.

[215] Y. Wang, E.L. Botvinick, Y. Zhao, M.W. Berns, S. Usami, R.Y. Tsien, and S. Chien. Visualizing the mechanical activation of src. *Nature*, 434(7036):1040–1045, 2005.

[216] G.M. Whitesides, E. Ostuni, S. Takayama, X. Jiang, and D.E. Ingber. Soft lithography in biology and biochemistry. *Annual review of biomedical engineering*, 3:335–373, 2001.

[217] M.R. Williamson, A. Shuttleworth, A.E. Canfield, R.A. Black, and C.A. Kielty. The role of endothelial cell attachment to elastic fibre molecules in the enhancement of monolayer formation and retention, and the inhibition of smooth muscle cell recruitment. *Biomaterials*, 28(35):5307–5318, 2007.

[218] E. Wilson, F. Vives, T. Collins, and H.E. Ives. Strain-responsive regions in the platelet-derived growth factor-a gene promoter. *Hypertension*, 31:170–175, 1998.

[219] B. Wojciak-Stothard, A. Curtis, W. Monaghan, K. MacDonald, and C. Wilkinson. Guidance and activation of murine macrophages by nanometric scale topography. *Experimental cell research*, 223:426–435, 1996.

[220] J.P. Xiong, T. Stehle, B. Diefenbach, R. Zhang, R. Dunker, D.L. Scott, A. Joachimiak, S.L. Goodman, and M.A. Arnaout. Crystal structure of the extracellular segment of integrin $\alpha_v\beta_3$. *Science*, 294(5541):339–345, 2001.

[221] J.P Xiong, T. Stehle, R. Zhang, A. Joachimiak, M. Frech, S.L. Goodman, and M.A. Arnaout. Crystal structure of the extracellular segment of integrin $\alpha_v\beta_3$ in complex with an arg-gly-asp ligand. *Science*, 296(5565):151–155, 2002.

[222] H. Yamada and H. Ando. Orientation of apical and basal actin stress fibers in isolated and subconfluent endothelial cells as an early response to cyclic stretching. *Mol Cell Biomech*, 4(1):1–12, 2007.

[223] W.P. Yang, E.K. Onuma, and S.W. Hui. Response of c3h/10t1/2 fibroblasts to an external steady electric field stimulation. reorientation, shape change, cona receptor and intramembranous particle distribution and cytoskeleton reorganization. *Exp Cell Res*, 155(1):92–104, 1984.

[224] Y. Yano, J. Geibel, and B.E. Sumpio. Cyclic strain induces reorganization of integrin alpha5beta1 and alpha2beta1 in human umbilical veon endothelial cells. *J Cell Biochem*, 64:505–513, 1997.

[225] M. Yin, Y. Yuan, C. Liu, and J. Wang. Development of mussel adhesive polypeptide mimics coating for in-situ inducing re-endothelialization of intravascular stent devices. *Biomaterials*, 30(14):2764–2773, 2009.

[226] M. Yoshigi, E.B. Clark, and H.J. Yost. Quantification of stretch-induced cytoskeletal remodeling in vascular endothelial cells by image processing. *Cytometry Part A*, 55(A):109–118, 2003.

[227] E. Zamir and B. Geiger. Components of cell-matrix adhesions. *J Cell Sci*, 114(Pt 20):3577–3579, 2001.

[228] M. Zhao, A. Agius-Fernandez, J.V. Forrester, and C.D. McCaig. Orientation and directed migration of cultured corneal epithelial cells in small electric fields are serum dependent. *Journal of cell science*, 109:1405–1414, 1996.

[229] M. Zhao, H. Bai, E. Wang, J.V. Forrester, and C.D. McCaig. Electrical stimulation directly induces pre-angiogenic responses in vascular endothelial cells by signaling through vegf receptors. *Journal of Cell Science*, 117:397–405, 2004.

[230] M. Zhao, A. Dick, J.V. Forrester, and C.D. McCaig. Electric field-directed cell motility involves up-regulated expression and asymmetric redistribution of the epidermal growth factor receptors and is enhanced by fibronectin and laminin. *Mol Biol Cell*, 10(4):1259–1276, 1999.

[231] S. Zhao, A. Suciu, T. Ziegler, J.E. Moore, E. Burki, J.J. Meister, and H.R. Brunner. Synergistic effects of fluid shear stress and cyclical circumferential stretch on vascular endothelial cell morphology and cytoskeleton. *Arterioscler. Thromb. Vasc. Biol.*, 15:1781–1786, 1995.

[232] B. Zhu, Q. Zhang, Q. Lu, Y. Xu, J. Yin, and J. Hu. Nanotopographical guidance of c6 glioma cell alignment and oriented growth. *Biomaterials*, 25:4215–4223, 2004.

Acknowledgments

It might be infeasible to mention everybody who supported me during the last three years. However, at this place I want to thank those, which made this thesis possible:
Professor Dr. Joachim P. Spatz, who gave me the opportunity, strong support and an interesting project to work on in his group. He inspired and motivated me to perform interdisciplinary research at the interface between biology and material science.
Professor Dr. Rainer H. A. Fink, who kindly adopted the second examiner tasks.
Dr. Ralf Kemkemer, who introduced me into the world of cell biology and scientific writing, and who furthermore gave me many suggestions and hints how to accomplish my research work in the beginning and how to consequently improve it.
Alexandra Goldyn and Borja Aragüés Rioja for help, discussion, the 'Feierabendbier' and unbreakable support.
Lindarti Purwaningsih, who will be desperately missed in the future as office mate and friend.
Dr. Simon Jungbauer for the charming and patient introduction and help with everything in the lab.
Su Yi, Emil Ruff, Anton Berthold, Britta Striegl, Marc Gronle, Chen Hao, Stefanie Korte, Jenny Diemer, and all other students I supervised. I hope, you all learned as much from me as I did from you.
There were many other people in the Kemkemer subgroup and the whole Spatz-group, who helped me or brightened up my day, thank you all! I want to mention especially Christine Mollenhauer, Ioanis Gregoridis, Peter Kaiser, Alex de Beer, Claudio Rolli, Wylie Ahmed, Magnus Johnson, Martin Deibler, Melih Kalafat and Tobias Busch.
For the motivation to perform a PhD work I thank Prof. Dr. Sven Oscarsson, Dr. Simon Berner and Hans Lidbaum, my master-thesis working group in Uppsala, Sweden. Furthermore thanks to my study-mates and professors in Heidelberg and Uppsala and my former physics teacher Joachim Schneider.
A big thank you to all people involved in proof-reading this thesis, first of all Alexandra Goldyn, Borja Aragüés Rioja, Kristen Mills and Emanuela Buyer, but also Claudio Rolli, Tobias Busch, Gudrun Fickenscher and Veronika Lenz.
I am very thankful to my parents, who supported me and gave me the first 20 years-basis to be capable of becoming a PhD student.
Last but not least thanks to the most wonderful friends Gudrun, Emanuela, Veronika, Elena, Tobias, Natalie, Nina, Julia, Linda, Eileen, Uli, Sarah and many more in Stuttgart and world wide. Thank you for entertainment, support, laughter, comfort, providing

hideaways, and so much more.
I am looking forward to a new part of my life now, thankful that I learned and gained a lot in this past three years, which I will never forget or lose again and which will help me to proceed my way.

Part V

Appendix

1 Abbreviations

AFM	Atomic force microscopy
BSE	Backscattered electrons
CCD	Charge-coupled device
DAPI	4'-6-Diamidin-2'-phenylindole
dcEF	Direct current electrical field
DNA	Deoxyribonucleic acid
EC	Endothelial cell
ECM	Extra cellular matrix
ELFP-EF	Extremely low frequency pulsed dc electric fields
FC	Fibroblast cell
SMC	Smooth muscle cell
HACEC	Human artery coronary endothelial cell
HACSMC	Human artery coronary smooth muscle cell
IrOx	Iridium oxide
PBS	Phosphate buffered saline
PDMS	Poly(dimethylsiloxane)
PEG	Polyethylene glycol
PSS	Platinum-electropolished stainless steel
REDV	Arg-Glu-Asp-Val peptide sequence
RGD	Arg-Gly-Asp peptide sequence
SE	Secondary electrons
SEM	Scanning electron microscopy
SS	Stainless steel
VAPG	Val-Ala-Pro-Gly peptide sequence
VE-Cad	Vascular endothelial cadherin
VEGF	Vascular endothelial growth factor
Z	Atomic number

2 Symbols

α_2	Signal characteristic of guding signal $\alpha_2 = (K_G^E E)^2$
E	Cell elongation
φ	Angle between the major cell ellipse axis and signal direction
$f(\varphi, t)$	Angle distribution function
$\Gamma(t)$	Stochastic signal
$g(\varphi, signal)$	Detection unit characteristics
k_2	Strength of the cellular reaction unit
K_G^E	Electric guidance coefficient $K_G^E = \sqrt{\frac{k_2^E}{q}}$
λ	De-Broglie-wavelenth of the electron $\lambda = \frac{h}{\sqrt{2em_0U}} = \frac{h}{p}$
M_x, M_y	Mean square displacements M_x and M_y
P	Polar order parameter $P = \langle \cos\varphi \rangle = \int g(\varphi) \cos\varphi d\varphi$
q	Strength of the stochastic source
S	Non-polar order parameter $S = \langle \cos 2\varphi \rangle$
τ_1	or τ_2 are characteristic times for order paramaters' temporal behavior
v_M	Total magnification of the microscope $v_M = \beta v_o$

3 Materials and methods

3.1 Human primary cells

Endothelial and smooth muscle cell culture Human coronary artery endothelial cells (HCAECs) and human coronary artery smooth muscle cells (HCASMCs) from PromoCell (Germany) were grown to confluence using Endothelial Cell Growth Medium and Smooth Muscle Cell Growth Medium, respectively, both with low serum concentration (2.5%). All cells had passage numbers less than six. Cells were washed with HepesBSS, and then trypsinized with trypsin/EDTA (0.25% trypsin/1mM ethylenediaminotetracetic acid) solution. When completely detached from the cell culture container, Trypsin Neutralizing Solution based on soy bean extract (all cell media and solutions by PromoCell) was added. The resulting cell suspension was spun down and resuspended in fresh media. Cells were counted using a Neubauer counting chamber. After cell seeding, the culture dishes were placed in a cell culture incubator (37 °C, 5% CO_2).

Human fibroblasts cell culture Human fibroblast cells were cultured in Dulbecco's modified Eagle's medium (DMEM, Gibco Laboratories, Eggenstein, Germany) supplemented with 2.5% fetal bovine serum and 2 mM L-glutamin (GIBCO) at 37 °C, 5% CO_2. FCs were isolated from the foreskin of a healthy young donor as described by Kaufmann *et al.* [103]. The cells were cultured in 25 cm^2 culture flasks until a subconfluent stage was reached. The media was changed every 2-3 days and for detaching, 0.25% trypsin/1mM EDTA was used.

3.2 Live cell staining

All staining procedures were performed one day before the start of the experiments to achieve a stable staining and to avoid toxic effects by fluorescence microscopy. Endothelial cells were stained with Vybrant CFDA SE Cell Tracer Kit (Molecular Probes, Invitrogen). Adherent Cells were incubated with a solution of $2\,\mu$M CFDA in PBS for 15 min. Then they were washed with prewarmed medium and incubated again for 30 min. After that the medium was changed again. Smooth muscle cells were stained with Vybrant FAST DiI^{TM}. Adherent cells were incubated for 20 min in prewarmed medium with $0.2\,\mu$M of FAST DiI^{TM}. Then they were washed three times for 10 min with prewarmed medium.

3.3 Antibody staining

The cells were fixed in 3.7% paraformaldehyde (Serva) for 10 min at room temperature. Then, the cells were permeabilized in 0.1% Triton X-100 (Sigma) in phosphate-buffered saline (Gibco) for 5 min. Before staining, cells were treated with bovine serum albuminum (BSA) for 5 min, to block unspecific antibody binding. The cells were incubated with 1st antibody (focal adhesion marker anti-paxillin [Y113], monoclonal, rabbit (Abcam), or anti-VE cadherin, monoclonal, mouse, (Abcam), or anti-smooth-muscle α-actin, mouse, polyclonal (Abcam), all 1:400 in PBS) for 60min, then they were washed with PBS and incubated with the secondary antibody (AlexxaFluor 568 anti-rabbit or anti-mouse, or AlexxaFluor 488 anti-mouse (all by Invitrogen)), 1:200 and depending on the experiment with $6,7\,\mu$M AlexaFluor 488 phalloidin (Invitrogen) for 30 min to stain for F-actin. DAPI (Invitrogen) staining was performed after antoboy staining, incubating the cell in a 1:1000 diluted solution for 5 min.

3.4 Analysis of actin stress fibers and focal adhesions

For analysis of actin stress fiber orientation (figure 2) a self-developed software macro embedded in ImageJ was used. Each cell was divided in several square-shaped subareas. Within each square the mean actin orientation was analyzed by texture analysis via a Fast Fourier Transformation (FFT) in analogy to Kemkemer *et al.* [107]. The angle for focal adhesion orientation was measured with ImageJ using background subtraction, threshold, and particle analysis. In total 15-30 cells from three independent experiments were evaluated and results were expressed as order parameter $\langle\cos(2\varphi)\rangle$ for each experiment.

3.5 Automatic controller model

Stochastic signal In the absence of a stochastic signal the differential equation (4.5) can be solved (small angle approximation) and the characteristic time, τ_2, is simply given by:

$$\tau_2(signal) = \frac{1}{2k_2(signal)^2} \tag{1}$$

This means that the cellular response is very fast for large guiding signals and very slow for small guiding signals. The temporal response in the small signal situation can be improved if a stochastic signal is introduced. The characteristic time, $\tau_2(0)$, is now given by the strength, q, of the stochastic signal

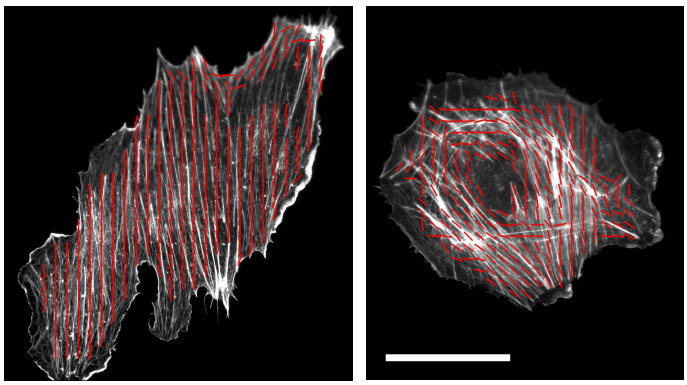

Figure 2: Example of analysis of actin stress fibres. A: endothelial cell after 6 h of applied stretch at 1 Hz, 8% amplitude, and B: control, cell after no applied stretch; scalebar represents 20 μm.

$$\tau_2(0) = \frac{2}{q} \tag{2}$$

Let us regard the following situation: The cells are oriented by a guiding signal. Then, at time $t = 0$ the signal is switched off. In the absence of a stochastic signal the cell orientation is frozen and stays forever. But in the case of a stochastic signal the cell orientation approaches the random orientation with the characteristic time, $\tau_2(0)$. Thus, in the signal-free situation, a stochastic signal is necessary if a finite response time is desirable. Obviously, the evolution of the cell has chosen a stochastic signal to respond quickly in case of low external signals.

Technical details of the controller (for cell orientation)

Symmetry properties The angle and signal characteristics of the cellular detection unit are predicted by using the symmetry of the system. The following experiments were performed to verify the symmetry: (1) The mirror symmetry holds true since the measured angle distribution function is symmetric in respect to zero degree (= direction of the guiding signal = x-axis): $f(\varphi) = f(-\varphi)$ or $f(x) = f(-x)$. The x-axis is a symmetry line for the cells and, therefore, cells cannot distinguish between left and right. (2) The apolar symmetry holds true since the measured angle distribution function is symmetric in respect to 90° (= perpendicular to the guiding signal = y-axis): $f(\varphi) = f(\varphi \pm 180°)$ or $f(y) = f(-y)$. The y-axis is a symmetry line for the cells and, therefore, cells like osteoblasts and fibroblasts cannot registrate the sign of the guiding field. This is an indirect proof. The direct one is: The steadystate angle distribution or the apolar order parameter does not change if the direction of the electric field is reversed.

Angle characteristics The angle characteristics, $g(\varphi)$, of the cellular detection unit are predicted by using the symmetry properties of the cells. This characteristic is basically described by the first nontrivial term: $sin(2\varphi)$. A straight line is predicted if the logarithm of the measured angle distribution function is plotted vs $\cos(2\varphi)$.

Cellular field standard The existence of a deterministic and a stochastic signal in the cellular automatic controller is the reason why the cells have an intrinsic field standard.

Actually the cells measure the deterministic signal in units of the stochastic signal. It can be shown in the following way:
The field-dependence of the cellular signal transformer can be predicted by using the symmetry properties of the cell. The dimensionless guiding field is described by the coefficient, α_2. The prediction is:

$$\alpha_2 = \frac{k_2}{q} b_2(signal) \tag{3}$$

Comparing the model predictions and the experimental results yields:

$$K_G^E = \sqrt{\frac{k_2^E}{q}} \tag{4}$$

$$b_2(signal) = E^2 \tag{5}$$

The power law for the field-dependent coefficient $b_2(signal)$ is verified having an even exponent ($n = 2$). The inverse of the guiding coefficient, K_G, is the cellular field standard in man-made units.

Symmetry properties of the detection unit The set point, φ_0, of the detection unit can be determined from the angle distribution function. Its maximum is at $\pm 90\,^\circ$) and its minimum at 0 and $\pm 180^\circ$. Thus, the examined cells like to orient perpendicular to the applied guiding signal. The desired angle of orientation in the summation point of the automatic controller is $\pm 90\,^\circ$ ($\varphi_0 = \pm 90^\circ$). This holds true for electric guiding fields and periodically stretched surfaces.
We are interested in cell orientation where the cellular automatic controller has the ability to recognize an extracellular guiding signal but not its sign. The coordinate system is defined in the following way: the x-axis is determined by the direction of the guiding signal. The cells orient in the xy-plane. The following symmetry properties are assumed:
Rotational symmetry: The physical state is unchanged if a cell is rotated in the xy-plane by $360\,^\circ$The angular dependence of the signal transformer is restricted by

$$g(\varphi) = g(\varphi + n360^\circ) \tag{6}$$

where n is an integer. Thus, the angular dependence of the signal transformer must be a cyclic function which can be described by a Fourier series

$$g(\varphi) = b_0 + b_1 sin(\varphi) + b_2 sin(2\varphi)... + c_1 cos(\varphi) + c_2 cos(2\varphi)... \tag{7}$$

with the guiding signal-dependent coefficients, $b_i(signal)$ and $c_i(signal)$. The rotary symmetry is evident and does not need an experimental verification.
Mirror symmetry: Next, it is assumed that the cellular automation cannot distinguish between left and right. Then, the physical state is unchanged if $+y$ is exchanged by $-y$ or the angle $+\varphi$ is exchanged by $-\varphi$ which means that the angular dependence of the signal transformer is restricted by

$$g(\varphi) = -g(-\varphi) \tag{8}$$

The consequence of this restriction is that all the coefficients c_i in (7) are zero. One has

now

$$g(\varphi) = b_0 + b_1 sin(\varphi) + b_2 sin(2\varphi) + ... \tag{9}$$

The mirror symmetry has to be verified by the experiment. Apolar symmetry: It is assumed that the cellular automaton can register the guiding signal but not its sign. Then, the physical state is unchanged if the x-direction is exchanged by $-x$, which means that the angular dependence of the signal transformer is restricted by

$$g(\varphi) = g(\varphi + 180^\circ) \tag{10}$$

All the coefficients b_i in equation 9 with odd i are zero. One has now:

$$g(\varphi, signal) = b_0 + b_2(signal) sin(2\varphi) + ... \tag{11}$$

In the case of an apolar symmetry the physical state of the cellular automaton is unchanged if the guiding field direction is reversed. This leads to an even integer, n, if b_i is approximated by a power law

$$b_i = (signal)^n \tag{12}$$

The predicted detection unit characteristics is then

$$g(\varphi) = b_0 + (signal)^n sin(2\varphi) + ... \tag{13}$$

only if the first nontrivial value is considered, b_0 has no physical meaning for the detection unit characteristics. Its only importance is for calibrating the angle distribution function.

4 Supplement material

All supplemental Material, which cannot be presented here is available on a DVD.

4.1 Stent coatings and stents

Details of the measurements with ECs of three different donors can be seen in figure 3. The data vary from donor to donor for PSS, IrOxI, IrOxII and IrOxIV. Only on IrOxIII and SS, cell growth is stable. These results confirm the short term measurements. The variations of donors made clear that it is necessary to perform cell culture essays on implant coatings with cells of more than three different donors to gain significant statistics. Particular emphasis should be given to the age of the donors and their medical background. It might be helpful to use cells from donors with a need for stent treatment.

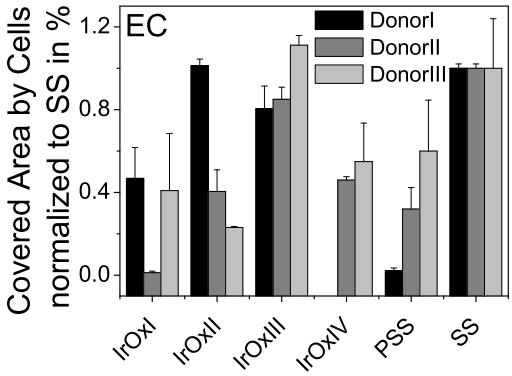

Figure 3: Covered area of endothelial cells (ECs) of three donors after 14 days on test strips, normalized to stainless steel (SS). Error-bars show the deviation from experiment to experiment.

Example images of ECs on stent struts immunostained with VE-cadherin antibody are depicted in figure 4.

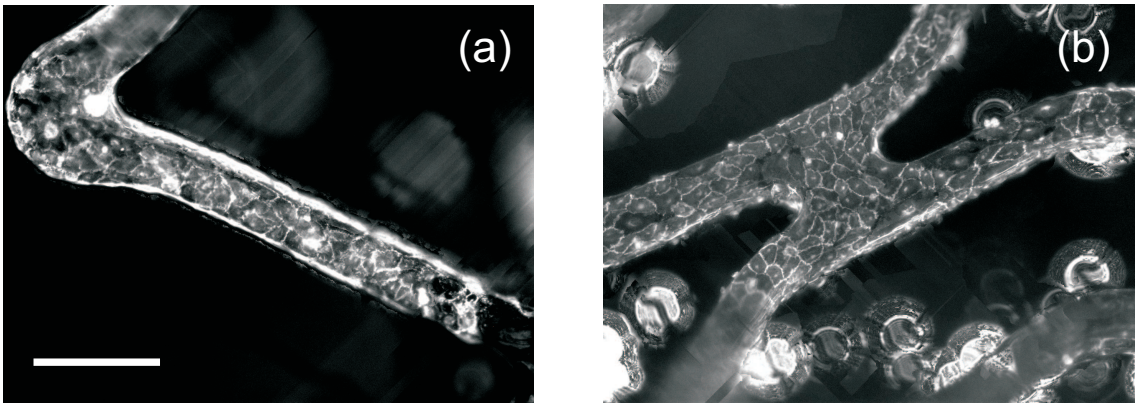

Figure 4: ECs after 14 days on a stent with IrOxIV-coating (a) and SS-coating (b), immunostaining with anti-VE-cadherin; the scalebar represents 200 μm.

4.2 Nano-micro topography

Supplementary movies are available on an attached CD:

Groove-Movie 1: Fibroblast cells (FCs) on 2 μm wide and 200 nm deep grooves, 24 h time lapse.

Groove-Movie 2: Endothelial cells (ECs) on 2 μm wide and 200 nm deep grooves, 24 h time lapse.

Groove-Movie 3: Smooth muscle cells (SMCs) on 2 μm wide and 200 nm deep grooves, 24 h time lapse.

4.3 Stretching

Supplementary movies are available on an attached CD:

Stretch-Movie 1: Endothelial cells (ECs) under applied stretch of a frequency of 1 Hz, amplitude of 8%, 6h time lapse. The stretch was applied in x-direction.

Stretch-Movie 2: Smooth muscle cells (SMCs) under applied stretch of a frequency of 1 Hz, amplitude of 8%, 6h tme lapse. The stretch was applied in x-direction.

4.4 Electrical fields

Supplementary movies are available on an attached CD:

EField-Movie 1: Endothelial cells (ECs) under an dc electrical field (dcEF) of 400 mV/mm; dcEF is directed in x-direction, switched on after fram 24, and switched off from frame 144; 15h time lapse.

EField-Movie 2: Smooth muscel cells (SMCs) under an dc electrical field (dcEF) of 300 mV/mm; dcEF is directed in x-direction, switched permanently; 6h time lapse.

An overview of perfomed experiments with endothelial (ECs) and smooth muscle cells (SMCs) in direct current electrical fields (dcEFs) is given in the figures 5 and 6.
An overview of perfomed experiments with endothelial (ECs) and smooth muscle cells (SMCs) in pulsed electrical fields (ELFP-EFs) is given in the figures 7 and 8.

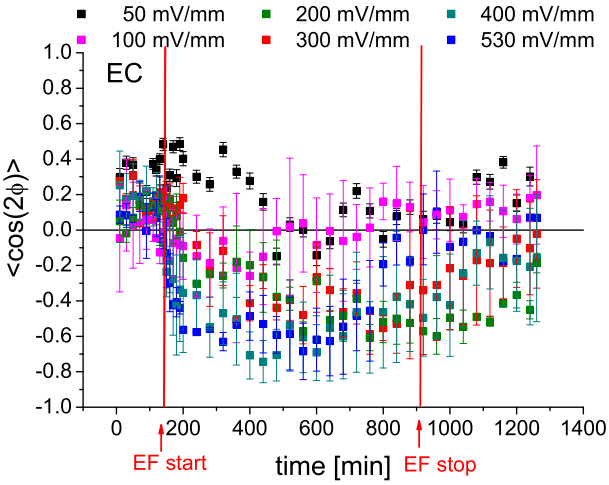

Figure 5: Time development of apolar order paramter ($\langle cos(2\varphi) \rangle$) of endothelial cell (EC) orientation for several electric field strengths (dcEFs); each color represents the average for 2-3 experiments.

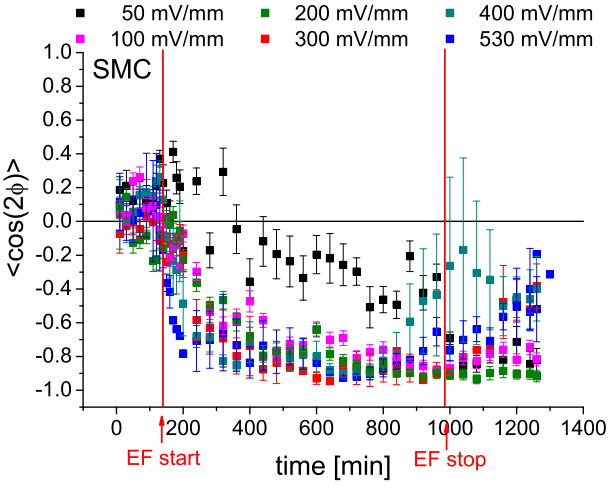

Figure 6: Time development of apolar order paramter ($\langle cos(2\varphi) \rangle$) of smooth muscle cell (SMC) orientation for several electric field strengths (dcEFs); each color represents the average for 2-3 experiments.

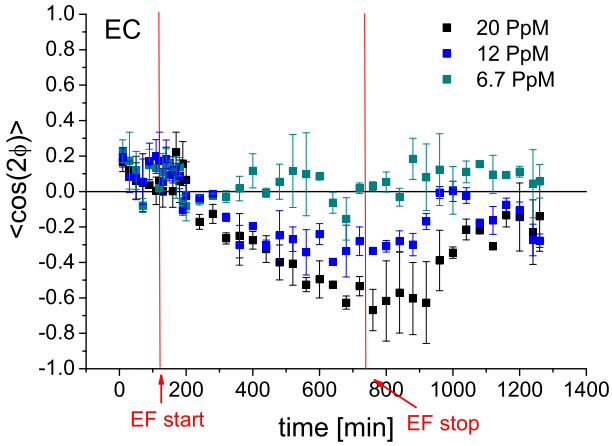

Figure 7: Time development of apolar order paramter ($\langle cos(2\varphi) \rangle$) of endothelial cell (EC) orientation for several pulse doses in an electrical field; the pulse doses are given in pulses per minute (PpM); each color represents the average for 2-3 experiments.

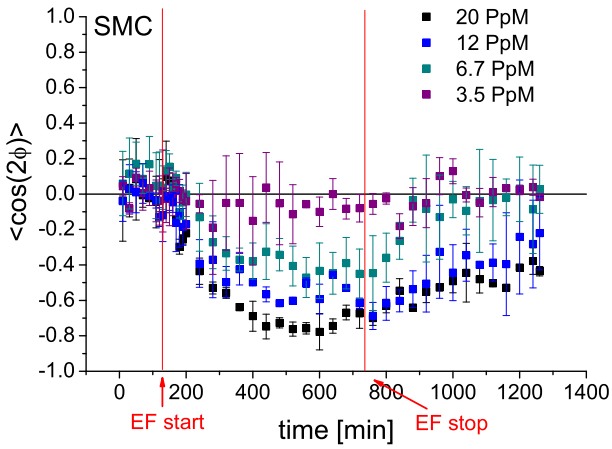

Figure 8: Time development of apolar order paramter ($\langle cos(2\varphi) \rangle$) of smooth muscle cell (SMC) orientation for several pulse doses in an electrical field; the pulse doses are given in pulses per minute (PpM); each color represents the average for 2-3 experiments.

Ich erkläre hiermit, dass ich die vorgelegte Dissertation selbst verfasst und mich keiner anderen als der von mir ausdrücklich bezeichneten Quellen und Hilfen bedient habe.

Heidelberg, den 27. April 2009 .....

Sarah Biela